AD-A114 627 VON KARMAN INST FOR FLUID DYNAMICS RHODE-SAINT-GENESE--ETC F/G 20/4
ROTATING STALL IN AN AXIAL FLOW SINGLE STAGE COMPRESSOR. ON-BLA--ETC(U)
APR 82 B GYLES, P LIGRANI, F A BREUGELMANS AFOSR-80-01198
UNCLASSIFIED EOARD-TR-82-10 NL

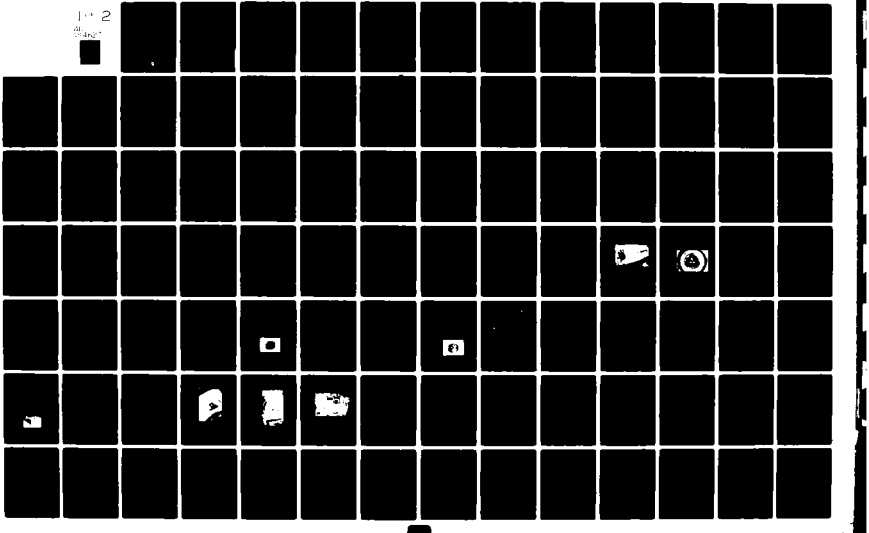

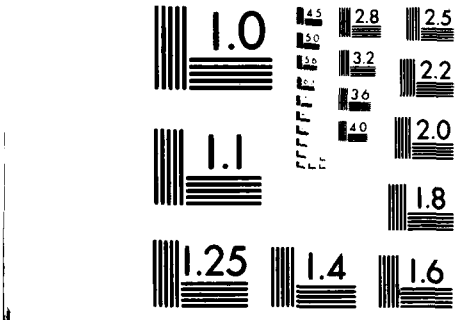

AD A114627

REPORT DOCUMENTATION PAGE		READ INSTRUCTIONS BEFORE COMPLETING FORM
1. Report Number EOARD-TR-82-10	2. Govt Accession No. AD-A114 627	3. Recipient's Catalog Number
4. Title (and Subtitle) Rotating stall in an axial flow single stage compressor. On-blade velocity measurements		5. Type of Report & Period Covered Final Scientific Report 15 Jan 80 - 14 Feb 82 6. Performing Org. Report Number
7. Author(s) B. Gyles, P. Ligrani, F.A.E. Breugelmans		8. Contract or Grant Number AFOSR 80-0119B
9. Performing Organization Name and Address von Karman Institute for Fluid Dynamics Ch. de Waterloo, 72 B-1640 Rhode Saint Genèse, Belgium		10. Program Element, Project, Task Area & Work Unit Numbers P.E.: 61102F Proj/Task: 2301/D1
11. Controlling Office Name and Address European Office of Aerospace Research and Development/LNT Box 14 FPO New York 09510		12. Report Date April 15, 1982 13. Number of Pages 112
14. Monitoring Agency Name and Address European Office of Aerospace Research and Development/LNT Box 14 FPO New York 09510		15.
16. & 17. Distribution Statement Approved for public release; distribution unlimited.		
18. Supplementary Notes		
19. Key Words Rotating stall; Flow separation; Axial compressor; Thermal tuft; Hot wire anemometry		
20. Abstract Three multiple hot wire sensors are developed and applied to a low speed axial compressor rotor blade. The multiple wire sensor design is based on the technique of the combined hot and cold wire in a parallel arrangement for the detection of flow separation and reversal. The sensors are used in the unstalled and stalled part of the compressor characteristics with one and two stall cells present. The signals are analyzed using the fast Fourier transform, power spectra and correlation techniques.		

EOARD-TR-82-10

This report has been reviewed by the EOARD Information Office and is releasable to the National Technical Information Service (NTIS). At NTIS it will be releasable to the general public, including foreign nations.

This technical report has been reviewed and is approved for publication.

Winston K Pendleton

WINSTON K. PENDLETON
Lt Colonel, USAF
Chief Scientist

Gordon L. Hermann

GORDON L. HERMANN
Lt Colonel, USAF
Deputy Commander

TABLE OF CONTENTS

ABSTRACT

Three multiple hot wire sensors are developed and applied to a low speed axial compressor rotor blade. The multiple wire sensor design is based on the technique of the combined hot- and cold wire in a parallel arrangement for the detection of flow separation and reversal. The sensors are used in the unstalled and stalled part of the compressor characteristic with one and two stall cells present. The signals are analyzed using the fast Fourier transform, power spectra and correlation techniques.

LIST OF FIGURES

1. INTRODUCTION

A current problem in the design of axial flow compressors is the prediction and control of the effects of rotating stall, a phenomenon which is characterized by one or more cells of retarded flow which propagate around the compressor annulus. This phenomenon occurs only when the compressor is operated along a part of the positive sloping portion of the performance map. The propagating stall cells may encompass all or part of the blade height and are known respectively as full-span and part-span stall cells. Viewed from the laboratory frame of reference, a stall cell moves in the direction of rotation of the rotor, but at a speed which is less than the rotor speed. Thus, viewed from a relative reference frame fixed to the rotor, the cell moves in a direction opposite to the direction of rotation, i.e., from the pressure side to the suction side of each blade.

The presence of rotating stall cells invariably results in a deterioration of the compressor performance (i.e., low flow rates and pressure ratios), and the periodic nature of the phenomenon introduces forced vibrations which are potentially harmful to the machine. From a design point of view, a good theoretical understanding of rotating stall would be useful in designing to avoid rotating stall and/or to minimize the harmful effects should rotating stall be unavoidable. At present, rotating stall theory is partially developed, and certain parameters of rotating stall can be predicted with reasonable accuracy. Among these are predictions of whether or not a rotating stall will occur at a given operating point and if so, whether a full-span or a part-span stall will occur. In addition, the total area of the annulus which will be blocked by stall cells, part-span or full-span, and the overall pressure ratio can be predicted within certain limits. Up to the present time, the speed of rotation of stall cells has defied accurate prediction.

In previous work on this subject, a number of experimental investigations were carried out in which were measured a number of gross characteristics of rotating stall. Primarily, these characteristics are the position on the performance map, the number and size of stall cells, and the cell rotational speed. In addition, the geometry of the machine is detailed in each case. Unfortunately, due to limitations on instrumentation, very little data is available on the detailed flow within a stall cell or on the stalling process occurring on the blades.

The rotating stall problem has been attacked theoretically by a number of authors. Two approaches are most commonly used. These are :

(1) an analysis which defines resonance conditions for a compressor system modelized as a Helmholtz resonator, and

(2) an analysis which determines the conditions for the growth of a small sinusoidal pressure disturbance across the blade rows. Most of the latter types of analyses use linearized equations of motion so that they are fundamentally unable to predict anything more than the conditions for the onset of an instability. Predictions obtained with these theories have been moderately successful in that the important non-dimensional system parameters have been defined, along with the relations between these parameters required for the existence of rotating stall. Unfortunately, these relations are not completely general in that something of the system behavior, such as the shape of the steady-state constant speed lines on the performance map, must be known in advance.

Attempts have also been made, with much less success, to predict some of the finer details of rotating stall such as the number of stall cells and the cell rotational speed. Some have conjectured that these parameters are strongly controlled by such things as blade shape, blade row spacing, etc., rather than by the gross parameters which induced the flow instability in the first place. If this is the case, then much more work

remains to be done to determine which variables are most important in controlling the flow processes once a rotating stall has been established.

Current research on rotating stall is being undertaken to further understanding of the basic mechanisms of rotating stall, with the aim of further developing the necessary theory. Of particular interest are detailed surveys of the flow field using fast response instrumentation, which can provide some insights into just how a stall cell propagates from blade to blade around the compressor annulus. Such measurements also provide a data base for attempts to calculate from basic principles the global parameters (stall size, stall speed, etc.) which are of interest to the designer.

For the present investigation, the authors have developed a directionally sensitive hot wire probe suitable for mounting on the suction surface of a rotor blade. Measurements were taken with this "thermal-tuft" probe in conjunction with hot wire measurements in the stationary reference frame ahead of and behind the rotor of a low-speed axial compressor. As a result, information has been obtained about the sequence of events as a rotor blade stalls and then unstalls during the passage of a rotating stall cell. The measurements also indicate that a stall cell has a distinct structure which is maintained with only minor random changes as the stall cell moves around the compressor annulus.

2. REVIEW OF PREVIOUS WORK

A large number of experimental investigations have been done in previous years on the problem of rotating stall in axial flow compressors. These investigations can be divided roughly into two categories :

(1) those concerned with measuring global parameters such as the number and size of stall cells, and;

(2) those concerned with very detailed measurements to gain insight into the dynamics of the stalling process.

The latter investigations generally involve the use of hot wires and/or fast response pressure probes. In a number of cases theoretical analyses of some particular aspects of rotating stall which attempt to reproduce the experimental results are included.

Perhaps the most striking aspect of the various experimental studies is the large number of parameters which strongly influence rotating stall. Any one experiment is able to vary only a limited number of these many parameters, making general conclusions about rotating stall quite difficult.

Of all the parameters of rotating stall which have been measured, there are perhaps three which are of real interest from a design point of view. These are :

(1) the area of the performance map where rotating stall will occur (i.e., the overall mass flows and pressure ratios);

(2) the passing frequency of the stall cells at a given operating point;

(3) the severity of the disturbance (to estimate the effects on blade life).

Each of these parameters is dependent on a large number of other parameters which can be varied by the designer within certain limits. A partial list of some of the more important variables follows :

(1) number of stages;

(2) hub to tip radius ratio;

(3) solidity of blading;

(4) geometry of blading;

(5) geometry of compressor inlet and exhaust ducting.

In addition, the dependent paramaters of rotating stall change as a function of the overall operating point of the compressor.

As a result of previous investigations, two aspects of rotating stall have been correlated with the same degree of accuracy. First, given the overall geometry of the compression system, it is possible to predict whether or not a rotating stall will occur. Second, for a given operating point where rotating stall is known to occur, it is possible to predict the overall pressure rise through the compressor. These predictions are possible because the most important non-dimensional variables in each case have been identified. Of course, there is a fair amount of uncertainty in the predictions since many variables having a second-order influence have been ignored.

Prediction methods employing a correlation approach and methods involving calculations from basic principles have been used to predict whether or not rotating stall will occur at a given operating point. Neither method seems to have any particular advantage, except that the correlations methods are much easier to apply. Greitzer (Ref. 33) describes a correlation method resulting from an analysis in which the compression system is modelled as a Helmholtz resonator. The steady-state performance map of the compressor, including the stall region, is needed as an input to the analysis. The end result of the analysis is the definition of a critical parameter for rotating stall. Given that the compressor is operating at a point on the performance map where stall might be expected to occur, there is a limit value of this parameter, below which rotating stall will occur, and above which surge

occurs. The essential input for this correlation method is the location of the stall limit on the performance map, information which is readily available even at the design stage.

In a later paper, Greitzer (Ref. 15) presents a correlation method in which the fraction of the annulus area blocked by stall cells and the overall pressure rise can be determined for any given operating point in the stalled zone. In addition, Greitzer found a limiting value of the blockage, above which full-span stall cells will occur, and below which part-span cells will occur. This method is an extension of the so-called parallel compressor theory, and requires the unstalled performance characteristic and the location of the stall limit as inputs. The overall pressure rise is found to be a linear function of the number of stages of the compressor.

Note that the above correlation-type prediction methods have been successful only in predicting the existence of rotating stall, the type and total size of stall cells which will be present, and the overall pressure rise in the compressor. While these predictions are indeed valuable, more detailed predictions of stall cell size, the severity of the disturbance, the number of stall cells, and the stall cell rotational speed are highly desirable. A number of attempts have been made at such predictions, but it is only within the past ten years that the methods have developed to the point where the results begin to approximate reality. Early prediction methods generally made use of steady, linearized equations of motion and did not consider the unsteady stalling characteristics of the blade row.

Tanaka and Murata (Ref. 44) have performed a number of rotating stall calculations using unsteady non-linear, inviscid equations of motion combined with a model of the unsteady stalling characteristics for the rotor blade row which was obtained experimentally for a particular set of blading. Four separate cases were calculated :

(1) a two dimensional isolated blade row;

(2) a three dimensional isolated blade row;

(3) a two dimensional rotor and stator at a finite axial distance;

(4) a single-stage compressor consisting of inlet guide vanes and a rotor separated by a finite axial distance followed by a stator at an infinitesimal distance form the rotor.

The case of the single-stage compressor is the most interesting since many features of rotating stall are evident in the calculation which do not appear in the simpler configurations.

For the single-stage compressor configuration, Takata and Nagano have been able to reproduce, at least qualitatively, the change from part-span to full-span stall as the compressor is throttled in the rotating stall region. The change from part-span to full-span stall is also accompanied by a decrease in the number of stall cells. These features are not found in any of the simpler configurations calculated by Takata or in any calculations by other authors using linearized equations of motion. Dependencies of the dependent stall parameters on a number of other independent variables are also predicted correctly, at least qualitatively. Among these dependencies are the dependence of the number of stall cells and the stall propagation velocity on the axial distance between the rotor and the inlet guide vane. This model also predicts where on the performance map rotating stall will occur, but the behavior of the unsteady total pressure loss coefficient of the blade rows is needed as an input to the calculation.

Day & Cumpsty (CUED/A-Turbo/TR 90)

Hot wire measurements between blade rows show both upstream and downstream flow within a given stall cell which might indicate the existence of a vortical structure.

Casalini & Breugelmans (VKI PR 1979-3)

Instantaneous velocities are measured during the single stall cell occurrence using crossed hot wires in front and downstream of the rotor at three different axial stations and five radial positions. An important return flow is observed near the blade tip, while a small axial component towards the impeller always exists at the hub. The representation with respect to the cell or the rotor blades demonstrates the "active cell" concept.

Cossar, Moffatt, Peacock (ASME P 79-GT-Isr-18)

Pressure measurements on blade suction and pressure surfaces show rapid changes in static pressure within stall cell which the authors feel may be due to flow reversal. At leading edge of stall cell, the authors saw a pressure disturbance passing over the suction surface of the blade. This disturbance moved from trailing edge to leading edge or from leading edge to trailing edge (in case of inlet flow distortion). Authors feel this may be boundary layer separation phenomenon.

Sexton, O'Brien, Moses (AGARD CP 177, Paper 33)

Pressure measurements on blade suction surface (at 1/4-span in part-span stall cell) show pressure disturbances during passage of stall cell. These disturbances appeared as a velocity peak moving from leading edge to trailing edge (on blade with 8° average incidence) or as a velocity peak occurring essentially simultaneously over the suction surface (on blade with 11° average incidence). The sequence of suction surface pressure profiles during stall cell passage is qualitatively similar to those which occur on an isolated airfoil during dynamic stall.

Work of Nagano, Machida & Tanaka

(1) Measurements taken of rotating stall in a counter-rotating axial flow compressor.

(2) Speed of rotation of blade rows was adjusted to hold stall cell stationary and flow angle, flow velocity and static pressure were measured before and after each blade row.

(3) Measurements in stationary plane show change in flow angle through clean flow region.

(4) Apparently, flow angle change relative to blade is seen as an increase in flow angle through clean flow region as stall cell is approached (same as seen in present work).

(5) Shape of loss curve and loss magnitude seems very dependent on rotational speed and geometry, but according to the authors, the non-dimensional time constant for boundary layer delay does not change much.

(6) Stall cell speed relative to first blade row is not very sensitive to changes in speed of second blade row.

Work of De Ponte & Baron (AGARD CP 296, Paper 12)

(1) Situation is a separated boundary layer exposed to a cyclically varying pressure gradient so that separation and reattachment points are unsteady.

(2) Delay time for reattachment is found to be larger than delay time for separation, apparently due to long wash-out time for low-speed stalled fluid.

Results of Kriebel, Seidel & Schwind (NASA TR R-61)

(1) Stall propagation in a circular cascade (quasi-linear).

(2) Observation made by use of schlieren photographs.

(3) Observed vortex shedding from airfoil leading edges as blades stalled at the stall cell leading edge.

(4) Observed vortex shedding from airfoil trailing edges as blades unstalled (possibly starting vortices) at the stall cell trailing edge.

General observations

All on-blade measurements have been of static pressures, which can be used to deduce the magnitude but not the direction of the flow. Thus we have no information on when and where reverse flow occurs on the blade during the passage of a stall cell.

Measurements outside of the blade rows indicate reversed flow in the stall cell as a whole. This occurrence should be seen also in on-blade measurements and should be distinguished from any boundary layer separation processes which occur.

3. DESCRIPTION OF FACILITY

3.1 The R-1 facility

The VKI low speed single stage compressor R-1 is used to study the overall and detail flow phenomena in all operating points of an axial flow compressor. The inlet and exhaust of the facility are atmospheric.

A 55 kW DC motor drives the rotor at rotational speeds ranging from 0 to 2000 RPM. The rotor is mounted in a overhang position with a long shaft through the inlet chamber. The contraction and inlet screen provide uniform flow conditions to the inlet guide vanes.

The test section has a tip diameter of 702 mm and a hub diameter of 554 mm, the diameters being of constant height over the axial extension of 515 mm of the test module. An inner conical hub diffuses the flow into the cylindrical duct downstream of the model. A radial throttle valve at the end controls the operating condition of the compressor.

3.2 The blading

The test model is equipped with inlet guide vanes (IGV), rotor blades and stator vanes. The IGV rotor distance is : 94 mm. The rotor-stator distance is : 57 mm.

The blade characteristics are shown in the following table. The stator vanes are constant thickness thin metal sheet airfoils of 35° camber, positioned for an average rotor outlet angle of 50° for an improved pressure recovery in the exhaust duct.

The bladings are described in Tables 1, 2 on page 14.

3.3 Instrumentation

The classical instrumentation consists of short prism type NACA probes connected to strain gage transducers with positioning accuracy of 0.1 mm radially; 0°2 angular and 0.1% of the full range for the transducer chain.

The hot wire signals are processed by a hot wire anemometer, a product of VKI-Instruments, using the constant temperature principle. Linearization can be performed using the King law. Time and RMS averaging is available.

The signals of the rotating frame are transmitted through the 8-channel Vibrometer mercury slip ring assembly. These rotating contacts are included in the hot wire bridges during the calibration procedure and are spun at the required rotational speed by an independent drive.

The signals can be acquired by different systems. A multi-channel, transient recorder, 4 K words per channel with a maximum of 200 kHz data rate, has been used in conjunction with a x-y plotter, an 8 track magnetic tape logger and an oscilloscope. The systematic large volume data acquisition is performed by the VKI medium speed DAS system of 16 channels (only 4 used for this purpose). The 16 channel signal conditioner contains an amplifier, a variable anti-aliasing filter and a sample-and hold for each data channel. This is followed by a multiplexer and analog/digital converter. The maximum sampling rate is 50 kHz. Both internal and external triggering capability is present. Data are processed as 12 bit words for transmission to a PDP 11/34 computer, via a serial line transmitter at frequency of the order of 1 M byte/sec, over distances in excess of 300 m. Parity-bit error detection system is provided by the transmission-reception hardware.

3.4 Performance map

The low speed compressor performance map is presented by the pressure coefficient Ψ_0 in function of the flow coefficient ϕ.

The over the blade height mass averaged values of axial velocity and pressure are used for the calculation of the non dimensional coefficients. These values are obtained in front of the IGV's and downstream of the stator vanes in order to have consistent measurements in the unstalled and stalled portion of the characteristic.

$$\phi = \frac{\int_H^T 2\pi\rho \; R \; V_a dR}{U_T} \qquad \text{with} \qquad \bar{P}_{0_i} = \frac{\int_H^T 2\pi R\rho \; V_{a_i} P_{0_i} \; dR}{\int_H^T 2\pi \; R \; \rho \; V_{a_i} \; dR}$$

$$\Psi_0 = \frac{\bar{P}_{02} - \bar{P}_{01}}{\frac{1}{2} \rho U_T^2}$$

The number of stall cells is determined by comparing the phase shift between two hot wire signals, simultaneously taken at two tangential locations. The angular separations used are 35°, 55°, 90° and 180°.

The ϕ-Ψ_0 characteristic is shown in figure 5. Zone A represents the region with 10 cells, followed by a transition zone where no periodic phenomenon could be observed and in which the flow reorganizes into one large cell (point B), and finally a break-up into two cells occurs (point C). Reopening the throttle valve allows the operating point to describe the hysteresis loop during which one cell exists.

The propagation velocities are 58.2% (A), 31.2% (B) and 32.7% (C) respectively for rotating stall frequencies of 97 Hz (A), 5.2 Hz (B) and 10.9 Hz (C) at 1000 RPM.

$\bar{h}$	0	0.25	0.50	0.75	1
ϕ	47.01	44.76	42.55	40.73	38.86
C_{L_0}	1.88	1.79	1.70	1.62	1.55
$(\frac{t}{c})_{max}$	0.06	0.06	0.06	0.06	0.06
γ	21.69	20.65	19.63	18.79	17.73
$\Delta\gamma$	3.96	2.292	1.90	1.06	0
g=c mm	44.5	47.5	50.5	53.5	56.5
σ	1	1	1	1	1

TABLE 1 - DATA OF INLET GUIDE VANE

$\bar{h}$	0	0.25	0.50	0.75	1
ϕ	22.34	18.34	14.83	11.74	9.23
C_{L_0}	0.89	0.73	0.59	0.47	0.36
$(\frac{t}{c})_{max}$	0.06	0.06	0.06	0.06	0.06
γ	24.56	31.54	37.33	42.11	46.03
$\Delta\gamma$	0	6.98	12.77	17.55	21.47
g (mm)	69.6	74.1	78.9	83.5	88.1
c (mm)	70.4	75.2	80.0	84.8	89.6
σ	1.01	1.012	1.015	1.017	1.018

TABLE 2 - DATA OF ROTOR

Remark : $\Delta\gamma = \gamma - \gamma_{tip}$ for IGV and stator

$\Delta\gamma = \gamma - \gamma_{hub}$ for rotor

4. SENSOR DEVELOPMENT

The objective was to study the flow on the rotating blade surface, to detect flow separation and reverse flow and to correlate these effects to the rotating stall cell. Different sensors are developed in this study and all of them are based on the thermal tuft technique and crossed hot wire principle. The usefulness of such a sensor for the investigation of the dynamic flow behavior is demonstrated in figure 6.

4.1 Thermal tuft techniques and flow reversal measurements

Hot wire or hot film techniques which allow determination of instantaneous changes in flow direction are numerous. Such measurement schemes generally employ sensors which detect heat wakes or which measure the time of flight of tracers of heated air or tracers of solid particles.

One of the earliest investigators to employ heated wake detection sensors to measure velocity was Kovasznay (1948). In his study, a wake with a sinusoidal periodic temperature fluctuation was detected using a hot wire. The velocity was determined by noting the phase shift between the current in the heated wire and the heating experienced by the detecting wire. Bauer (1965) extended the Kovasznay technique using a constant current hot wire as a resistance thermometer. This wire was placed downstream of the heated wire. As before, velocity magnitudes were determined by measuring time differences between pulses in the two wires. Velocity direction was also determined by moving one wire relative to the other until the wakes were aligned.

Bradbury (Ref. 2) and Bradbury & Castro (Ref. 5) improve Bauer's method by placing a pulsed heated wire at right angles to and between two hot wires operated as resistance thermometer. The probe allows measurement of components of velocity perpendicular to the plane of the three wires, but also requires a check

of yaw sensitivity since it is intended to be used away from a wall where highly unsteady mean flow may assume large direction changes. The technique was later used for a variety of applications, including measurements in the turbulent wake produced by a flat-plate placed normal to the flow direction (Bradbury, Ref. 3). Tombach (Ref. 28) also employed a technique similar to that of Bradbury in turbulent jet of foreign gas with very small turbulent scales.

Downing (Ref. 12) developed a technique using a geometric arrangement like that of Bradbury (Ref. 2), however, instead of a pulsed heated wire, Downing's probe contained an ordinary constant-temperature wire. This wire allowed direct detection of the magnitude of one component of velocity, and produced a thermal wake which allowed the direction to be determined by two resistance-thermometer wires placed on either side. Instead of a digital output like that obtained with the Bradbury method, a continuous analog signal was produced.

Gunkel, Patel and Weber (Ref. 16) used a pair of constant temperature wires in an arrangement similar to one described by Moon (Ref. 24). Flow direction was deteched when the wake of one hot wire was sensed by a second wire placed parallel to and directly behind the first. However, in contrast to the Moon technique, the Gunkel et al. method has two wires contained within a ring enclosure shield so that the sensors were unaffected by the component of velocity perpendicular to the plane of the wires. The method was demonstrated to be useful for measuring one component of rapidly reversing flows. Cook and Redfearn (Ref. 8) advanced the Gunkel et al. method by employing an improved shield to better contain one component of velocity. It was mentioned that such techniques are accurate for low velocity flows containing turbulence structures larger than the inner diameter of the shield. Bradbury (Ref. 4) discusses another variation of the Gunkel et al. and Cook et al. methods, in which the shroud contains a constant-temperature hot wire followed by a resistance thermometer at right angles.

In contrast to all of the previous methods described which may be used to detect flow reversals away from walls, several methods have also been developed to detect reversals near walls. Such techniques are commonly used as diagnostic tools to detect boundary layer separation. One of the earliest of these is described by Moon (Ref. 24). The author developed a near wall direction sensing system which employs two hot wires. Either the ratio or the difference of the two hot wire signals serves as an indicator of the direction of the flow. Indication is possible since the relative magnitude of each hot wire signal depends on which wire is contained in the wake of the opposite wire.

Horstman and Owen (Ref. 18) used thin platinum film gages operated in a constant-temperature mode and mounted flush with the surface adjacent to the flow to be tested. Fluctuating voltages from these films provide measurements related to flow fluctuations above the films. Rubesin, Okuno, Mateer and Brosh (Ref. 25) developed a three-element wall sensor. The design consists of buried-wire skin friction gauges : a heated wire center element with two temperature sensors on either side. Generally, the Rubesin et al. technique appears to be most useful for separation measurements when the location of separation does not change rapidly in magnitude or with time. An example of measurements using the technique is shown in figure 7, where the output voltage from the two temperature sensors is shown as a shock wave passes. The difference between the two voltage levels gives an indication of flow separation (S) and reattachment (R) as shown.

Some of the most recent techniques devised to detect flow reversals near walls are described by Eaton et al. (Ref. 13), Carr & McCroskey (Ref. 6), and Westphal et al. (Ref. 29). The sensors in these studies all employ three hot wires mounted very near the wall. Both flow reversal and velocity magnitude may be detected using the probes described in the latter two papers. However, all of the probes are limited in that they

may be used to measure direction changes caused only by quasi one dimensional flow reversals, and not when the flow reversals occur near the wall in a direction which is not roughly perpendicular to the wires. No probes known to the present authors for near wall measurements provide information for situations other than quasi one dimensional flow reversals.

All of the three hot wires employed in the Carr & McCroskey (Ref. 6) technique are powered by constant temperature anemometry circuits. Two 5 μm diameter wires are placed with a 25 μm wire directly between them. The center wire is sensitive to velocity magnitude, and the outside wires indicate direction as they sense the wake produced by the center wire. The technique was demonstrated to give an unambiguous indication of the direction of flow over a helicopter rotor airfoil during dynamic stall. An example of such measurements for one airfoil oscillation is shown in figure 8, where an ordinary hot wire signal is compared with their thermal tuft measurements at different locations along the blade surface. The locations where the signal passes the zero voltage intercept indicate locations of flow reversal (FR) and reattachment (R) as shown.

The Eaton et al. (Ref. 13) thermal tuft consists of two resistance thermometers (5 μm diameter) mounted on either side of a center wire (125 μm diameter) heated with a DC current. The probe is used for several purposes, including measurement of the fraction of time that the flow near the wall is forward or backward. An example of such a measurement is shown in figure 9, where the time averaged percent of downstream flow for a diffuser is shown. In the figure, S is the coordinate along the wall measured from the diffuser throat and W is the length of the diffuser.

The probe described by Westphal et al (Ref. 19) employs a pulsed wire heater-tracer technique similar to the method described by Bradbury et al. (Ref. 5). The device may be used to measure the streamwise flow velocities between -8 m/sec

and +8 m/sec. The instantaneous wall shear stress is deduced from the velocity assuming that the near wall velocity profile remains similar and scales on the wall shear stress, even when the flow direction changes rapidly.

4.2 Thermal-tuft design and development for flow measurement near a compressor blade - Two wire sensor

The initial stages in hot wire thermal tuft development for measurement of flow near compressor blades are described by Ligrani et al. (Ref. 22) and by Gyles et al. (Ref. 17) The probe design is simple, consisting of two hot wires mounted parallel to each other and spaced a small distance apart as shown in figures 10 and 11. The wires are oriented in the x-y plane, perpendicular to the coordinate x of figure 10. The wires are connected to two pairs of prongs mounted on a small plexiglas plug which may be inserted into calibration fixtures or mounted directly onto a compressor blade.

Of the probe designs described earlier, the present design is most similar to the one described by Moon (Ref. 24) since near wall measurements are made using two closely spaced wires driven by constant temperature bridges. When the flow moves in the +x direction (i.e., when $\alpha = 0°$ and $\Theta = 0°$), wire number 1 in figure 10 produces a heated wake which is detected by wire number 2. For all the measurements, wire number 1 was operated at an overheat ratio of 1.6, while wire number 2 was operated at an overheat ratio of 1.1, following recommendations by Carr & McCroskey (Ref. 6). Such an approach provides a greater velocity ratio sensitivity to flow reversals than is possible if the same overheat ratio is used for both wires. Two parallel wires, instead of two perpendicular wires like those in the Bradbury et al. (Ref. 5) technique were chosen for the present probe since a greater resolution of signal changes is expected as wire 2 senses a large part of the heated wake from wire 1 for flow moving in the +x direction. This results in a greater

change in velocity ratio when the heated wakes moves off wire 2, an important consideration for the highly turbulent flow expected near the compressor blade.

Typical calibration characteristics for the hot wire thermal tuft are shown in figures 11, 13 and 15. Figure 11 shows calibration characteristics of the probe as the velocity and pitch angle of the probe are changed. In this figure, the ratio of the indicated average velocities from the two hot wires, $\frac{U_{i_2}}{U_{i_1}}$ is plotted on the vertical axis. If a complete reversal of flow direction (i.e., from $\theta=0°$ $\alpha=0°$ to $\theta=0°$ $\alpha=180°$) occurs then the magnitude of $\frac{U_{i_2}}{U_{i_1}}$ goes from a value less than one to a value greater than one. Such a situation is equivalent to a one dimensional flow reversal. For the data in the figure, $\frac{U_{i_2}}{U_{i_1}}$ increases with pitch angle when wire 1 is upstream, and decreases with pitch angle when wire 2 is upstream. The variations of $\frac{U_{i_2}}{U_{i_1}}$ with α and velocity, V, are caused by variations in the way that the downstream wire is contained within the thermal wake convected from the upstream wire.

Figure 12 shows how $\frac{U_{i_2}}{U_{i_1}}$ varies with yaw angle α for -5 degree pitch angle and velocities of 15.0 m/sec, 25.0 m/sec, and 35.0 m/sec. Generally, the indicated velocity ratio increases as the yaw angle increases, a trend consistent with data in the previous graph. From figures 11 and 12, it is evident that one value of the velocity ratio $\frac{U_{i_2}}{U_{i_1}}$ can correspond

to infinitely many combination of yaw and pitch angle, unless $\frac{U_{i_2}}{U_{i_1}} \approx 0.1\text{-}0.2$. For this case, the flow moves in a direction from wire 1 to wire 2, the yaw angle is 0°, the pitch angle is 0°, and the flow direction is in the plane of the two wires.

A further check on the behavior of the thermal tuft was made using the apparatus shown schematically in reference 17. The thermal tuft was mounted on the plate in the figure, which was then placed in a calibration duct. The character of the boundary layer developing over the plate was changed by changing the plate pitch angle relative to the oncoming flow. For negative pitch angles, a strong favourable pressure gradient was induced on the wall boundary layer. For positive pitch angles, the boundary layer separated and a one dimensional flow reversal was present at the thermal tuft location. The $\frac{U_{i_2}}{U_{i_1}}$ output from the tuft clearly indicates a change in flow behavior as the pitch angle changes from negative to positive angles. Considering the calibration data presented earlier in figures 11 and 12, two different types of flow behavior may be distinguished : (1) for $\frac{U_{i_2}}{U_{i_1}} \lesssim 0.2$, the flow moves in the +x direction, (2) for $\frac{U_{i_2}}{U_{i_1}} > 0.2$, the flow does not move in the +x direction. Thus, the present thermal tuft probe allows one to conclude when a measured flow is well behaved (i.e., when the flow moves directly from wire 1 to wire 2) and when it is not.

During compressor operation, when the flow is not well behaved near compressor blade surfaces, boundary layer separation, skewing and three dimensionality will be common features. Thus, quasi one dimensional flow reversals are not expected. Consequently, three wire thermal tuft designs may

not provide more information than the present design since they are designed for quasi one dimensional flow reversals where the direction of flow before and after reversal is in the plane of the wires and approximately perpendicular to the wires.

4.3 The thermal tuft crossed hot wire - Four wire sensors

A standard crossed hot wire probe suffers from the usual problem that the flow angle cannot be found uniquely. That is, for a given measurement, there will be four possible flow angles. Some of these can be removed by using a directional thermal tuft probe. Each of the single wires on a crossed hot wire are replaced by a pair of parallel hot wires. One wire is operated at an overheat ratio of 1.5 and the other at O.H.R. of 1.1. The signal differences can now be used to determine from which quadrant the flow is coming, thus determining which of the four possible flow angles is the correct one. This capability is particularly useful in rotating stall work where strong radial flows and flow reversals are expected when the stall cell passes (Fig. 13a, 13b).

The four wires are denominated as follows :

Wires	R_w (Hot)	OHR	$\frac{1}{2\pi\tau}$	Prongs
1	4.3 Ω	1.5	3980 Hz	short
2	3.0 Ω	1.1	1060 Hz	short
3	4.1 Ω	1.5	5305 Hz	long
4	2.9 Ω	1.1	1224 Hz	long

The response time was determined by the square wave test at 27 m/sec flow velocity.

The wires 1, 3 and 2, 4 are considered as normal crossed hot wire pairs (Fig. 14). The calibration curves for the four wires are shown in figures 15a and 15b where the upper curves are for the wires on the longer pronges. The ratio of the indicated velocities $\frac{U_{i_3}}{U_{i_1}}$ and the difference $\frac{U_{i_3}-U_{i_1}}{U_{actual}}$ in function of the yaw angle are the basic calibration curves (Figs. 15c, 15d).

The procedure for flow angle detection is as follows :

- The comparison of the indicated velocities U_{i_1} with U_{i_2} for one pair of wires and U_{i_3} with U_{i_4} for the other will determine from which quadrant the flow is coming (Fig. 16a).

- The crossed hot wire calibration curves are afterwards used to determine the yaw angle within the quadrant. However, this sensor has in principle a 360° resolution.

The dimensions do not allow to make a point measurement and an angular variation can be induced through velocity gradient existing over the separation height of the different wires. The error analysis of references 21, 22 and the pitch angle influence is also applicable here.

A small amount of yaw angle ambiguity will still exist for flows parallel with ±20° to one of the wires 1 or 3 (Fig. 16b). This is a consequence of the yaw angle response of a two parallel wire sensor (Fig. 12).

The application of such a sensor to a rotor blade became possible due to the availability of an 8 channel slip ring.

4.4 The thermal tuft probe - Triple wire sensor

This sensor allows the determination of separation and flow reversal in the chordwise direction.

The geometrical characteristics are similar to the two and four wire sensors. The central wire (3) is 1.7 mm longer and the distance between the wires is 0.8 mm (Figs. 17a, 17b).

Wire	R_w	OHR	$\frac{1}{2\pi\tau}$
1	3.0 Ω	1.1	1650 Hz
2	2.7	1.1	1990 Hz
3	3.8	1.5	4974 Hz

The response time was determined by the square wave test at 30 m/sec flow velocity.

The calibration curves (Fig. 18) indicate a non symmetrical behavior for the central wire (3) at yaw angles 0° (wire 1) and 180° (wire 2 upstream). This is caused by geometrical inaccuracies in wire mounting and alignment.

5. TEST CONDITIONS

5.1 Measurement chain

The measurement chain used for the compressor testing is shown schematically in figure 19. The signal is taken from the compressor rotor by means of a mercury slip ring, which was tested for noise from 2 Hz to 10000 Hz using a frequency analyser. No contributions from the slip ring were evident for the frequencies of interest in the tests. The slip ring was also included in the calibration measurement chain between the probe and the bridges. Figure 20 shows the hot wire thermal tuft probe in place on the compressor blade, while the slip ring assembly inside the compressor housing is shown in figure 21.

The 9 micron diameter hot wires on the thermal tuft were platinum plated tungsten with copper plating on the ends connected to the prong supports. The sensing length of the two wires was approximately 2.0 mm, and the spacing between them was 0.6 mm, as shown on figure 10. The frequency responses of the wires were lower with the mercury slip ring contained in the circuit than when direct connections were made to the bridges. With the slip ring in place, the hot wire with the 1.1 overheat ratio was found to have a response frequency of 1500 Hz, and the 1.6 overheat ratio wire responded at 4000 Hz. The two hot wire probes were driven by constant temperature bridges designed and constructed at the von Karman Institute.

From the bridges, the signals were passed through amplifiers and 2000 Hz low pass filters to an analog digital converter providing 12-bit signal resolution. This was followed by a multiplexer which allowed transmission of the data to a PDP 11/34 computer. For each run, 1024 data points were taken at a sampling rate of 3125 Hz and stored on floppy disks for processing using FORTRAN programs. These programs include digital filtering routines to further process data. In some cases to be discussed, low pass digital filtering at a cut off

frequency of 600 Hz was applied to the data. A plotter was also available with which plots of the reduced data were made.

The hot wire signals were linearized during computer processing using the relation between voltage, E, and velocity, U, given by

$$u = \left(\frac{E^2 - E_0^2}{B} \right)^{\frac{1}{n}}$$

The values of E_0, n and B were determined from calibration runs, and were found to provide an excellent fit to measurement points for the range of velocities encountered in the present tests. During calibration, the measurement chain included only the probe, the mercury slip ring and the bridges. Additional details of the measurement chain and the calibration procedure are discussed by Gyles et al. (Ref. 17). Figure 22 shows the equipment used in this study.

5.2 Probe location

The on-blade multi-wire sensors have been used at the mid-blade height, mid-chord position. The four wire sensor is positioned at 45° or the bisectrix parallel to the blade chord. The other sensors are positioned with the wires vertical.

The inlet crossed hot wire is located in a plane 7 mm ahead of the rotor blade leading edge, the downstream location was 20 mm with the possibility of radial exploration of the flow field.

5.3 Data reduction and analysis procedure

The data reduction and analysis consist of the application of the following procedures :

a. Calculation of the instantaneous velocity field (two components) using the crossed hot wire signals.

b. Ensemble averaging over a sample of 20 stall cells using a 12800 word sample size from which the periodic event is determined by a spectrum analysis.

c. Determination of low frequency and high frequency spectra using a 5.000 and 25.000 Hz sampling rate.

Spectra measurements

f_R frequency resolution

n number of samples in one acquisition

f_s sampling rate

f_{Ny} Nyquist folding frequency

T_{max} length of time of sample

f_L lowest frequency resolution possible

N number of samples required for ensemble averaging

SE statistical error

$$f_r = \frac{f_s}{2b} \qquad f_{Ny} = \frac{f_s}{2} \qquad f_L = \frac{1}{T_{max}}$$

$$T_{max} = \frac{n}{f_s} \qquad SE = \frac{1}{\sqrt{N}}$$

Case 1 - Low frequency spectra

f_s = 5000 hertz

n = 1024 pts

N = 10 samples

f_r = 2.44 Hz $\qquad f_{Ny}$ = 2500 hertz

f_L = 4.883 Hz $\qquad T_{max}$ = 0.205 seconds

SE = 0.316

Case 2 - High frequency spectra

f_s = 25000 hertz

n = 1024

N = 10 samples

f_R = 12.21 hertz $\qquad$ f_{N_y} = 12500 hertz

f_L = 24.41 hertz $\qquad$ T_{max} = 0.041 seconds

SE = 0.31

d. Determination of the autocorrelation

Autocorrelation measurements

$$R(\tau) = \frac{\overline{u'(t)\, u'(t+\tau)}}{\bar{u}'^2} = \text{autocorrelation}$$

$$\text{frequency spectra } \phi(\omega) = \frac{2}{\pi} \int_0^\infty \overline{u'(t)\, u'(t+\tau)} \cos\omega \, d$$

Comments :

- each value of $\overline{u'(t)\, u'(t+\tau)}$ represents the autocorrelation at a given value of τ for all time t

- all frequencies of a signal will contribute to the autocorrelation for a given τ

- autocorrelation measurements near the viscous sublayer were made by Kim, Kline & Reynolds (JFM, Vol. 50, Part 1, 1971, pp 133-160)

- the autocorrelation is a relevant quantity in highly turbulent flows where Taylor's hypothesis may break down or where intermittent structures exist

- the peaks in correlations measured in rotating stall are due to contributions due to the presence of rotating stall cells. Signal strongly correlates at the passage frequency of the rotating stall cells.

e. Averaging the spectra

Summary

N° of samples	Words per sample	Processing type	Filter (Hz)	Sampling rate (Hz)	Channels
2	12800	EN.AV	3125	6250	2
10	1024	L.S.	2000	5000	2
10	1024	H.S.	12500	25000	2
2	11264	A.C.	1562	3125	2

EN.AV. ensemble averaged

L.S. low frequency spectra

H.S. high frequency spectra

A.C. autocorrelation

6. EXPERIMENTAL RESULTS

The performance map of figure 5 is studied for the following operating points

- unstalled or clean flow (US, CL)
- 10 cell part-span stall zone A, S1 (STALL 1) condition
- 1 cell full-span stall zone B, S2 (STALL 2) condition
- 2 cell full-span stall zone C, S3 (STALL 3) condition

The observations in the absolute motion are shortly summarized, the main effort of this study being the on-blade measurements.

6.1 Absolute motion

The absolute flow field has been intensively studied by Ktenidis, Casalini, Muzzu, Asturaro and Mathioudakis (Ref. 7).

Stall inception occurs at maximum Ψ_0 when bursts of separated flow are observed in the downstream flow field.

A periodic phenomenon established itself in zone A and is called S1. It is a part-span stall at the tip region and consists of a 10 cell structure, the absolute flow vector changes by +10° in direction and +30% in magnitude from the clean flow condition to the stall cell (Fig. 23). The relative inlet flow has an increased incidence by +5°. At the hub radius, no rotor blade incidence change is observed.

Further throttling does not provide a periodic flow phenomenon between A and B in figure 5. Occasionally, the operating point would be kept in between A and B long enough to gather data for a fast Fourier analysis. A small increase in RPM (+3%) is noticed when point B is established. This stall structure S2 consists of one large cell. This configuration has been extensively studied by other authors and a few

characteristic flow fields are shown in figure 24. The return flow at the tip radius is clearly seen and the velocity in the cell approaches the rotor speed.

The operating condition C shows the stall configuration S3 with a two cell structure. The detailed investigation for this condition is in progress.

Operating condition	Stall code	N° cells	Freq. Hz	Propagation % U
0	US,CL	-	-	-
A	S1	10	97	58.2%
B	S2	1	5.2	31.2%
C	S3	2	10.9	32.7%

6.2 On-blade measurements

For the present series of measurements, the thermal tuft probes were fixed to a rotor blade as indicated in the sensor description section at the mid-chord, mid-height position.

The two wire sensor was successful in the determination of the local velocity, velocity fluctuations and separation detection.

The four wire probe has been used but suffered during the application of strong interferences between prongs and wires, while at the same time some problems developed in two channels of the slip ring assembly. Indication has been obtained of strong radial flows during the stall cell passage.

The three wire sensor did not perform as was expected from a one dimensional calibration. The probe provided no more information than the two wire sensor. The central wire,

used for the velocity determination, suffered from the presence of the upstream wire and flow reversals in a simple 0° → 180° manner probably do not occur in the phenomenon being investigated.

(a) The two wire sensor - single stall cell

The flow behavior at the measuring station during the presence of a single stall cell is described using the velocity indication from the two wires.

Figures 24 through 26 show representative examples of the data which has been taken in the presence of a rotating stall. Figure 24 is the velocity seen by the upstream wire, while figure 25 is the velocity seen by the downstream wire during the same events. In figure 26, the ratio of these two wire velocities is shown to indicate distinct regions where the flow moves in the nominal direction and regions where the flow does not. One can see that the flow velocity appears to change magnitude and direction in some way as the blade passes into the stall cell. This is evident since the indicated velocity ratio jumps from its nominal value of 0.2 to values on the order of 0.6. The change in flow behavior near the hot wire resulting from stall cell passage occurs in the reference frame relative to the blade at a frequency of 11.9 Hz, or at 4.8 Hz in the absolute frame of reference.

In figures 27, 28 and 29, the data seen before in figures 24, 25 and 26 is shown after being digitally filtered with a 600 Hz low pass filter. Since the passage of the inlet guide vane blade wakes occur at around 650 Hz, most of the fluctuations due to the upstream blade wake passage have been filtered out. Lower frequency events thus become more evident, and the effect of the rotating stall cell, or the velocity ratio is more obvious. Three different flow regions can be defined, the locations of which are indicated on figures 24-29. In region I, the flow moves in the nominal +x flow direction

and $\frac{U_{i_2}}{U_{i_1}} \lesssim 0.2$. In regions II and III, the flow does not move in the +x direction, and higher values of $\frac{U_{i_2}}{U_{i_1}}$ exist then for for region I. Region III is different from region II because of the distinct and repeatable velocity peak which appears there, as opposed to the more random velocity fluctuations appearing in region II. The flow behavior in regions II and III is believed to be a consequence of a stall cell passage, and region III shows characteristics similar to those observed by McCroskey et al. (Ref. 23) during vortex shedding occurring during the dynamic stall of oscillating airfoils.

In region I, where the flow moves in the nominal direction, the velocity ratio varies from 0.15 to greater than 0.2 as the stall cell disturbance approaches. Since the velocity ratio increases and the velocity decreases, from inspection of the calibration data one can say that the yaw angle is increasing and/or the pitch angle is increasing. This conclusion seems reasonable, since the yaw angle would be expected to increase due to centrifugal forces which have a larger influence as the flow velocity decreases. When the instrumented blade enters region I, an abrupt decrease in the velocity ratio is seen to occur. This is followed later by an equally abrupt increase in velocity ratio as the blade passes into the disturbed flow of region III.

In regions II and III, where the stall cell is believed to be passing, the velocity ratio appears to be more constant than in the well ordered flow region and fluctuates between 0.5 and 0.65. As expected, the velocity ratios never reach values which would indicate a quasi one dimensional flow reversal. The lower indicated velocity ratios in these regions may then be the consequence of three dimensional separation and flow reversals. Increased turbulent diffusion resulting in reduced temperature differences in the thermal wakes from

the hot wires may also partially account for the lower ratios. An additional observation which can be made from the qualification tests is that the velocity ratio becomes much less sensitive to changes in both velocity and yaw angle when the flow is reversed. Such a decrease in sensitivity for reversed flow could be one reason why large changes in velocity ratio are not seen in the stall cell even though large velocity and yaw angle fluctuations may be occurring.

The present measurements show qualitative similarity to the measurements of McCroskey et al. (Ref. 23), taken on an oscillating airfoil undergoing dynamic stall. The $x/c = 0.54$ trace of figure 6 shows a large region of well behaved flow for $1.2\pi \lesssim \omega t \lesssim 2.3\pi$ which corresponds to region AB for the upstream wire velocity trace on figure 27. In both situations the magnitude of the velocity decreases with time. Point B on figure 27 then seems to be analogous to what McCroskey calls "onset of flow reversal at a distinct minimum". The velocity peak at C in figure 27 appears to have a character which is closely similar to a velocity peak occurring due to vortex shedding on the oscillating airfoil. The peaks can be seen to occur in the measurements of dynamic stall just after the points of flow reversal labelled "R" in figure 6. Regions of low velocity DE then follow in figure 27 and the cycle then repeats itself in much the same way as for the measurements shown in figure 6. Such agreement supports the idea that the behavior of flow near compressor blades passing through a rotating stall cell may be similar to fluid behavior near the suction surface of a single oscillating airfoil undergoing dynamic stall.

(b) Power spectra, auto-correlation, average and fluctuating velocity components

The signals from the hot wire sensor were analysed for the clean flow (CL) or unstalled (US) condition, the 10 cell configuration (S1), the single cell (S2) and the two cell (S3) rotating stall patterns.

The analysis is carried out on a large sample of the signal (i.e., 11.264 words). The signals of wire 1, the hot wire with OHR of 1.5, are filtered by low pass filters of 1562 Hz and 125 Hz. The signal of wire 2 is only used to calculate the indicated velocity U_{i_2} which is needed for the detection of separated flow. This principle is applicable for the two, three and four wire sensor. The detection of separated flow during stall is treated in references 22 and 23.

The unstalled flow condition : the power spectra (Fig. 30) and autocorrelation (Fig. 31) as obtained from wire 1 do not show any particular feature. The inlet guide vane wakes at 645 Hz are not shown in this analysis. The filter setting for the data for the low frequency power spectra is 2000 Hz and sampling rate at 5000 Hz.

Condition S1 or a 10 cell part span rotating stall: The part span stall, as observed in the absolute motion, renders it difficult to make any conclusions on the flow behavior at the mid-blade height and mid-chord position and to obtain a perfect synchronous phenomenon with figure 23a which is at tip radius. The indicated velocities from the wire are presented in figure 32. The autocorrelation in figure 33 does not show a pronounced feature at τ = 14 m/sec which corresponds to the 10 cell passage in the relative frame with its oscillatory flow fluctuation at the tip section.

Condition S2 or a 1 cell full span rotating stall cell: Large indicated velocity fluctuations are observed for the single and two cell structure (Fig. 34). The power spectra show clearly the single cell at 11.5 Hz and the harmonics (Fig. 35). Figure 36 indicates a strong correlation at τ = 87 m/sec which is the cell period in the relative frame and a strong negative correlation at 28% and 71% of τ = 87 m/sec Opposite velocity fluctuations do occur at these time intervals. The flow stalls, reverses and returns to the original direction during the unstalled period of the cycle. It seems to be very

difficult for the flow to achieve complete restoration in the case of large stall cells. The recovery takes longer than simply the ratio stalled/unstalled percentage of the circumference.

Condition S3 or the double cell full span rotating stall cell: The double frequency is already described in figure 37 when comparing to figure 34. The power spectra (Fig. 38) show the frequency of 22.4 Hz for the two cells and the harmonics. Strong correlation is again obtained for τ = 45 m/sec or the passage frequency of each cell. Within this time interval, strong negative correlation is seen at 30% and 70% of 45 m/sec (Fig. 39).

The high frequency power spectra of figure 40 are obtained from a different set of large samples of wire signals with the filter setting at 12500 Hz and sampling rate of 25000 Hz. The power spectra for the three rotating stall cell structures are presented, i.e., S1, S2 and S3.

The averaged velocities and fluctuating component are determined from a sample of 30 stall cells

$$\bar{u} = \frac{\sum_{i=1}^{n} U_i}{n}$$

$$U_{RMS} = \sqrt{\frac{\sum_{i=1}^{n} (U_i - \bar{U})^2}{n-1}}$$

The three rotating stall conditions S1, S2, S3 are shown in figures 41, 42 and 43. The indicated velocity U_i over a time interval of 200 m/sec is presented together with the averaged velocity $\bar{U}$ over 30 stall events, $\sqrt{u'^2}$ the

averaged fluctuating component and $u'^2/\bar{u}^2$.

The high level of fluctuations over the total time interval is observed for the S1 stall condition, the recovery to the clean flow velocity level or at least an attempt to it is not observed. The velocity level of 5.5 m/sec is too low for a relative inlet velocity to the rotor blade of 29.9 m/sec. A permanent separated flow can cause this condition. The low indicated velocity (5.5 m/sec) can also be caused by a radial flow along the blade surface which is in the low sensitivity region of the multi-wire sensor.

The S2 or single stall condition does exhibit large variation of the mean velocity and the fluctuating components during a stall cycle (Fig. 42). The same observations can be made for the S3 or double cell stall condition of figure 43.

7. CONCLUSIONS

The thermal tuft technique is applicable to blade surface velocity measurements and detection of flow separation.

The three types of sensors: double, triple and quadruple wire sensors, developed in this program showed a variable rate of success.

The triple wire did not yield more information than the two wire sensor and therefore did not fulfill the expectations of flow reversal detection similar to applications in two dimensional configurations.

The strong three dimensional flow nature in turbomachines during the stall event made that all measurements and conclusions had to be made on the indicated velocity, namely, the component normal to the wire sensor.

The quadruple wire probe has been applied to the rotor blade. Different problems made it impossible to draw any valid conclusions upon the success of such a sensor.

The quasi sinusoidal change of the inlet flow at the S1 condition does not show up in the on-blade measurements. A very weak correlation occurs at τ = 14 m/sec. The relative angle changes are of the order of 1°5 and the velocity changes are 4%, probably insufficient to cause a strong effect at the central location of the blade.

The blades undergo a dynamic stall at the beginning of the cell, higher energy levels are observed at all frequencies where three harmonics of the stall cell passage are visible in the power spectra.

A strong correlation exists between the stall cells (S2, S3) with a high negative correlation of events within the stall cell at 30% and 70% of the cell.

The fluctuating components of the velocities are large compared to the average velocity level. Important variations do occur for the S2 and S3 stall condition.

A new insight has been given into the detailed flow on the blade surface of a compressor rotor blade during three types of rotating stall using different sensors and analysis methods. This approach has cleared up some phenomena, has generated further questions and will help in an improved mode··zation of the rotating stall phenomenon.

REFERENCES

1. BAUER, A.B.: Direct measurement of velocity by hot wire anemometry.
   AIAA Journal, Vol. 3, No. 6, 1965, pp 1189-1191.

2. BRADBURY, L.J.S.: A pulsed wire technique for velocity measurements in highly turbulent flows.
   NPL Aero Report 1284, 1969.

3. BRADBURY, L.J.S.: Measurements with a pulsed wire and a hot wire anemometer in the highly turbulent wake of a normal flat plate.
   J. of Fluid Mechanics, Vol. 77, Part 3, 1976, pp 473-497.

4. BRADBURY, L.J.S.: Reverse flow sensing shrouded hot wire anemometer for use in highly turbulent flows.
   Euromech Conference 132 : Hot Wire, Hot Film Anemometry and Conditional Measurements, Ecole Centrale de Lyon, France, July 2-4, 1980.

5. BRADBURY, L.J.S. & CASTRO, I.P.: A pulsed wire technique for velocity measurements in highly turbulent flows.
   J. of Fluid Mechanics, Vol. 49, Part 4, 1971, pp 567-691.

6. CARR, L.W. & McCROSKEY, W.T.: A directionally sensitive hot wire probe for detection of flow reversal in highly unsteady flows.
   ICIASF Record, 1979, pp 154-162.

7. CASALINI, F. & BREUGELMANS, F.A.E.: Rotating stall in axial flow compressors.
   VKI PR 1979-3.

8. COOK, N.J. & REDFEARN, D.: The calibration and use of a hot wire probe for highly turbulent and reversing flows.
   J. Ind. Aerodynamics, Vol. 1, No. 3, 1976, pp 221-231.

9. COSSAR, B.F.J.; MOFFATT, W.C.; PEACOCK, R.E.: Compressor rotating stall in uniform and non-uniform flow.
   Transact. ASME, Series A : J. Engineering for Power, Vol. 102, No. 4, Oct. 1980, pp 762-769.

10. DAY, I.J. & CUMPSTY, N.A.: The measurements and interpretation of flow within rotating stall cells in axial compressors.
    University of Cambridge, CUED/A-Turbo/TR 90, 1977.

11. DAY, I.J.; GREITZER, E.M.; CUMPSTY, N.A.: Prediction of compressor performance in rotating stall.
Transact. ASME, Series A : J. Engineering for Power, Vol. 100, No. 1, 1978, pp 1-14.

12. DOWNING, P.M.: Reverse flow sensing hot wire anemometer.
J. Sci. Instruments, Vol. 5, No. 9, 1972, pp 849-851.

13. EATON, J.K.; JEANS, A.H.; ASHJAEE, J.; JOHNSTON, J.P.: A wall-flow-direction probe for use in separating and reattaching flows.
Transact. ASME, Series I : J. Fluids Engineering, Vol. 101, No. 3, 1979, pp 364-366.

14. EMMONS, H.W.; KRONAUER, R.E.; ROCKETT, J.A.: A survey of stall propagation experiment and theory.
Transact. ASME, Series D : J. Basic Engineering, Vol. 71, 1959, pp 409-416.

15. GREITZER, E.M.: Review - axial compressor stall phenomena.
Transact. ASME, Series I : J. Fluids Engineering, Vol. 102, No. 2, 1980, pp 134-151.

16. GÜNKEL, A.A.; PATEL, R.P.; WEBER, M.E.: A shielded hot wire probe for highly turbulent flows and rapidly reversing flows.
Ind. Eng. Chem. Fundam., Vol. 10, No. 4, 1971, pp 627-631.

17. GYLES, B.R.; LIGRANI, P.M.; BREUGELMANS, F.A.E.: Boundary layer separation on low speed compressor bladings.
VKI PR 1980-22.

18. HORSTMAN, C.C. & OWEN, F.K.: New diagnostic techniques for the study of turbulent boundary layer separation.
AIAA Journal, Vol. 12, No. 10, 1974, pp 1436-1438.

19. IURA, T. & RANNIE, W.D.: Experimental investigations of propagating stall in axial flow compressors.
Trnasact. ASME, Vol. 76, No. 3, 1954, pp 463-471.

20. JOHNSON, W; & HAM, N.D.: On the mechanism of dynamic stall.
J. of the American Helicopter Society, Vol. 17, No. 4, 1972, pp 36-45.

21. KOVASZNAY, L.S.G.: Hot wire investigation of the wake behind cylinders at low Reynolds number.
Proc. Roy. Soc., A198, No. 1053, pp 174-190.

22. LIGRANI, P.M.; GYLES, B.R.; BREUGELMANS, F.A.E.: A hot wire probe for measurement of flow near the surface of a compressor blade.
Euromech Conference 132 : Hot Wire, Hot Film Anemometry and Conditional Measurements, Ecole Centrale de Lyon, France, July 2-4, 1980.

23. McCROSKEY, W.J.; CARR, L.W.; McALISTER, K.W.: Dynamic stall experiments on oscillating airfoils.
AIAA Journal, Vol. 14, No. 1, 1976, pp 57-63.

24. MOON, I.M.: Direction sensitive hot wire anemometer for two dimensional flow study near a wall.
ASME Symposium on Measurement in Unsteady Flow, 1962, pp 71-75.

25. RUBESIN, M.W.; OKUNO, A.; MATEER, G.G.; BROSH, A.: A hot wire surface gage for skin friction and separation detection measurements.
NASA TM-X 62 465, 1975.

26. SEXTON, M.R.; O'BRIEN, W.F.; MOSES, H.L.: An on-rotor investigation of rotating stall in an axial flow compressor.
in Unsteady Phenomena in Turbomachinery, AGARD CP 177, 1975, Paper 33.

27. SOVRAN, G.: The measured and visualized behaviour of rotating stall in an axial flow compressor and in a two dimensional cascade.
Transact. ASME, Series A : J. Engineering for Power, Vol. 81, No. 1, 1959, pp 24-34.

28. TOMBACH, I.H.: Velocity measurements with a new probe in inhomogeneous turbulent jets.
Ph.D. Thesis, California Institute of Technology, Pasadena, California, 1969.

29. WESTPHAL, R.V.; EATON, J.K.; JOHNSTON, J.P.: A new probe for measurement of velocity and wall shear stress in unsteady, reversing flow.
Transact. ASME, Series I : J. Fluids Engineering, Vol. 103, No. 3, Sept. 1981, pp 478-482.

30. McALISTER, K.W. & CARR, L.W.: Water tunnel visualizations of dynamic stall.
Transact. ASME, Series I : J. Fluids Engineering, Vol. 101, No. 3, Sept. 1979, pp 376-380.

31. EVANS, R.L.: Turbulence and unsteadiness measurements downstream of a moving blade row.
Transact. ASME, Series A : J. Engineering for Power, Vol. 97, No. 1, 1975, pp 131-139.

32. EVANS, R.L.: Boundary layer development on an axial-flow compressor blade.
Transact. ASME, Series A : J. Engineering for Power, Vol. 100, No. 2, 1978, pp 287-293.

33. GREITZER, E.M. et al.: A fundamental criterion for the application of rotor casing treatment.
Transact. ASME, Series I : J. Fluids Engineering, Vol. 101, No. 2, 1979, pp 237-243.

34. DE PONTE, S. & BARON, A.: Experiments on a turbulent unsteady boundary layer with separation.
in Boundary Layer Effects on Unsteady Airloads, AGARD CP 296, 1980, Paper 12.

35. CARTA, F.O. et al.: Determination of airfoil and rotor blade dynamic stall response.
J. Amer. Helicopter Soc., Vol. 18, No. 2, 1973, pp 31-39.

36. McCROSKEY, W.T. & FISHER, R.K.: Detailed aerodynamic measurements on a model rotor in the blade stall regime.
J. Amer. Helicopter Soc., Vol. 17, No. 1, 1972, pp 20-30.

37. MARTIN, J.M. et al.: An experimental analysis of dynamic stall on an oscillating airfoil.
J. Amer. Helicopter Soc., Vol. 19, No. 1, 1974, pp 26-32.

38. BEDDOES, T.S.: A qualitative discussion of dynamic stall.
in Special Course on Unsteady Aerodynamics, AGARD R 679, 1980, Paper 3.

39. McCROSKEY, W.J.: Prediction of unsteady separated flows on oscillating airfoils,
in Three Dimensional and Unsteady Separation at High Reynolds Numbers,
AGARD LS 94, 1978, Paper 12.

40. CARLSON, R.G. et al.: Dynamic stall modeling and correlation with experimental data on airfoils and rotors,
in Rotorcraft Dynamics,
NASA SP 352, 1974, pp 13-23.

41. DUNHAM, J.: Observations of stall cells in a single stage compressor.
ARC CP 589, 1961.

42. COSTILOW, F.L. & HUPPERT, M.C.: Rotating stall characteristics of a rotor with high hub-tip radius ratio.
NACA TN 3518, 1955.

43. EMMONS, H.W.; PEARSON, C.E.; GRANT, H.P.: Compressor surge and stall propagation.
Transact. ASME, Vol. 77, 1955, pp 455-469.

44. TANAKA, S. & MURATA, S.: On the partial flow rate performance of axial-flow compressor and rotating stall (First report, Influences of Hub-Tip Ratio and Stators),
Bull. JSME, Vol. 18, No. 117, 1975, pp 256-263.

45. KRIEBEL, A.R.; SEIDEL, B.S.; SCHWIND, R.G.: Stall propagation in a cascade of airfoils.
NASA TR R 61, 1960.

46. STENNING, A.H. & KRIEBEL, A.R.: Stall propagation in a cascade of airfoils.
Transact. ASME, Vol. 80, 1958, pp 777.

47. FABRI, J.: Rotating stall in axial flow compressors.
in Internal Aerodynamics (Turbomachinery),
Symposium on Turbomachinery, Cambridge, 1957.
Published by I. Mech. Engrs., 1970.

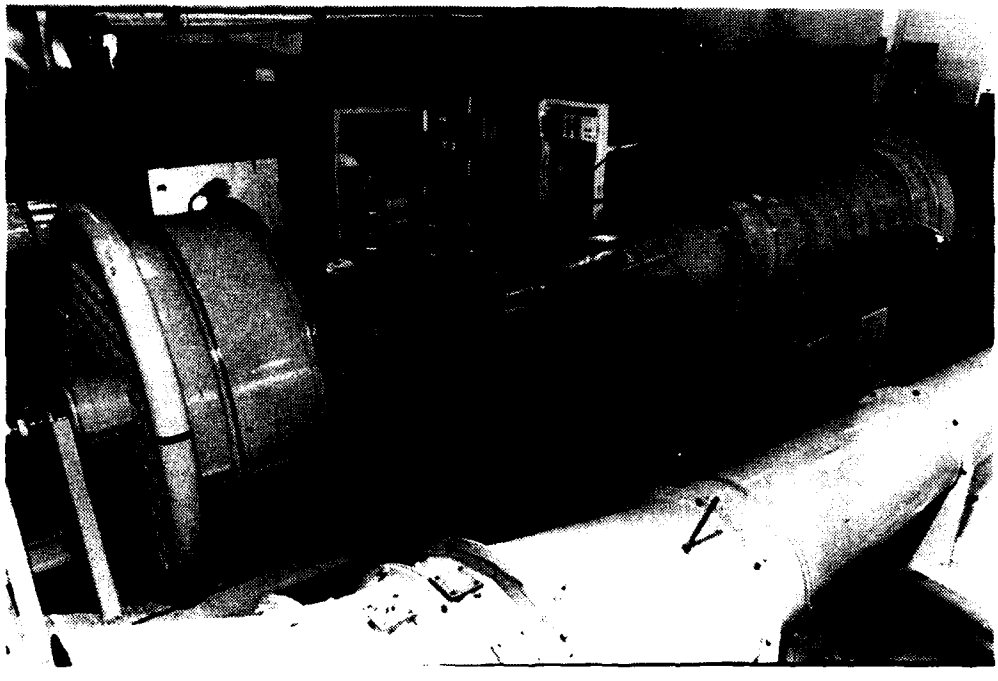

FIG. 1 - R-1 FACILITY

FIG. 2 - ROTOR ASSEMBLY

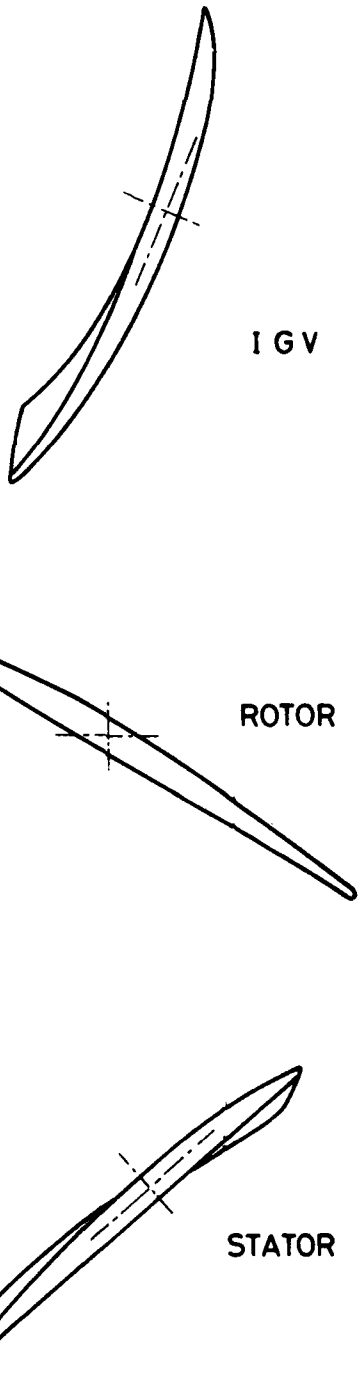

FIG. 3 - BLADING.

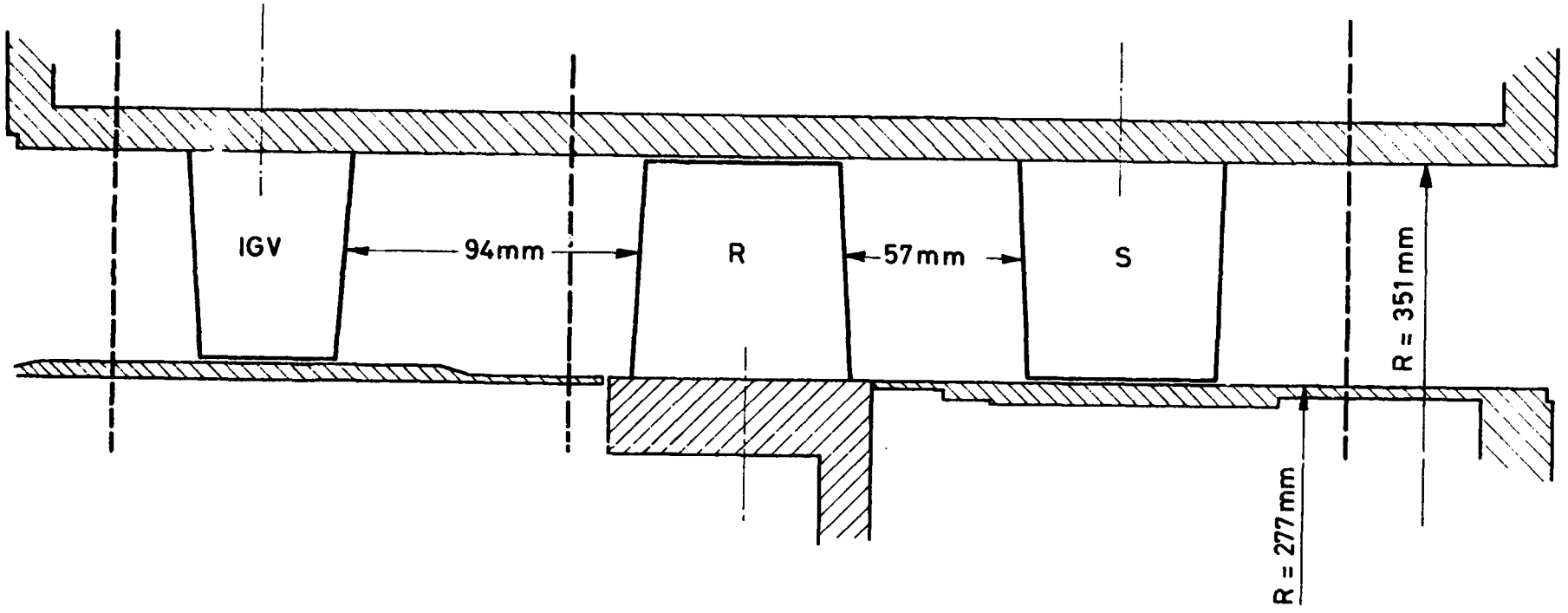

FIG. 4 - TEST SECTION

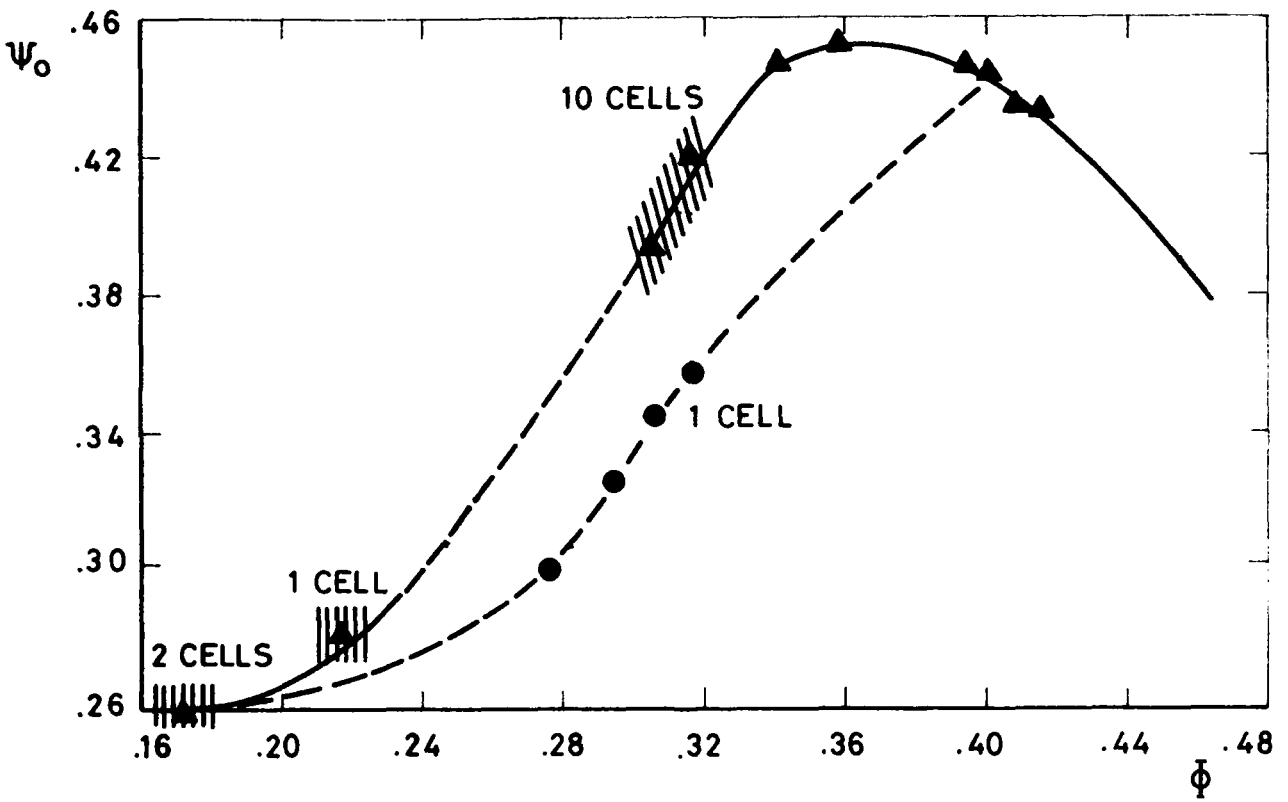

FIG. 5 - STAGE CHARACTERISTIC

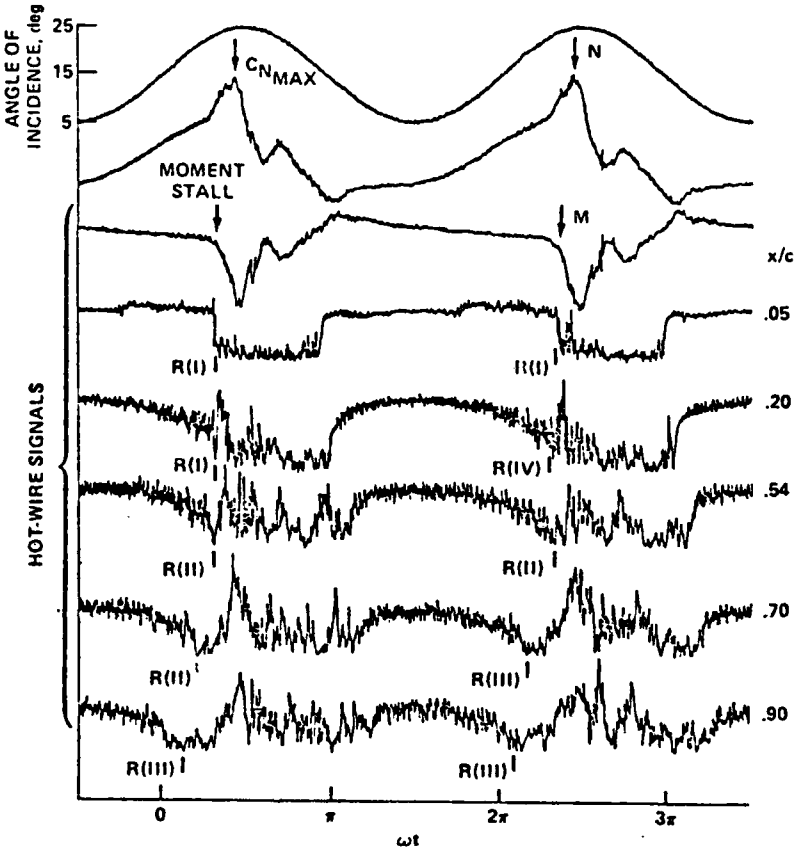

FIG. 6 - TYPICAL VELOCITY FLUCTUATIONS ON SUCTION SURFACE OF AN OSCILLATING AIRFOIL DURING DYNAMIC STALL from Mc CROSKEY et al. (1976)

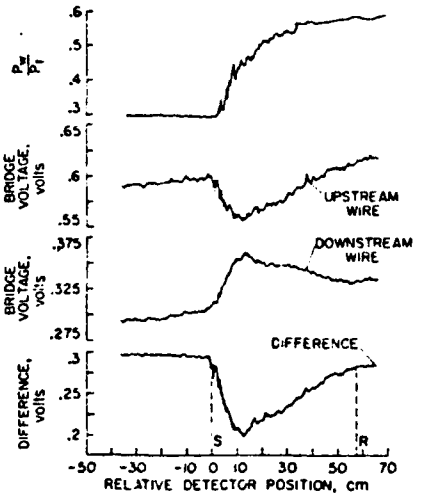

FIG. 7 - RESPONSE OF SEPARATION DETECTOR TO SHOCK WAVE TRAVERSE RUBESIN et al. (1975)

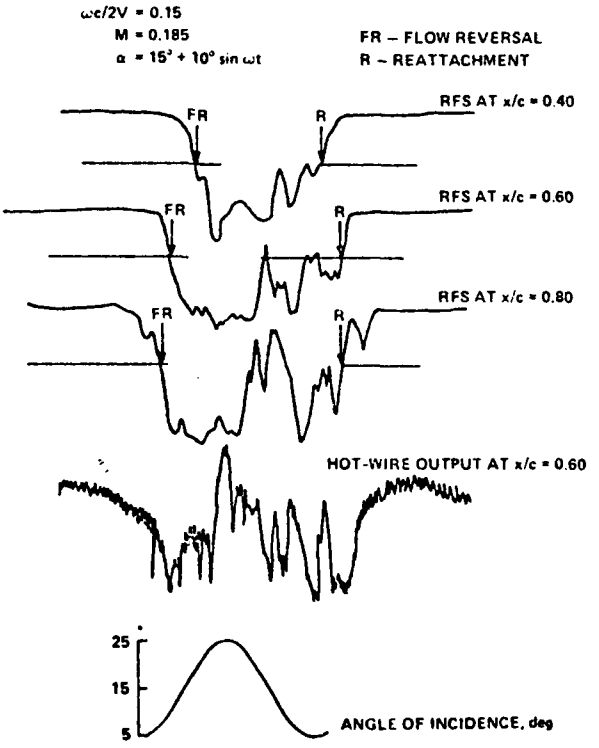

FIG. 8 - PROGRESSION OF FLOW REVERSAL UP AIRFOIL DURING DYNAMIC STALL CARR et al. (1979).

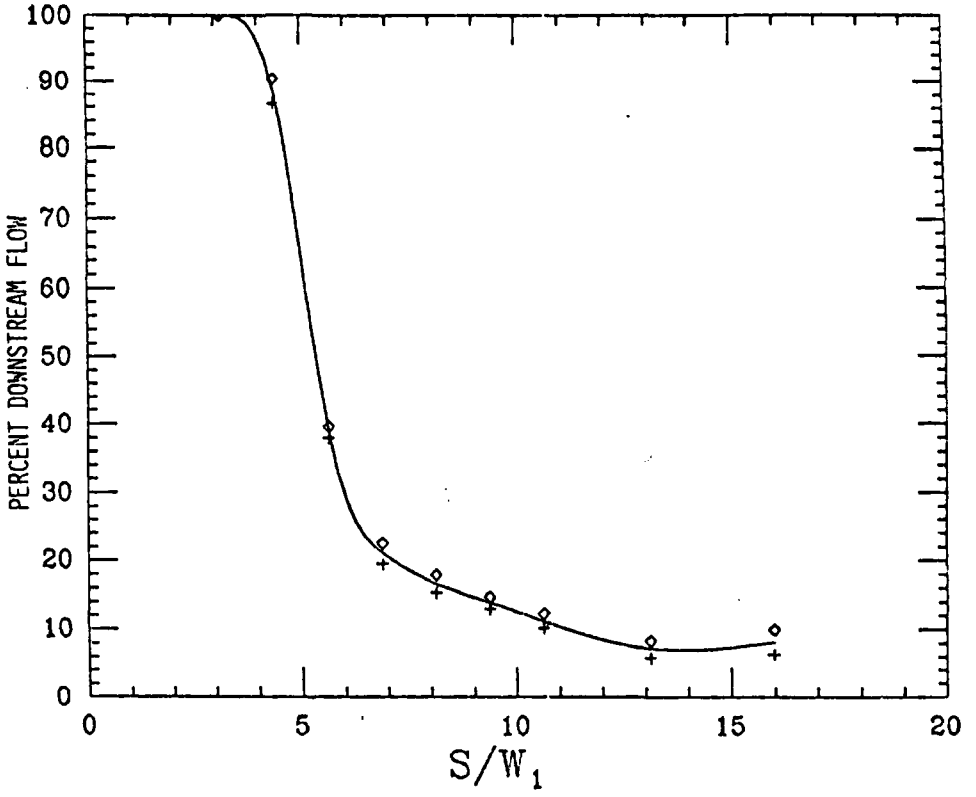

FIG. 9 - SEPARATING FLOW DATA DETERMINED USING THE THERMAL TUFT PROBE EATON et al. (1979).

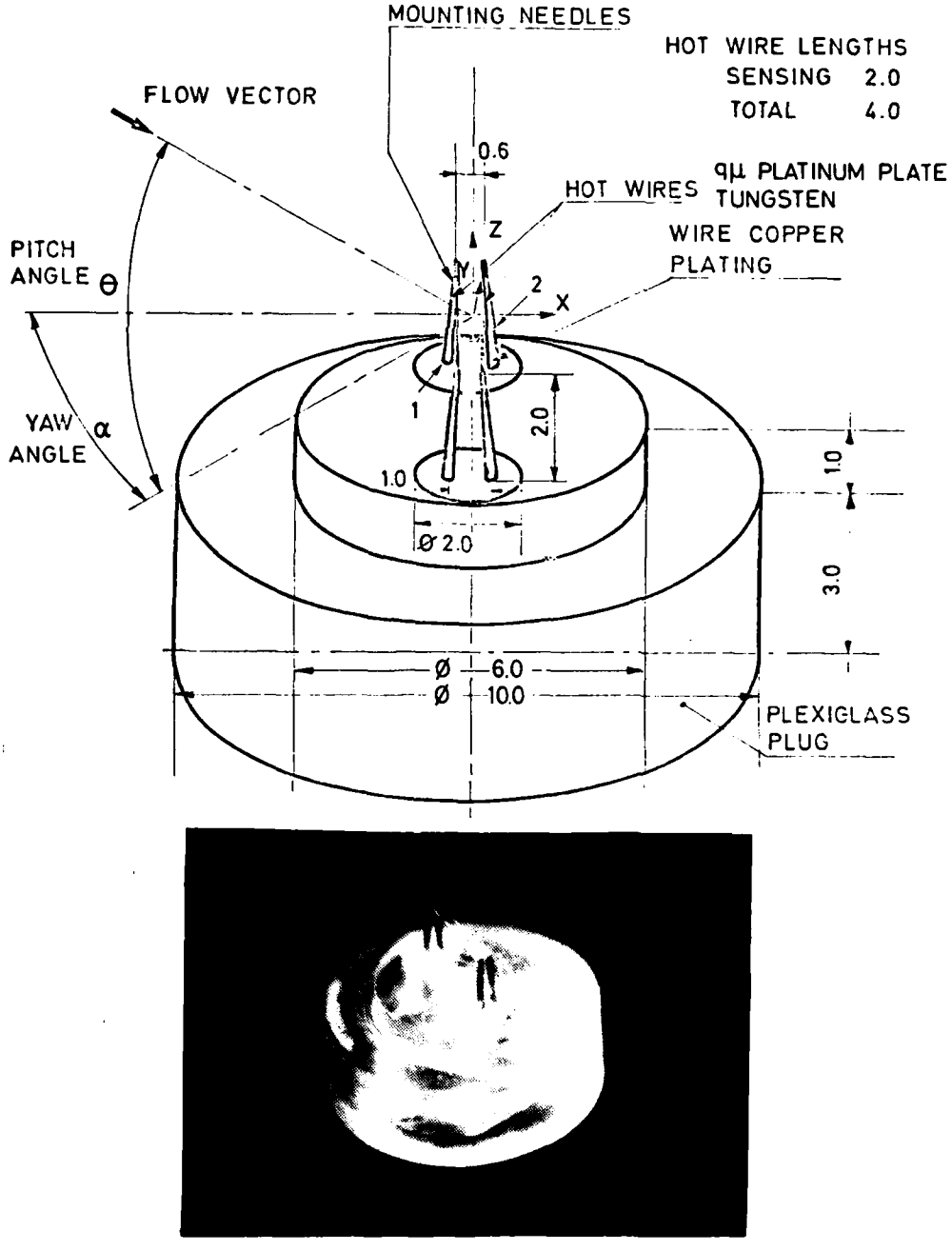

FIG. 10 - SCHEMATIC OF HOT WIRE PROBE AND PLUG FOR MOUNTING.

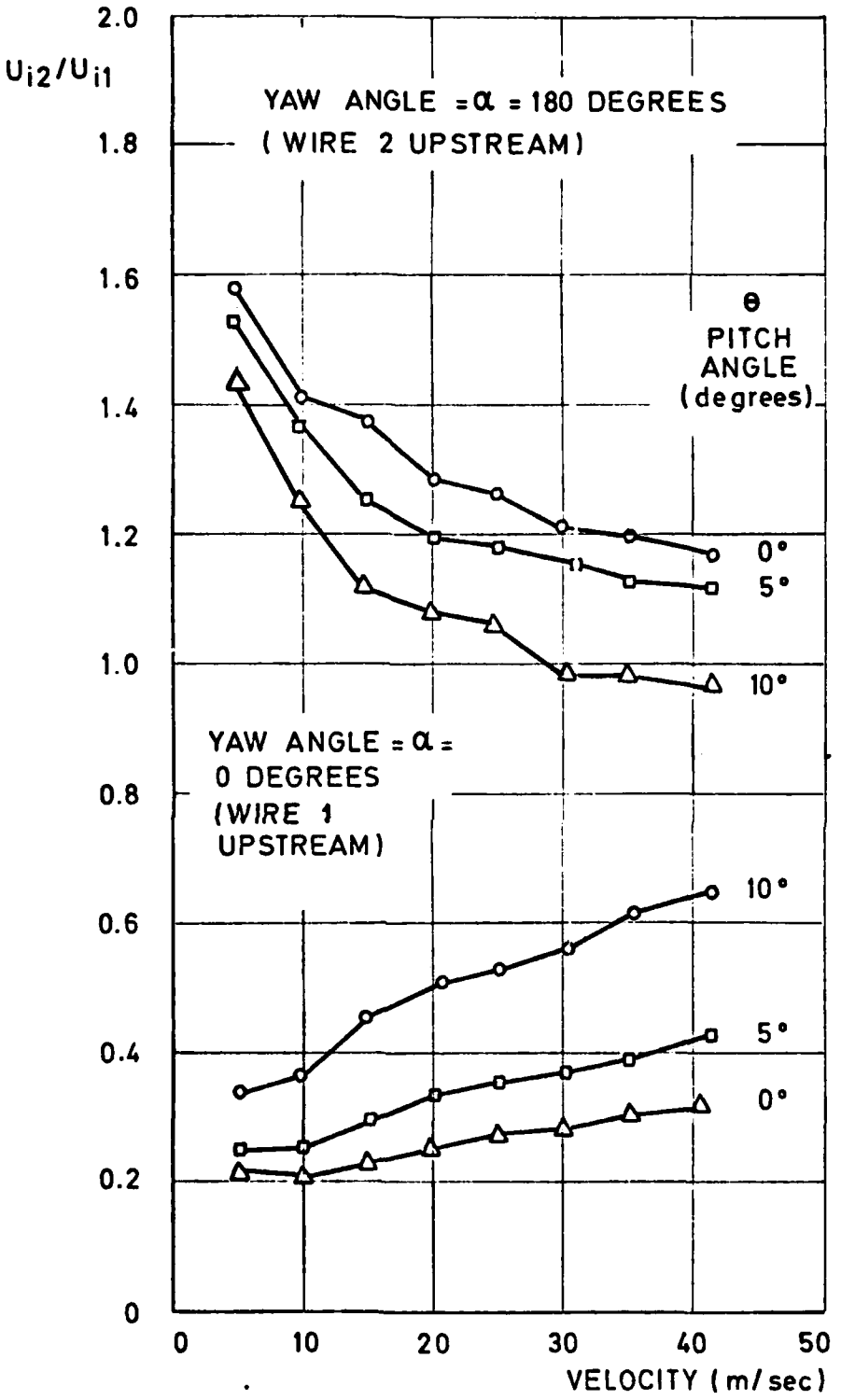

FIG. 11 - TYPICAL HOT-WIRE THERMAL TUFT CALIBRATION FOR VARIABLE VELOCITY AND VARIABLE PITCH ANGLE AT CONSTANT YAW ANGLE.

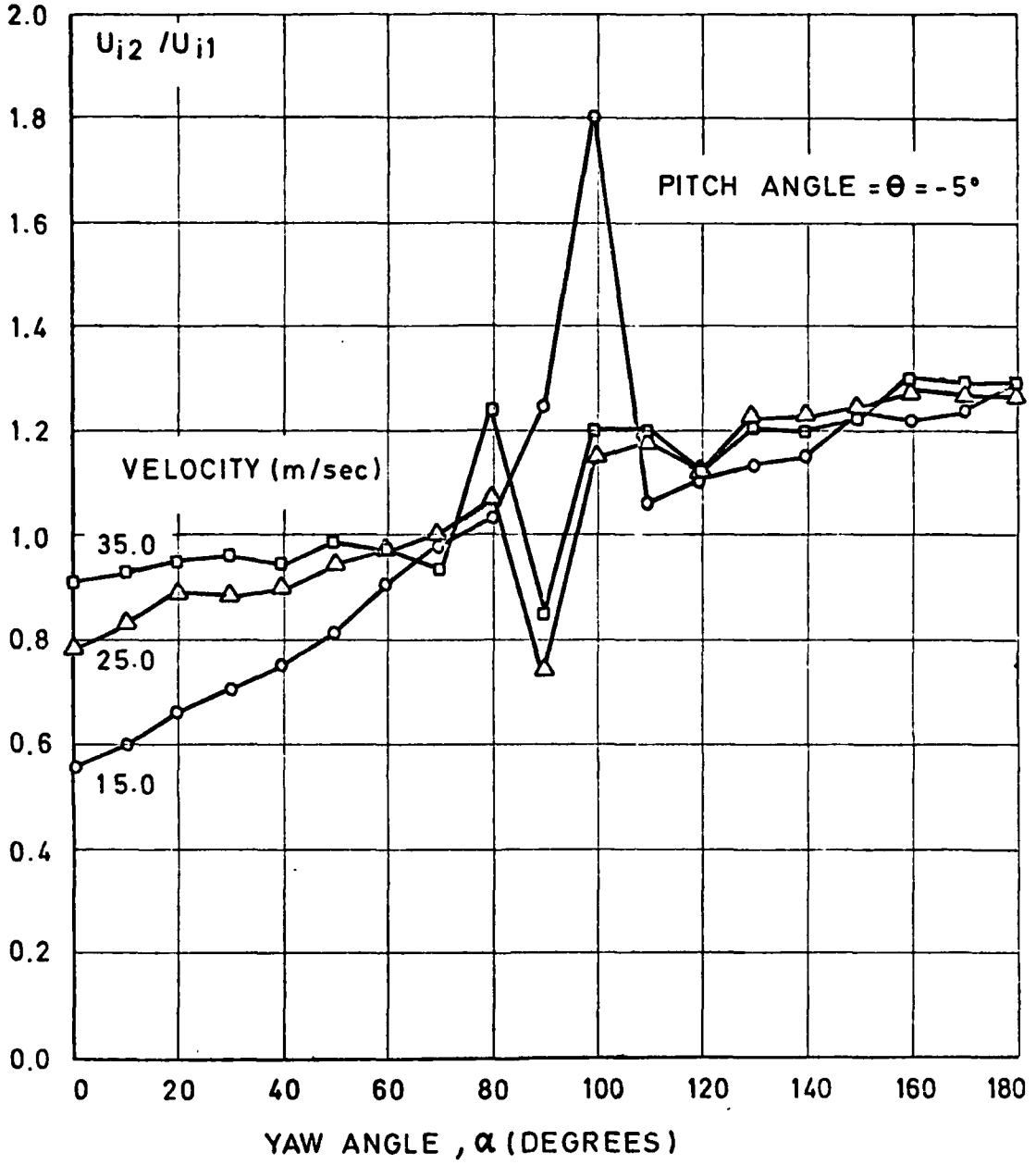

FIG. 12 - TYPICAL HOT-WIRE THERMAL TUFT CALIBRATION FOR VARIABLE YAW ANGLE AT CONSTANT VELOCITY AND CONSTANT PITCH ANGLE.

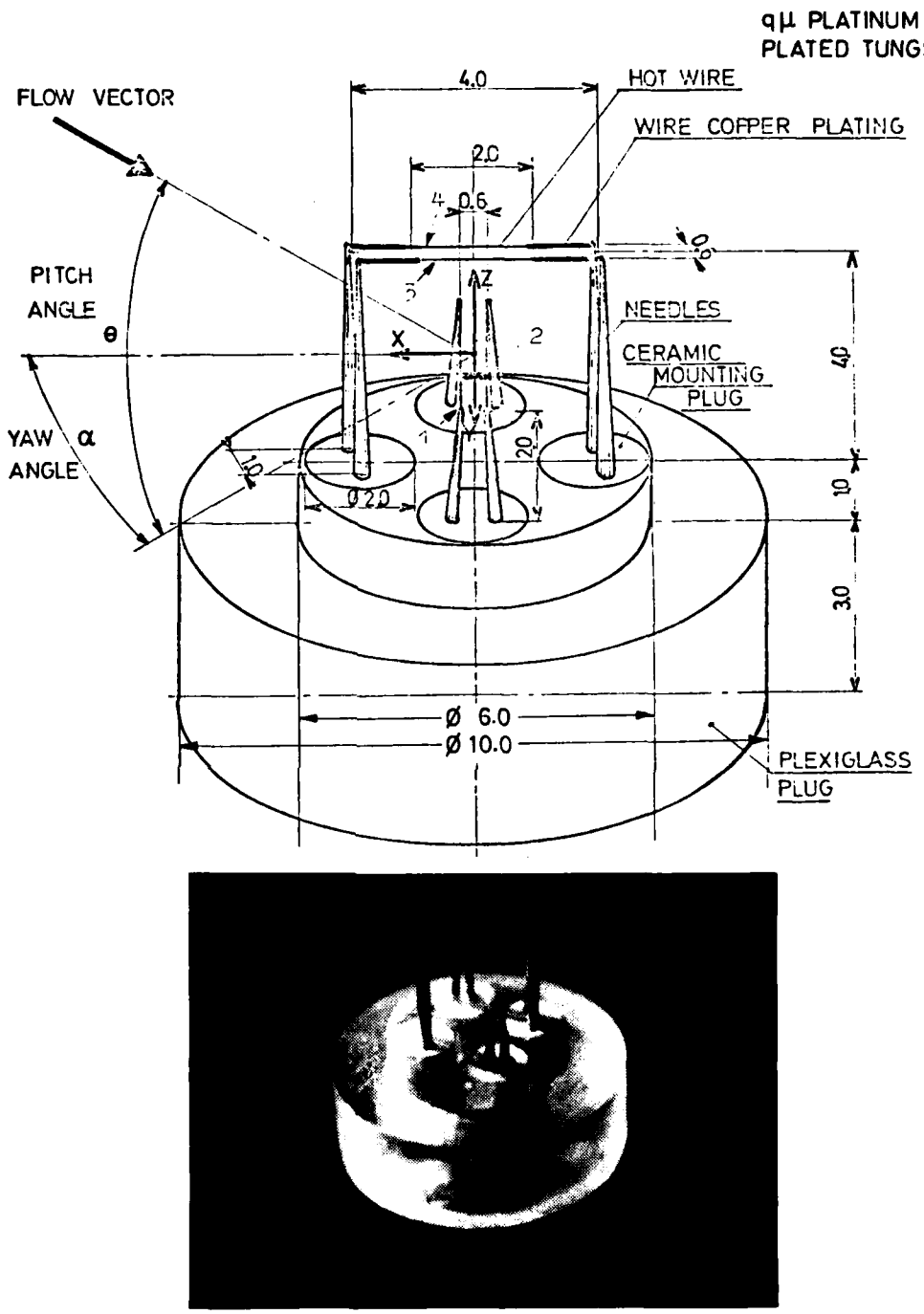

FIG. 13 - SCHEMATIC OF HOT WIRE PROBE AND PLUG FOR MOUNTING.

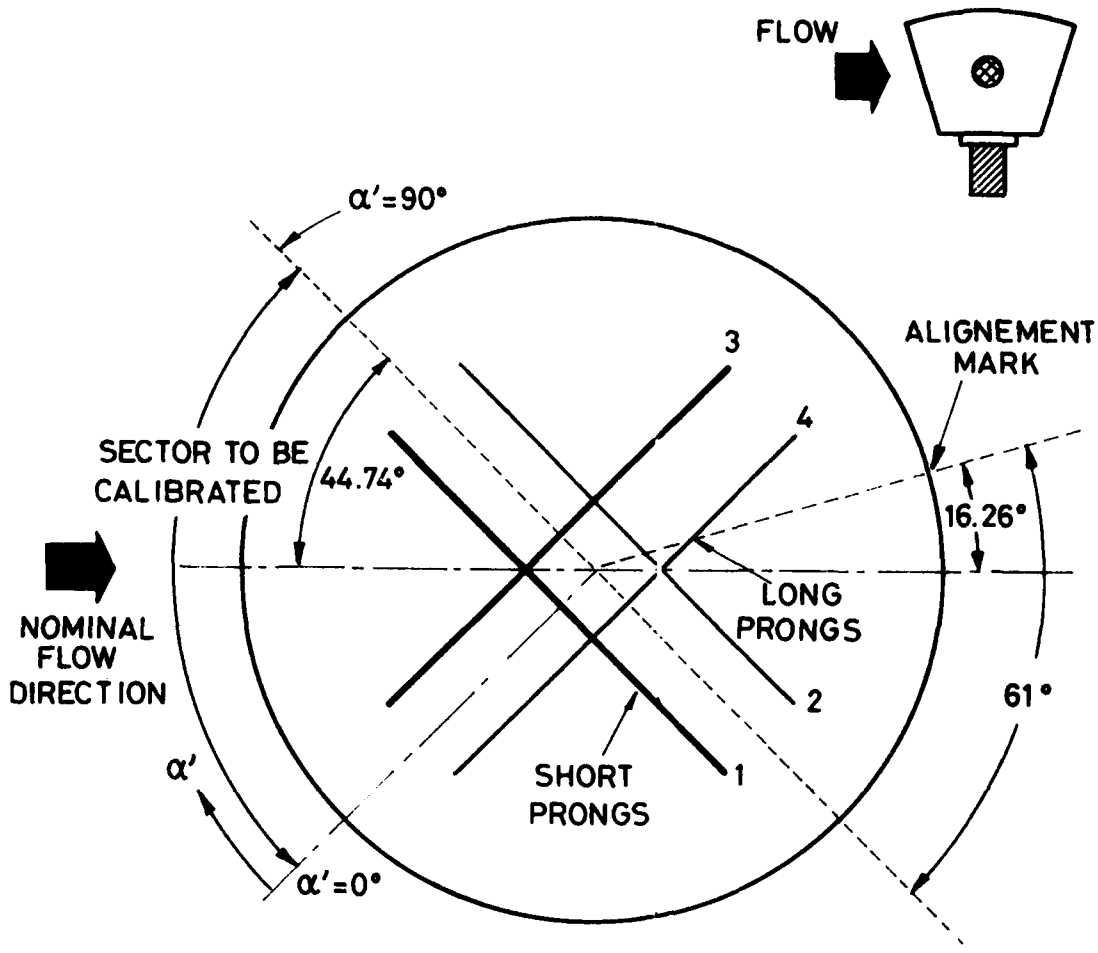

FIG. 14 - VIEW OF PROBE FACE AS MOUNTED ON BLADE

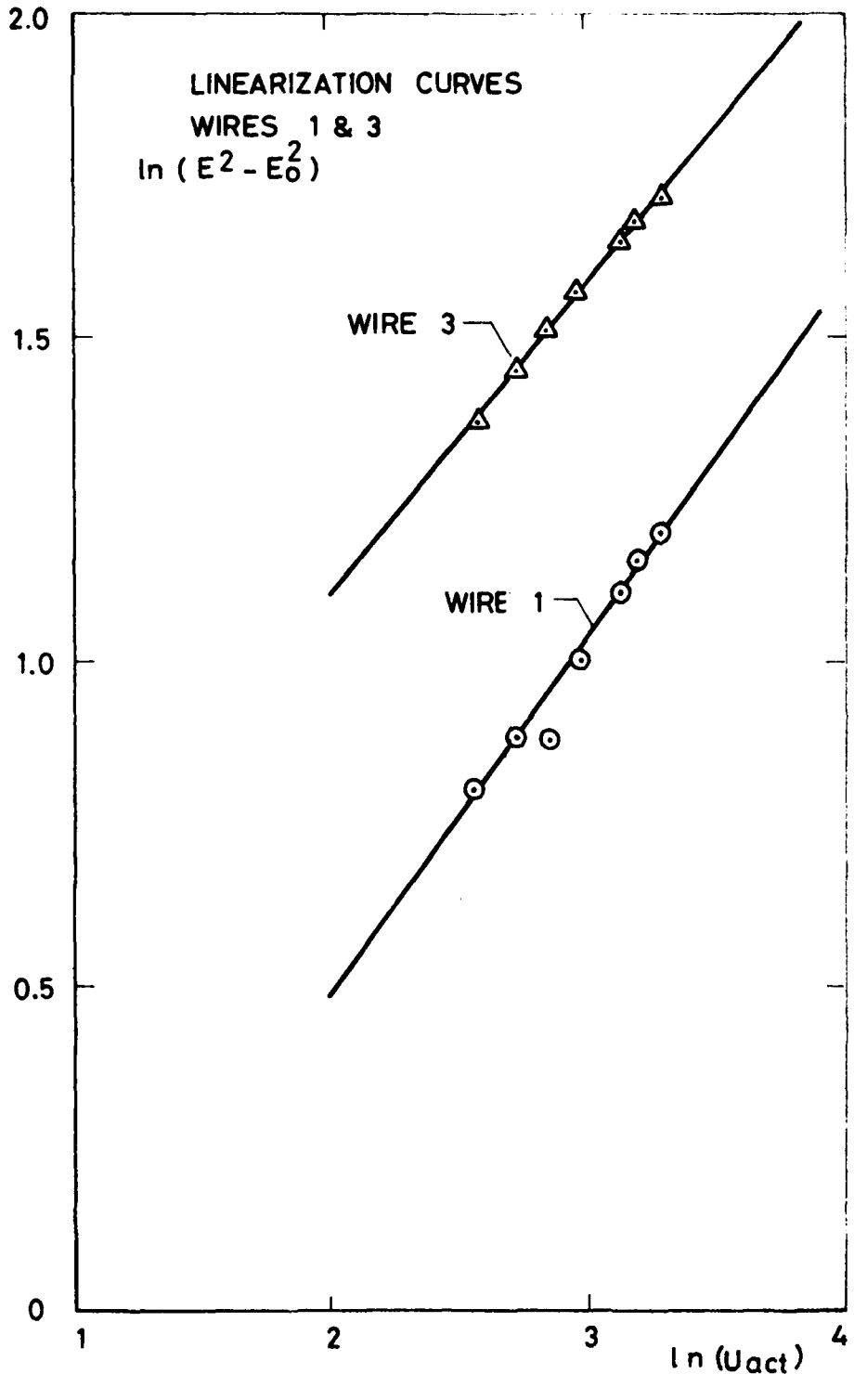
LINEARIZATION CURVES
WIRES 1 & 3
ln (E² - E₀²)
WIRE 3
WIRE 1
2.0
1.5
1.0
0.5
0
1
2
3
4
ln (Uact)

FIG. 15 a

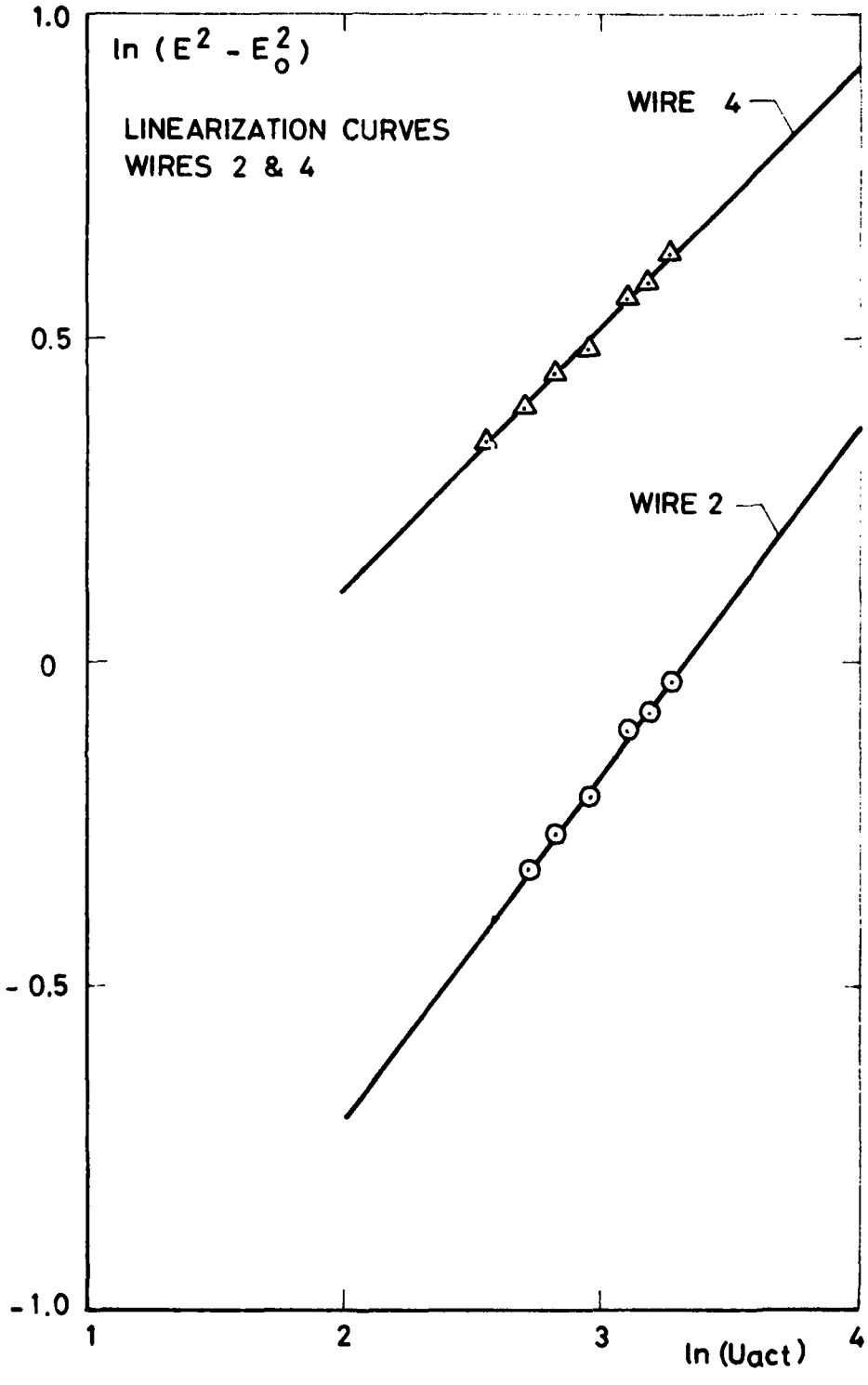
1.0
ln (E² - E₀²)
LINEARIZATION CURVES
WIRES 2 & 4
WIRE 4
WIRE 2
0.5
0
- 0.5
- 1.0
1
2
3
4
ln (Uact)

FIG. 15 b

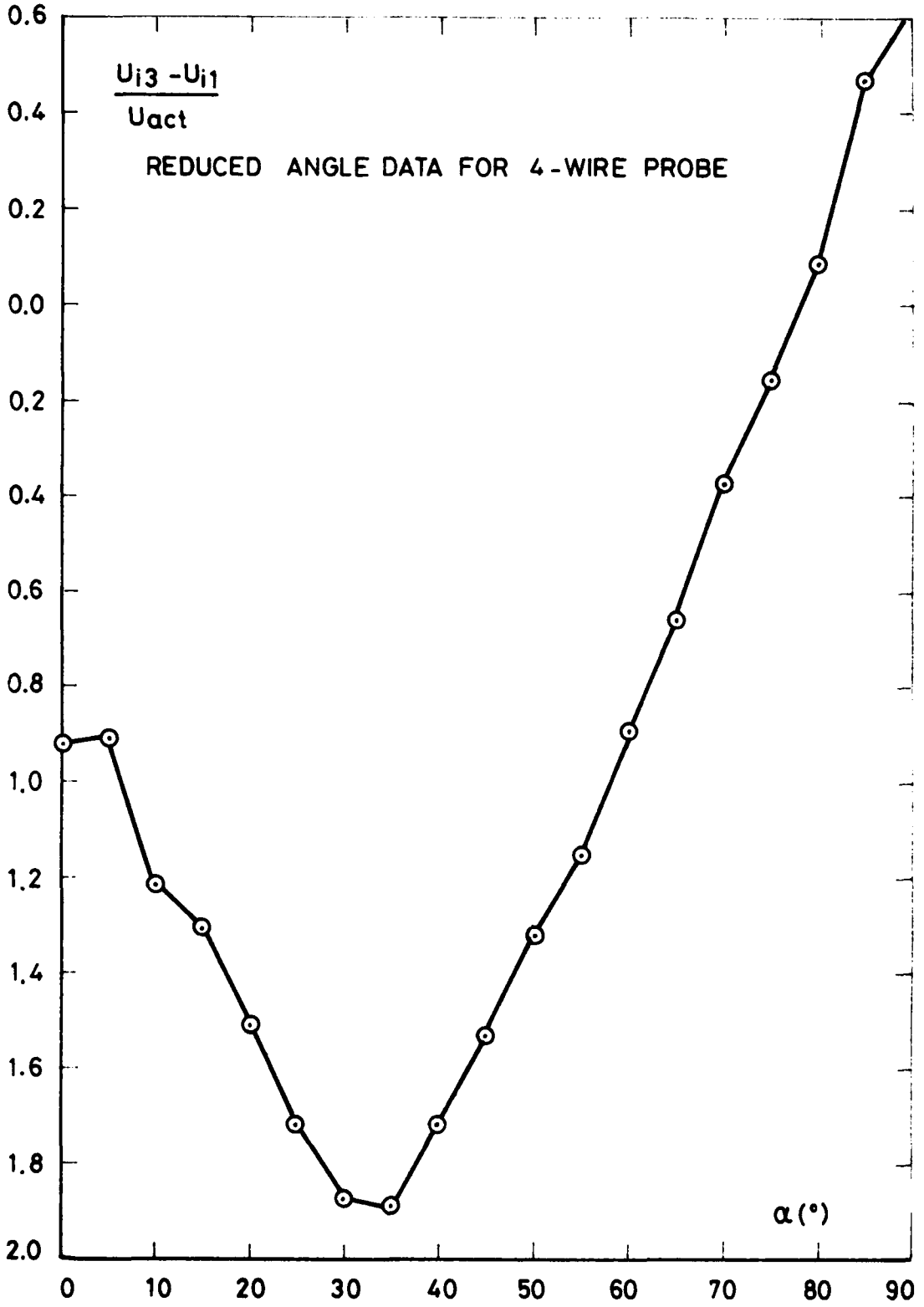
$\frac{U_{i3} - U_{i1}}{U_{act}}$
REDUCED ANGLE DATA FOR 4-WIRE PROBE
0.6
0.4
0.2
0.0
0.2
0.4
0.6
0.8
1.0
1.2
1.4
1.6
1.8
2.0
0
10
20
30
40
50
60
70
80
90
α (°)

FIG. 15 c

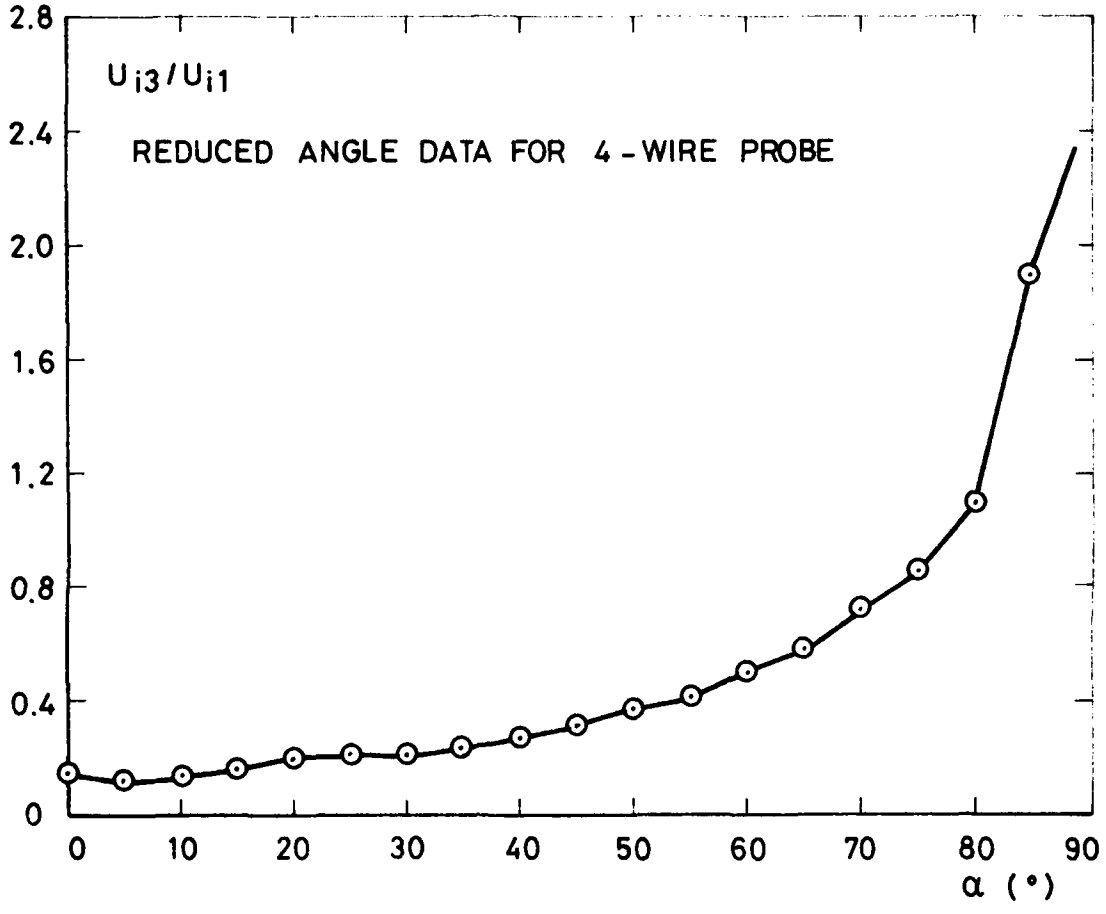
2.8
U_{i3}/U_{i1}
2.4
REDUCED ANGLE DATA FOR 4-WIRE PROBE
2.0
1.6
1.2
0.8
0.4
0
0
10
20
30
40
50
60
70
80
90
α (°)

FIG. 15 d

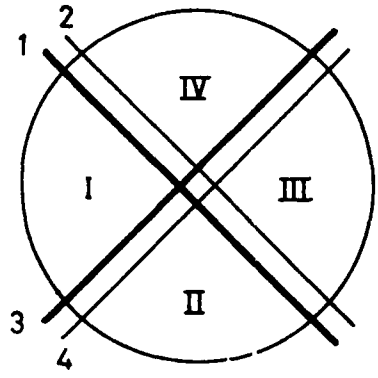

	U_{12}	U_{34}
I	+	+
II	+	-
III	-	-
IV	-	+

FIG. 16 a - FLOW FROM SIDE OF COLD WIRE.

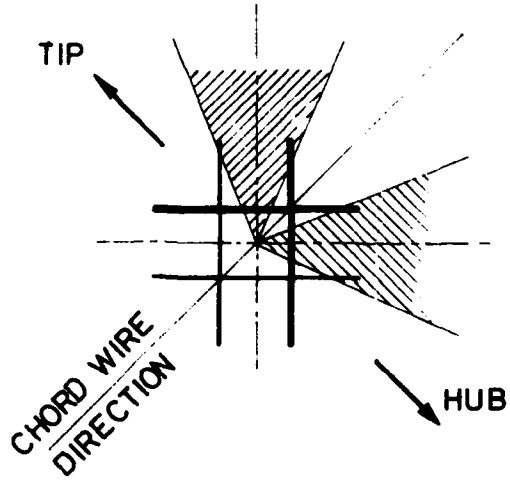

FIG. 16 b

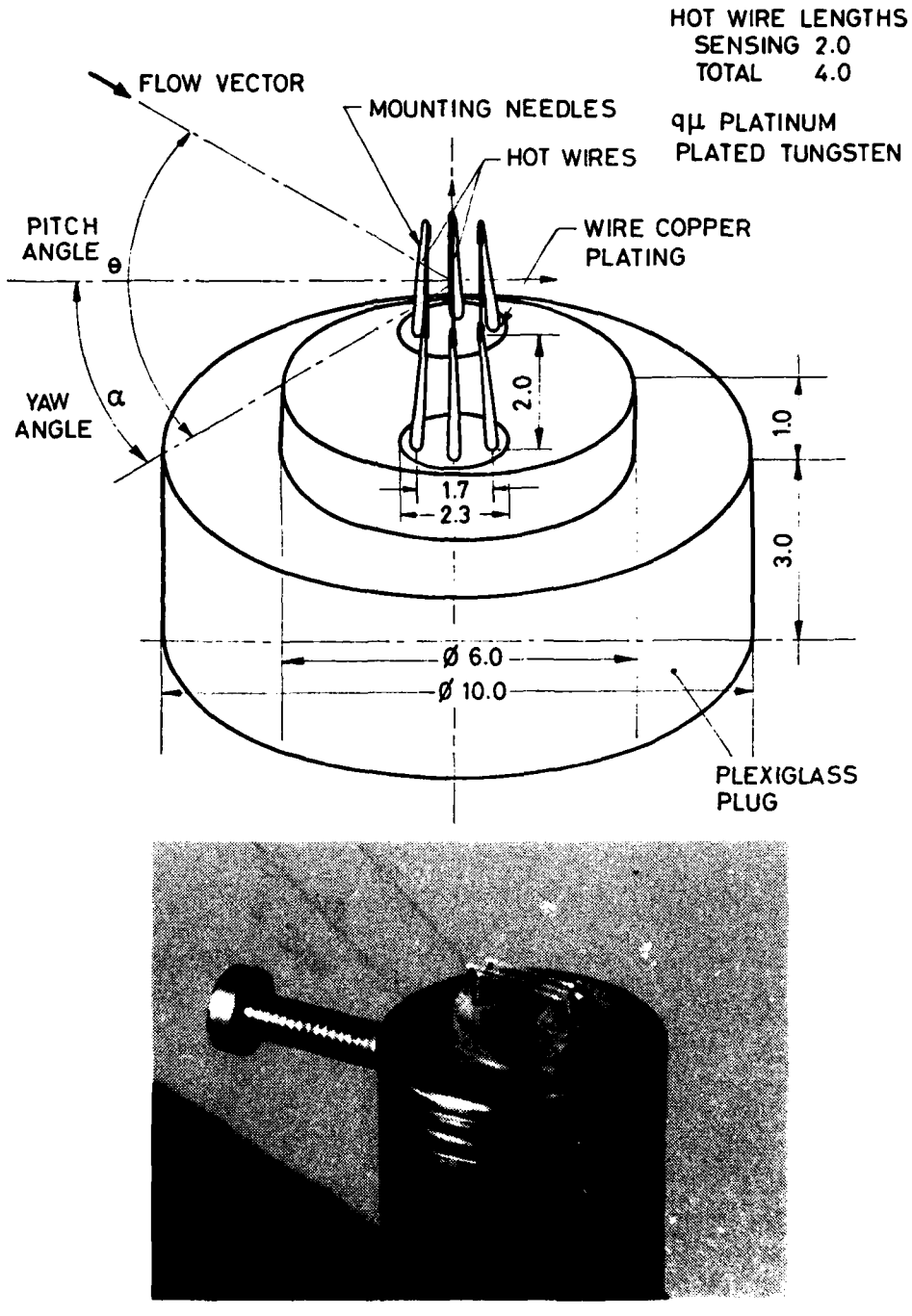

FIG. 17 - SCHEMATIC OF HOT WIRE PROBE AND PLUG FOR MOUNTING.

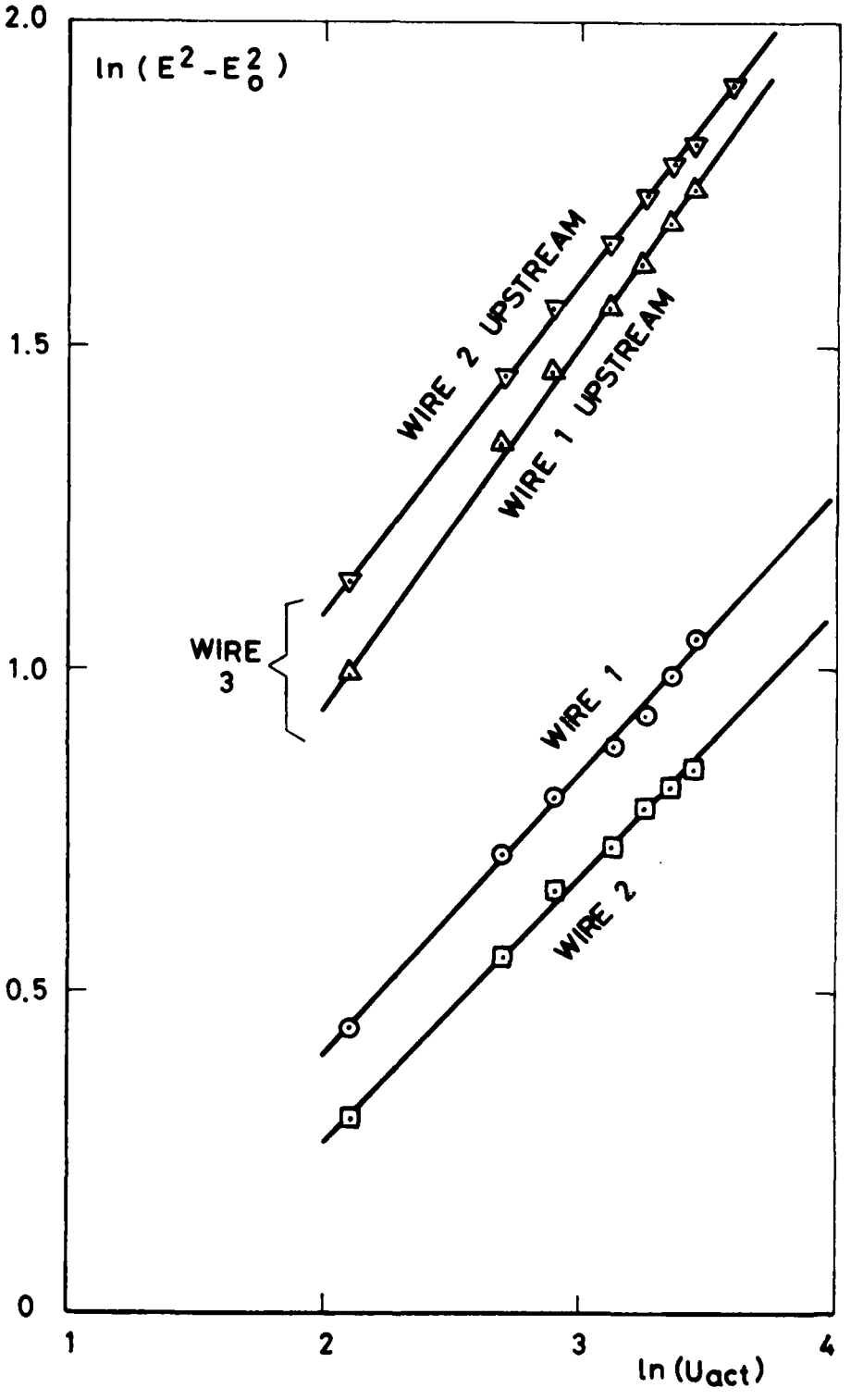
2.0
1.5
1.0
0.5
0
1
2
3
4
ln (E² - E₀²)
ln (Uact)
WIRE 2 UPSTREAM
WIRE 1 UPSTREAM
WIRE 3
WIRE 1
WIRE 2

FIG. 18

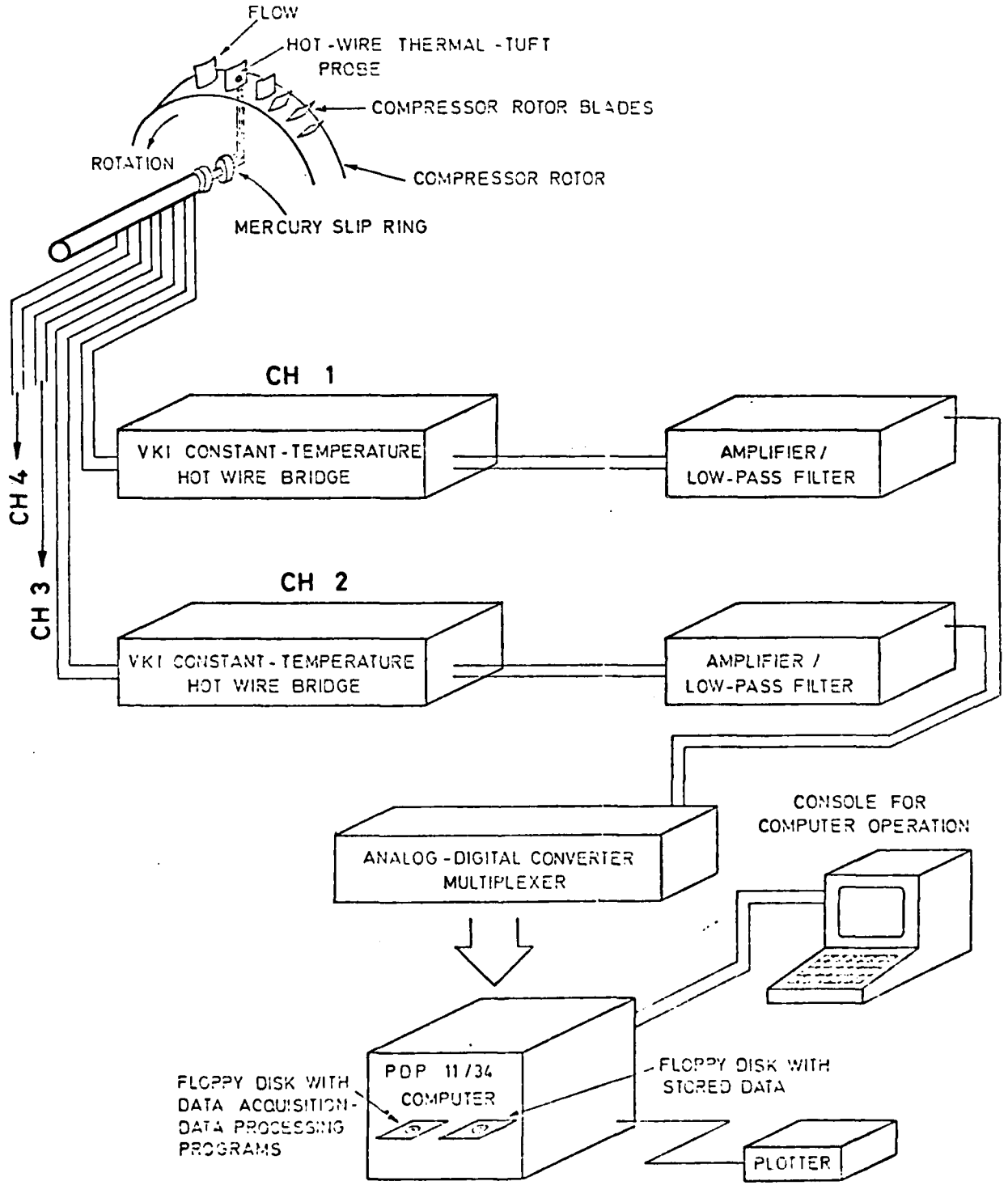

FIG. 19 - MEASUREMENT CHAIN AND DATA ACQUISITION SYSTEM

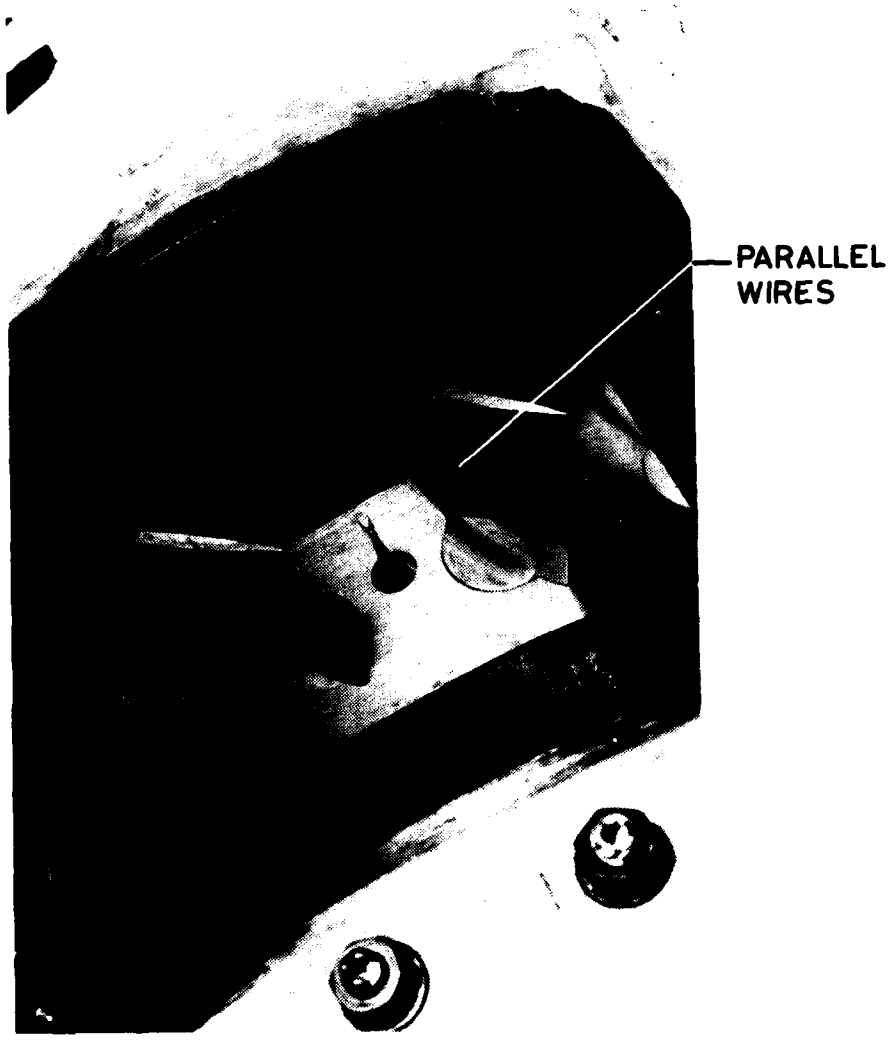

FIG. 20 - INSTRUMENTED CHANNEL .

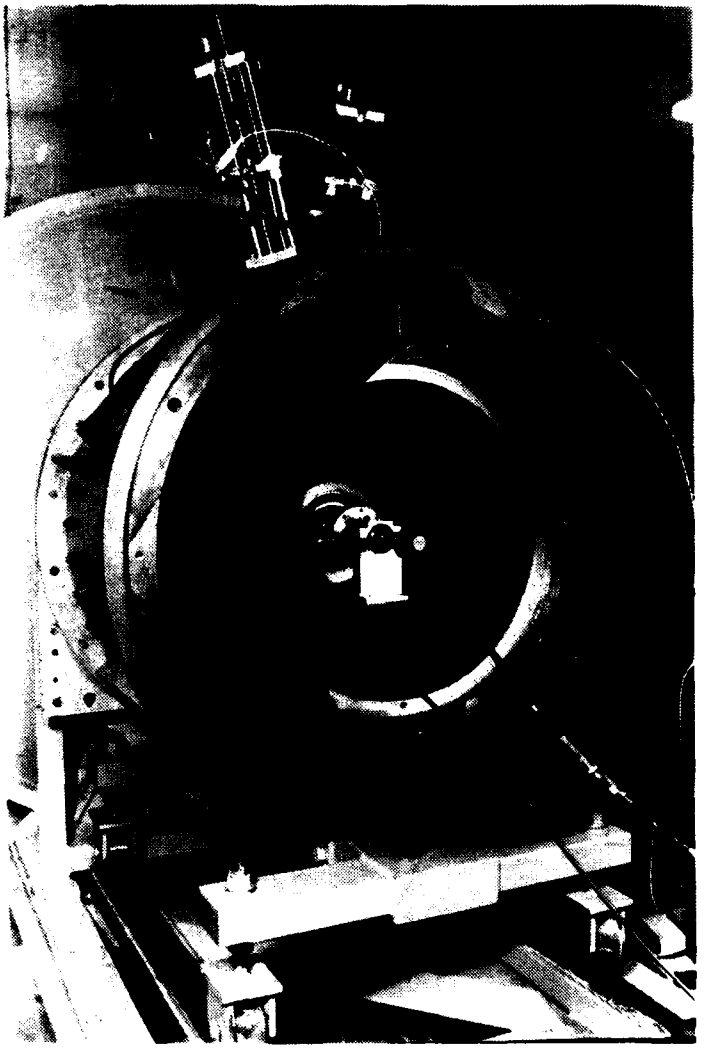

FIG 21 - SLIPRING ASSEMBLY

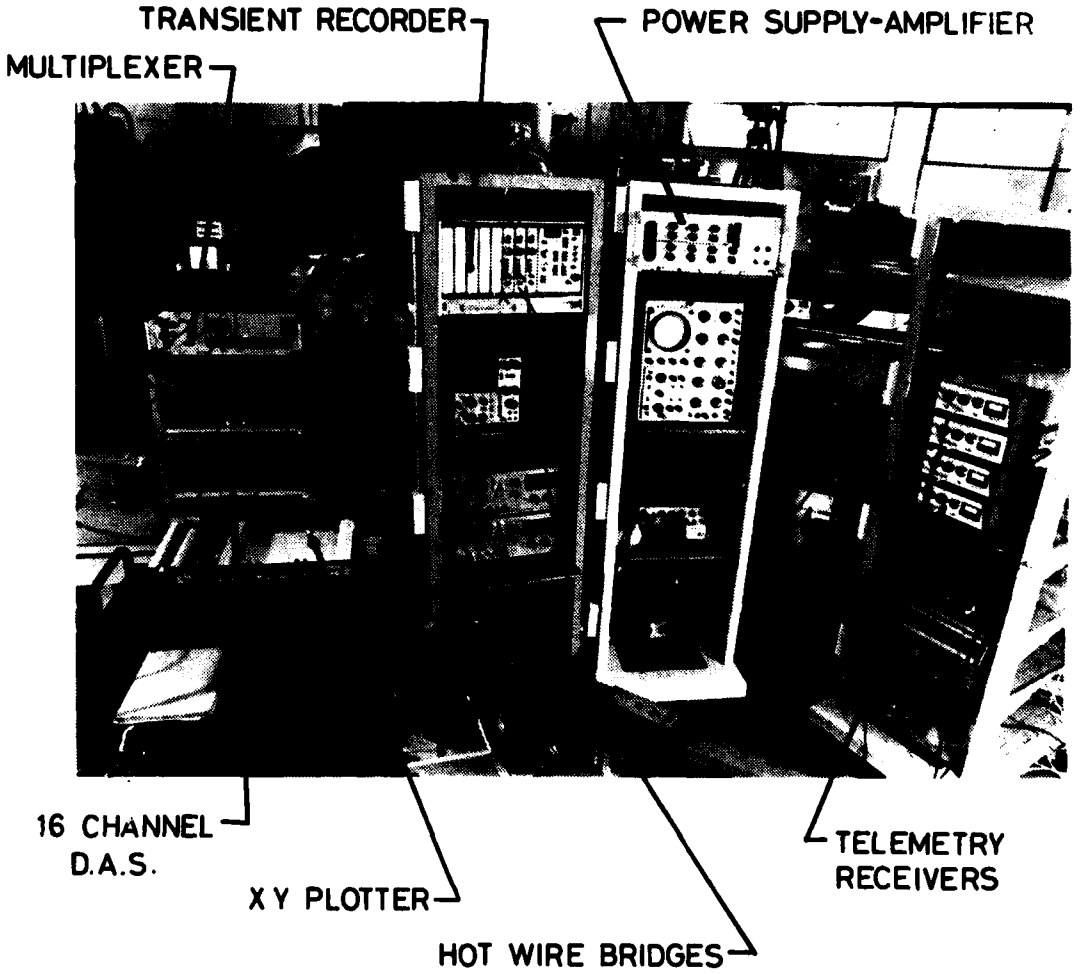

FIG. 22 - INSTRUMENTATION

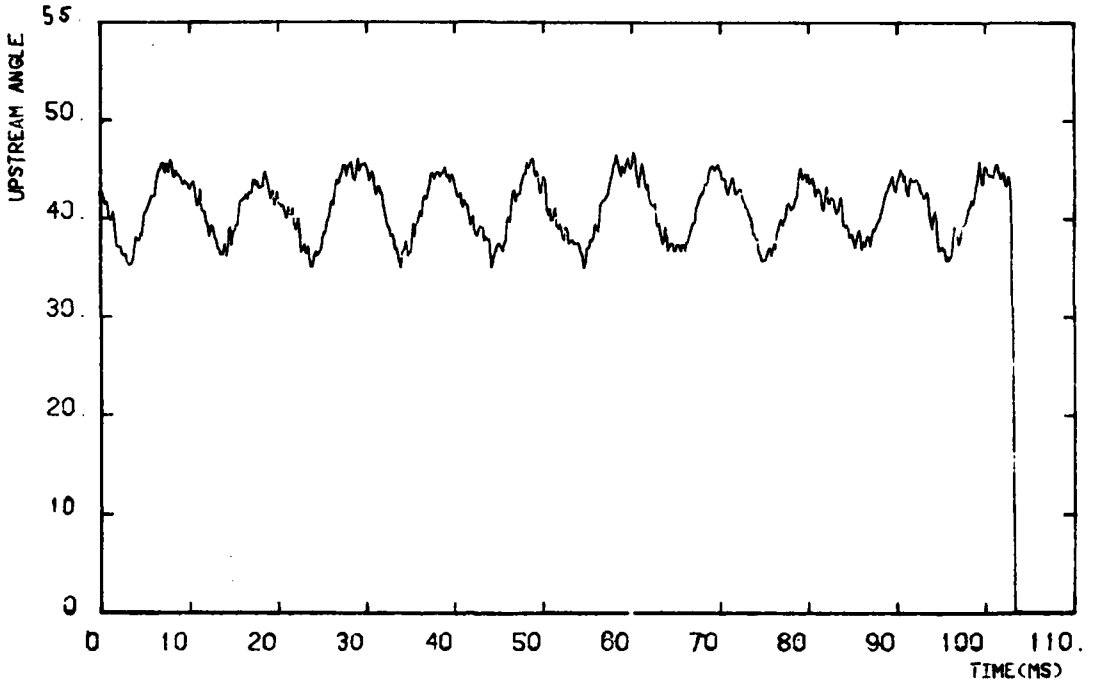

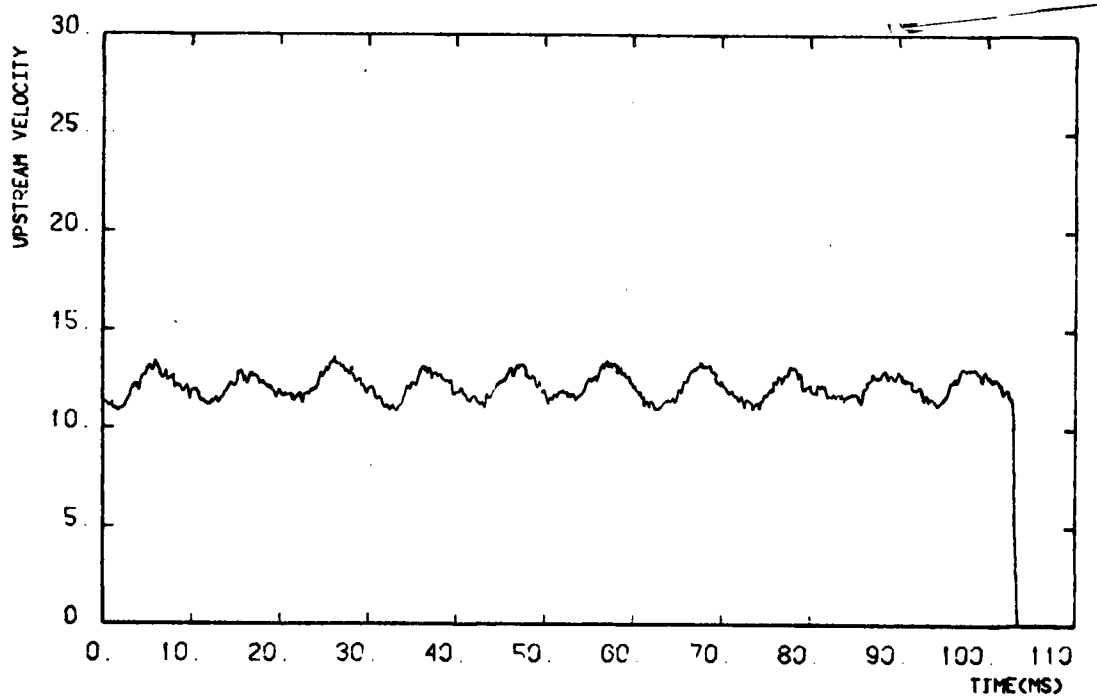

FIG. 23 a - S-1 CONDITION.

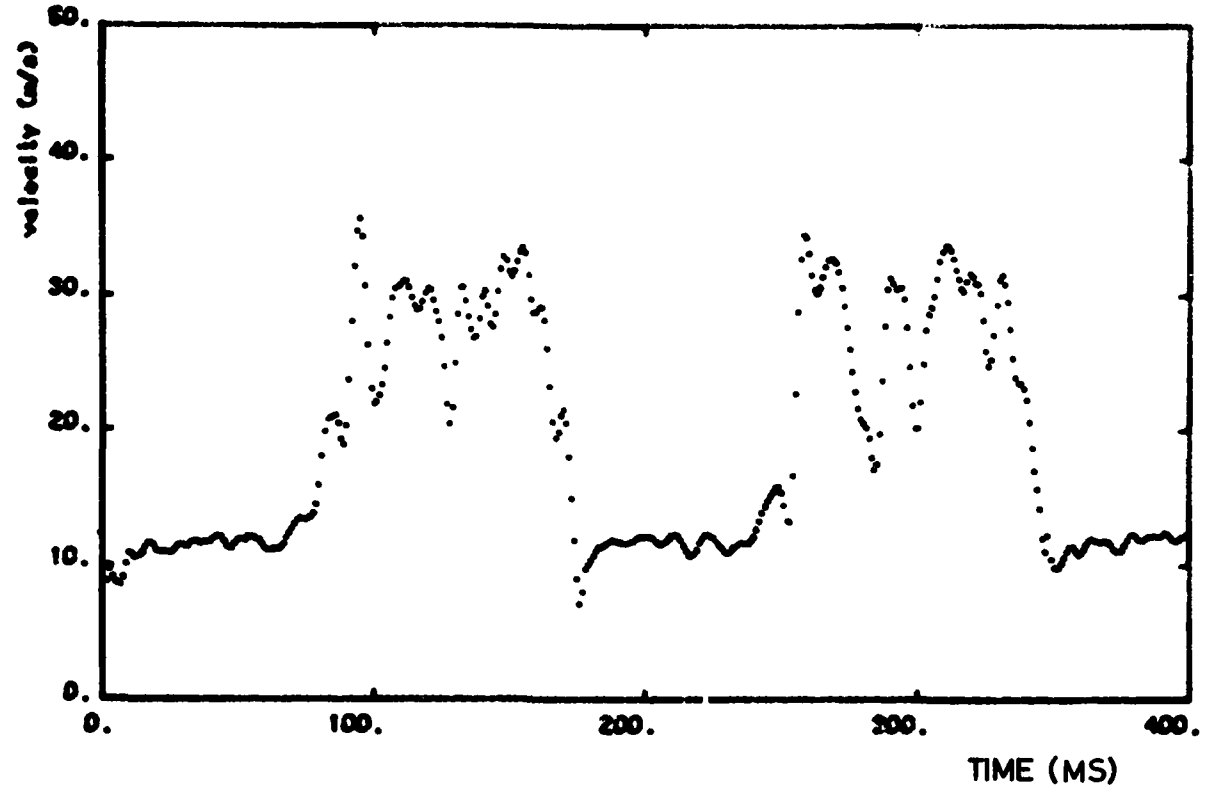

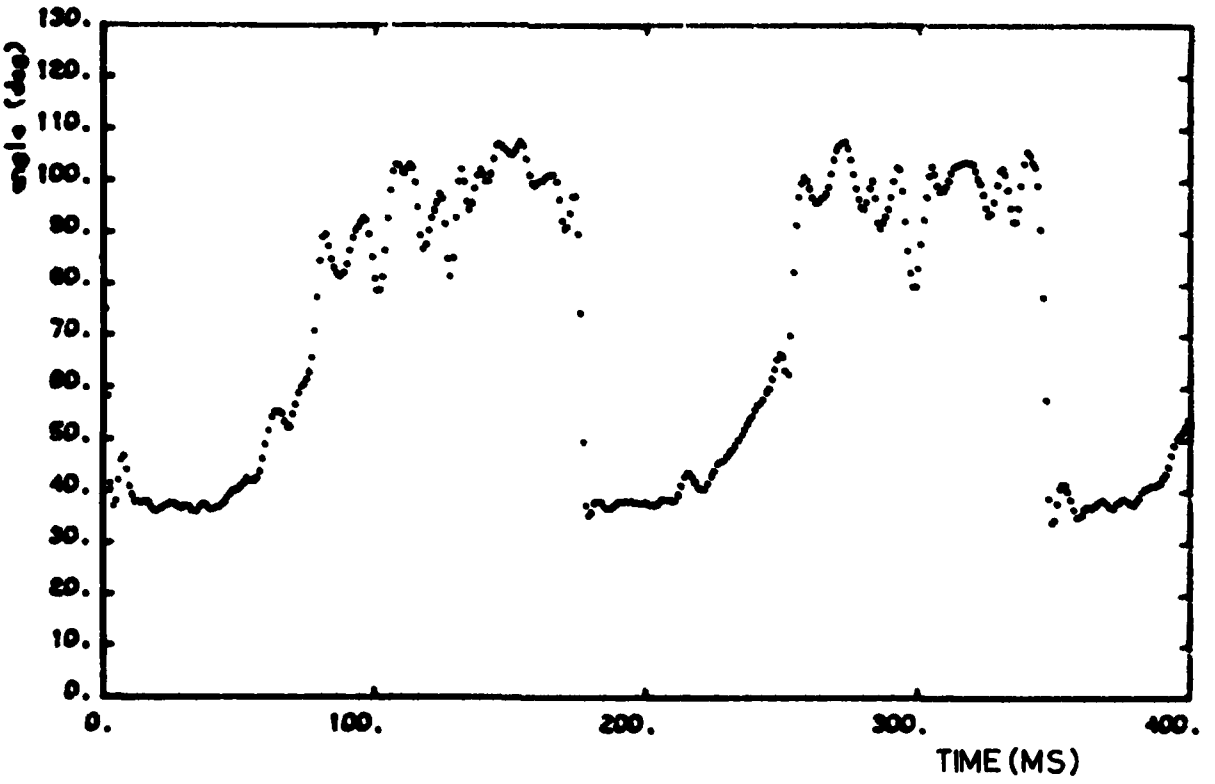

FIG. 23 b- S-2 CONDITION

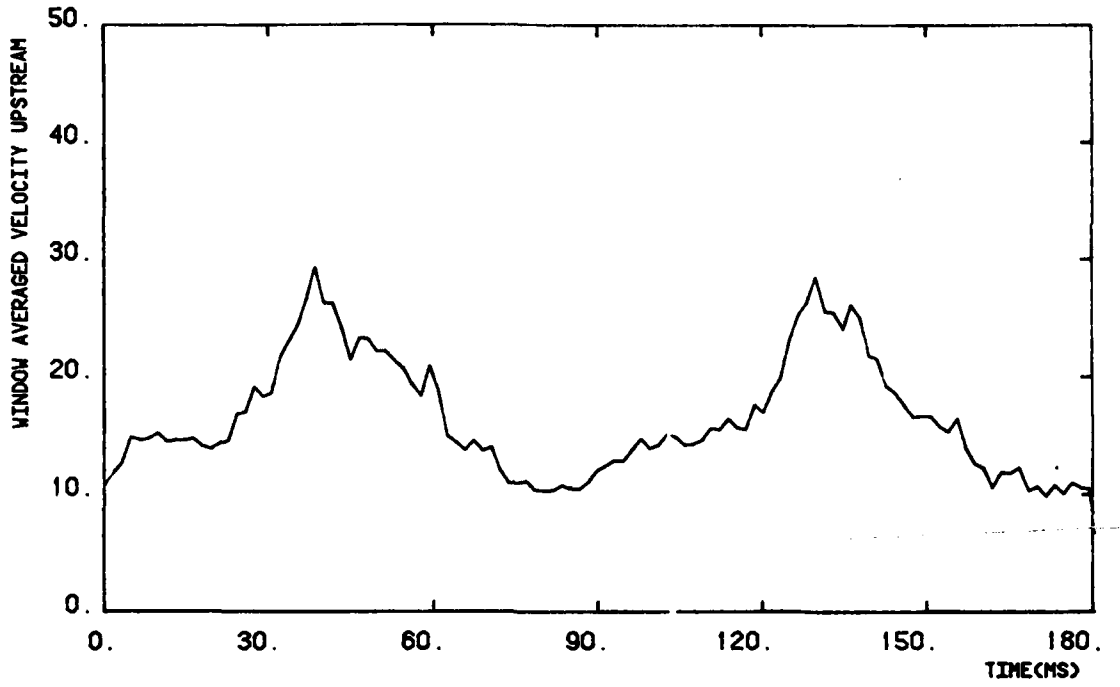

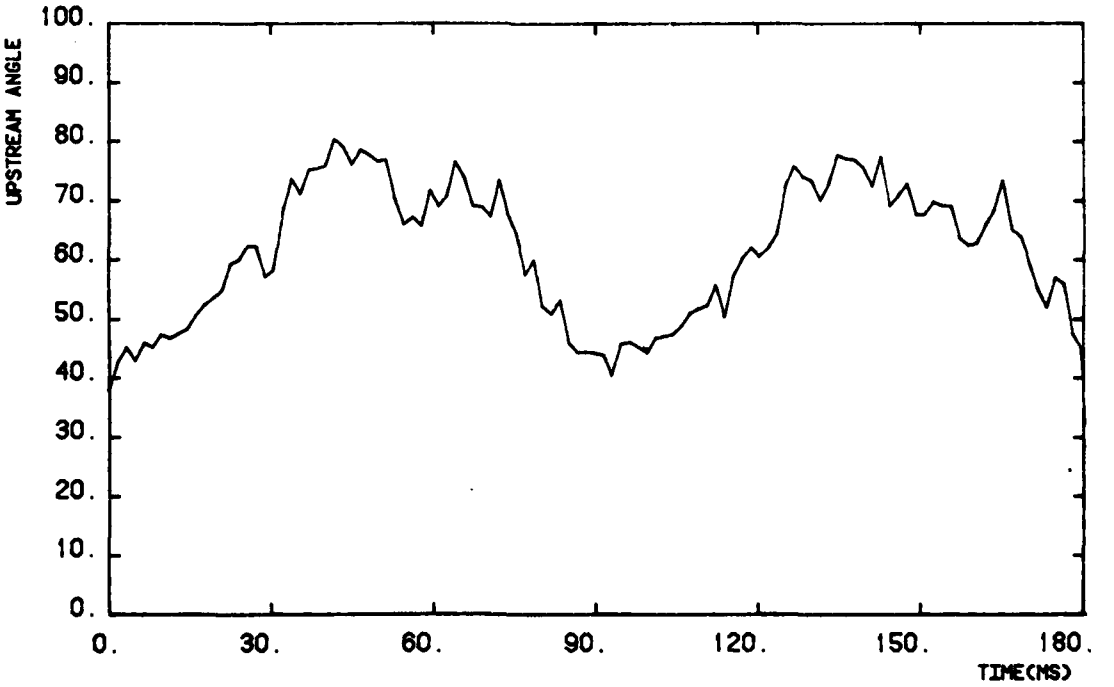

FIG. 23 c - S-3 CONDITION.

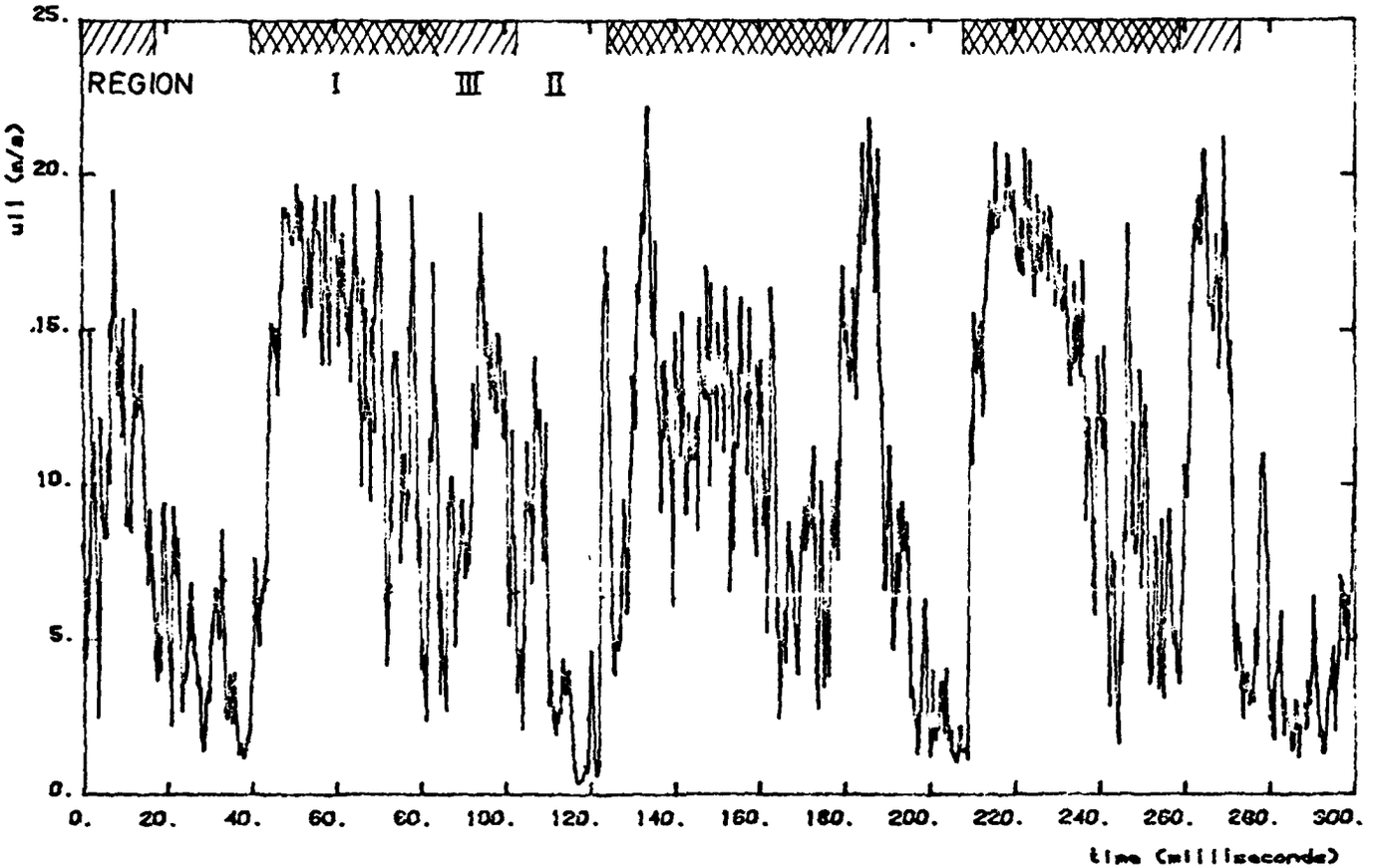

FIG. 24 - WIRE 1 VELOCITY, STALLED FLOW S-Z CONDITION

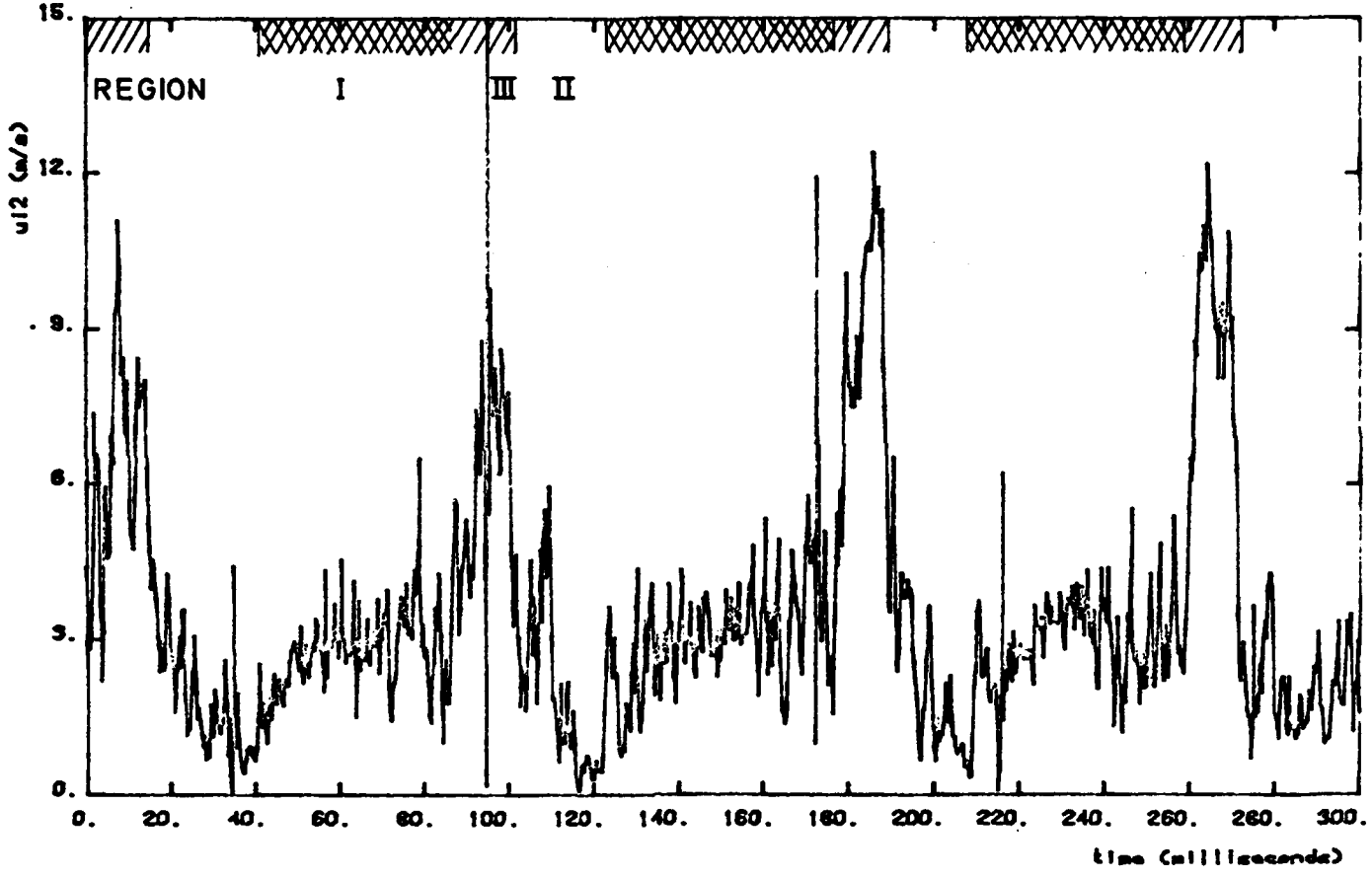

FIG. 25 - WIRE 2 VELOCITY, STALLED FLOW. S-Z CONDITION

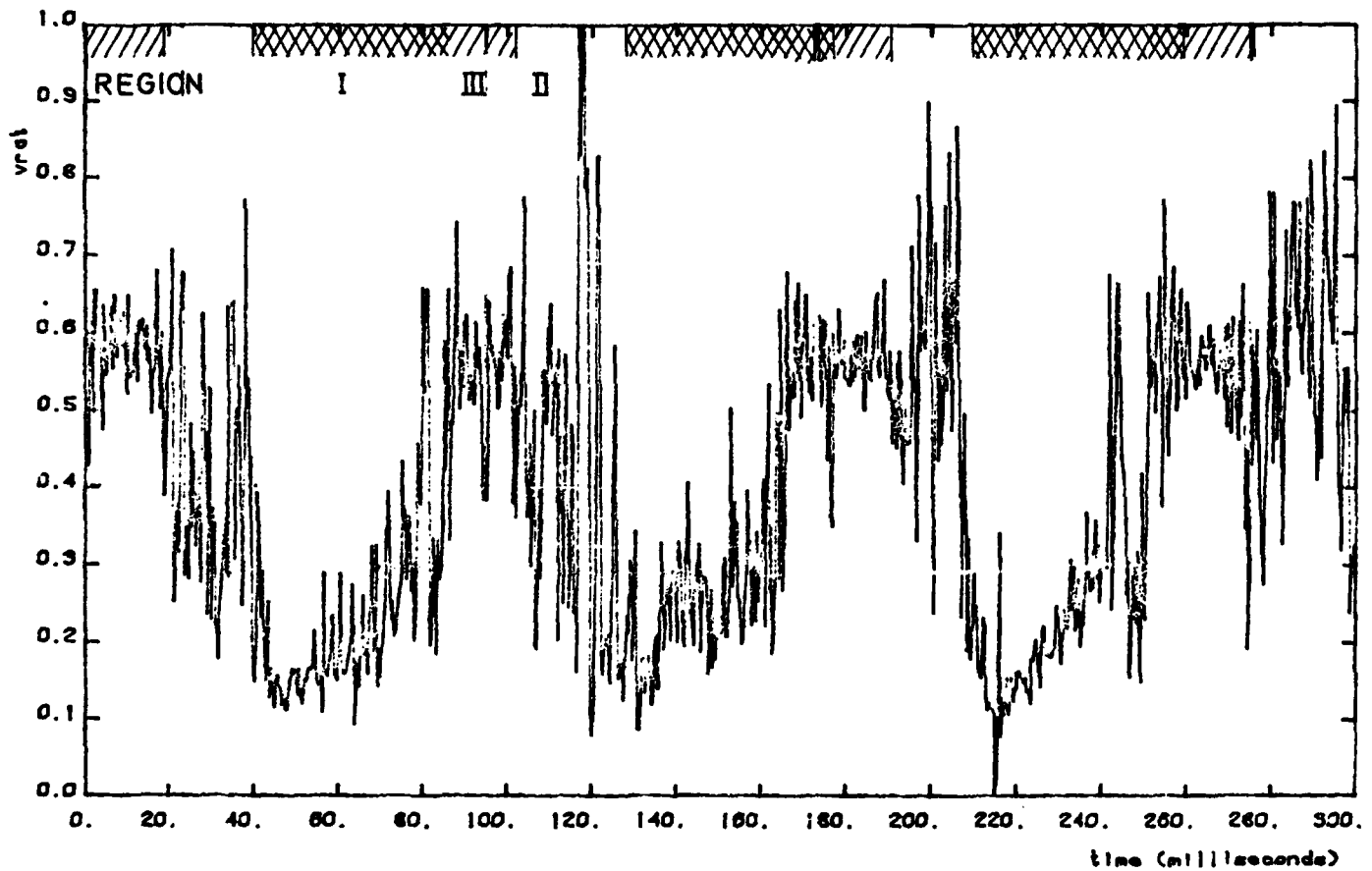

FIG. 26 - VELOCITY RATIO , STALLED FLOW . S-2 CONDITION

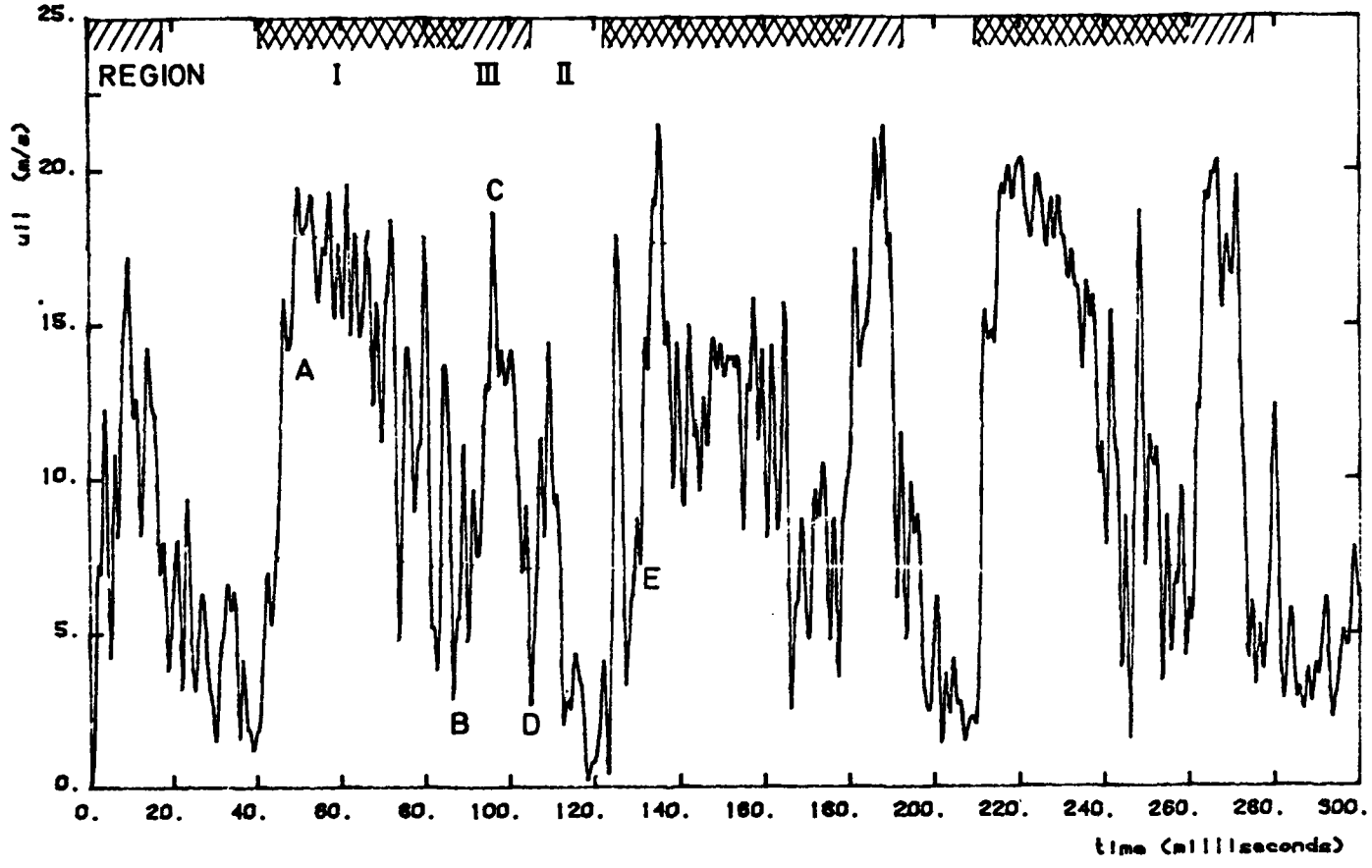

FIG. 27 - WIRE 1 VELOCITY, STALLED FLOW, SIGNAL LOW PASS FILTERED AT 600 H Z S-2 CONDITION

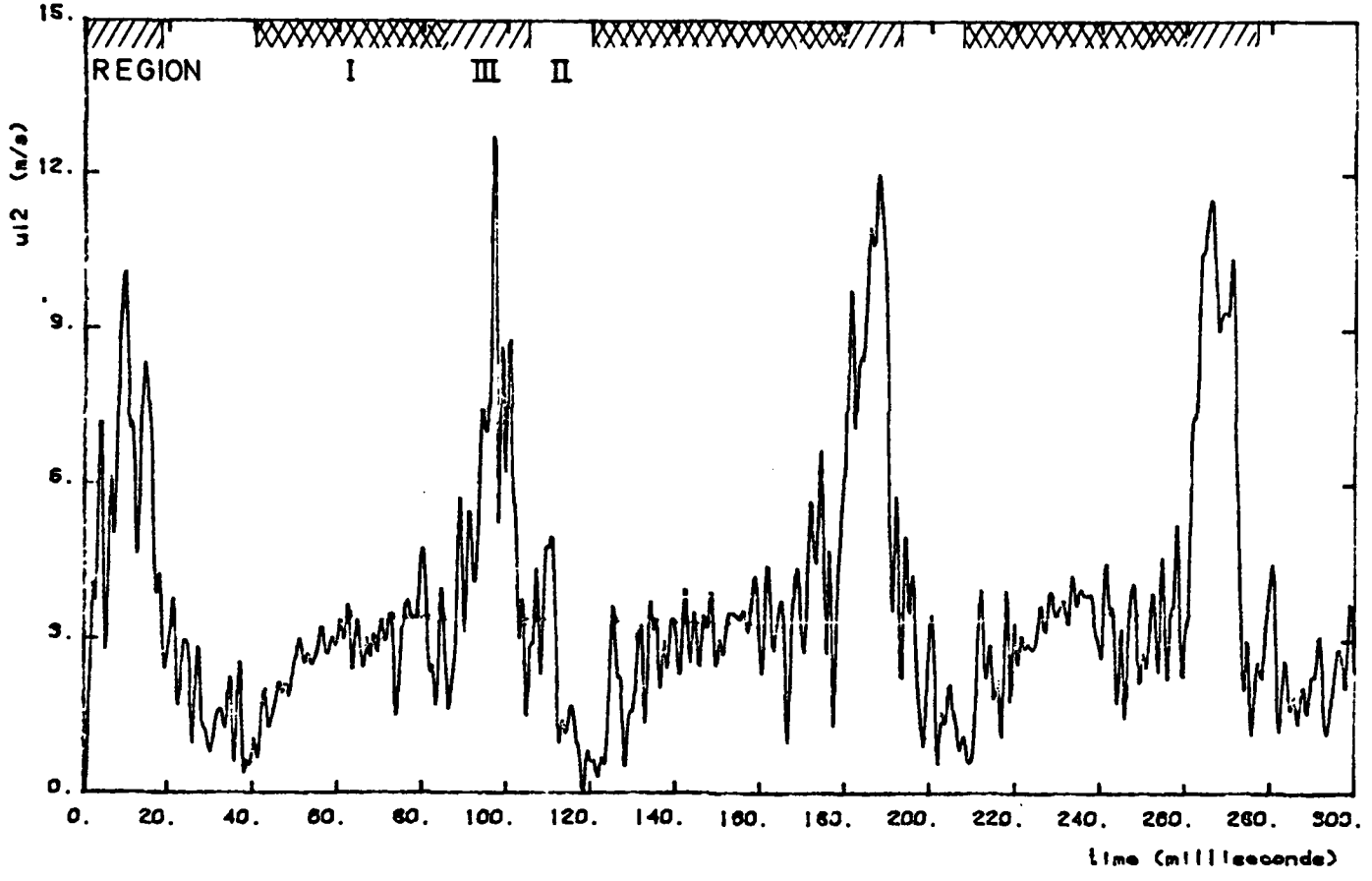

FIG. 28 - WIRE 2 VELOCITY, STALLED FLOW, SIGNAL LOW PASS FILTERED AT 600 HZ S-2 CONDITION

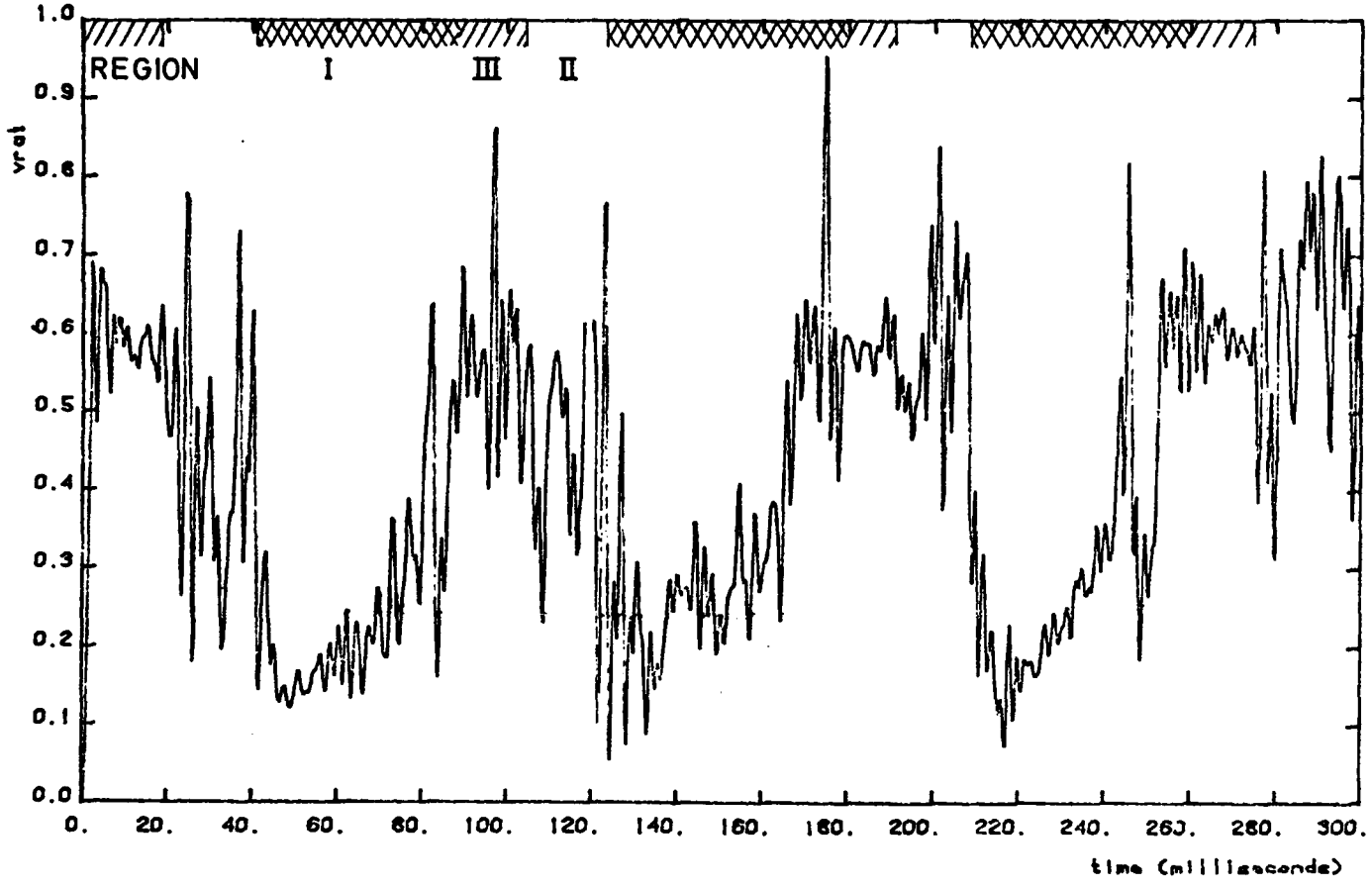

FIG. 29 -VELOCITY RATIO, STALLED FLOW, SIGNAL LOW PASS FILTERED AT 600 HZ. S-2 CONDITION

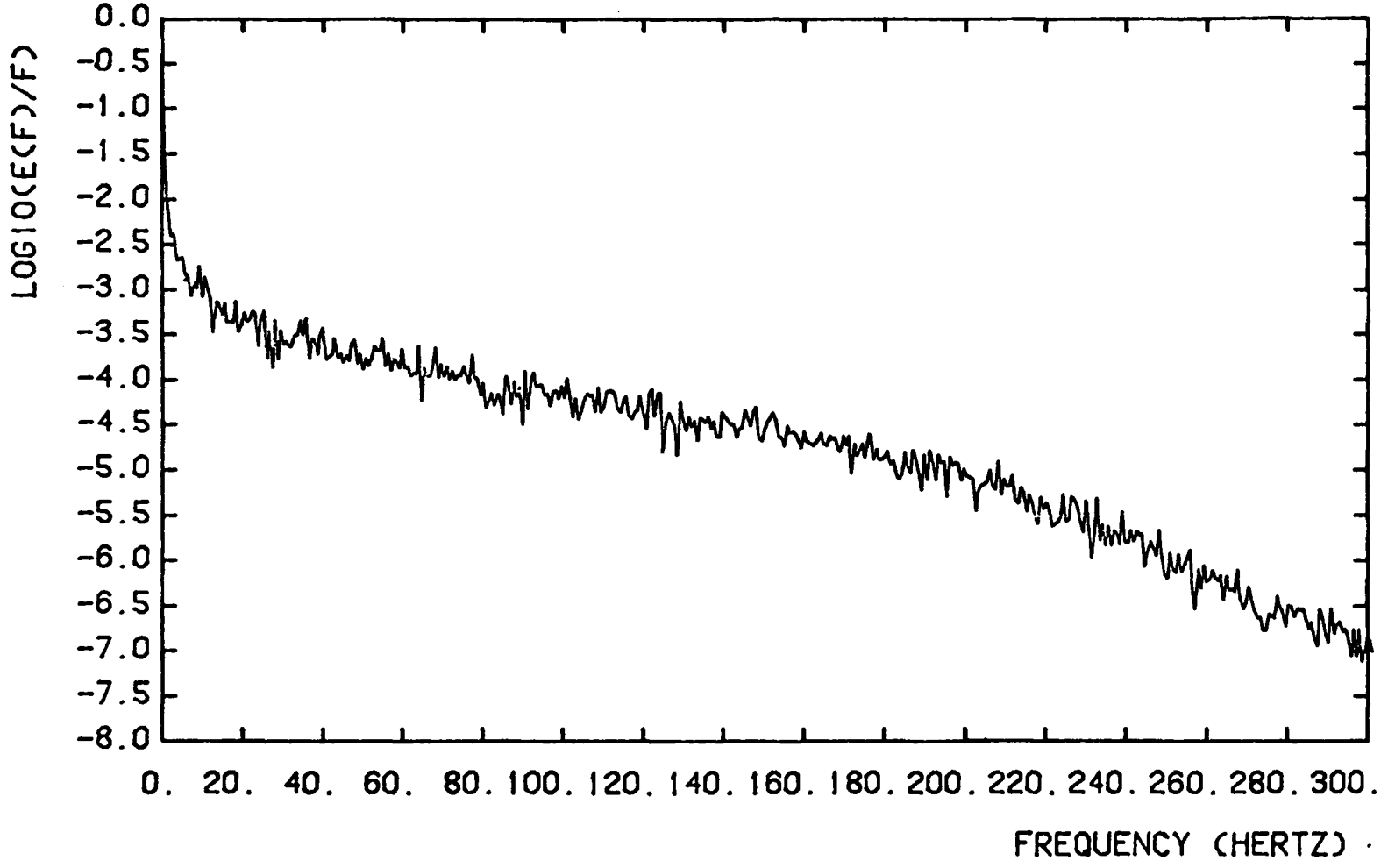
LOG10(E(F)/F)
0.0
-0.5
-1.0
-1.5
-2.0
-2.5
-3.0
-3.5
-4.0
-4.5
-5.0
-5.5
-6.0
-6.5
-7.0
-7.5
-8.0
0. 20. 40. 60. 80. 100. 120. 140. 160. 180. 200. 220. 240. 260. 280. 300.
FREQUENCY (HERTZ)

FIG. 30

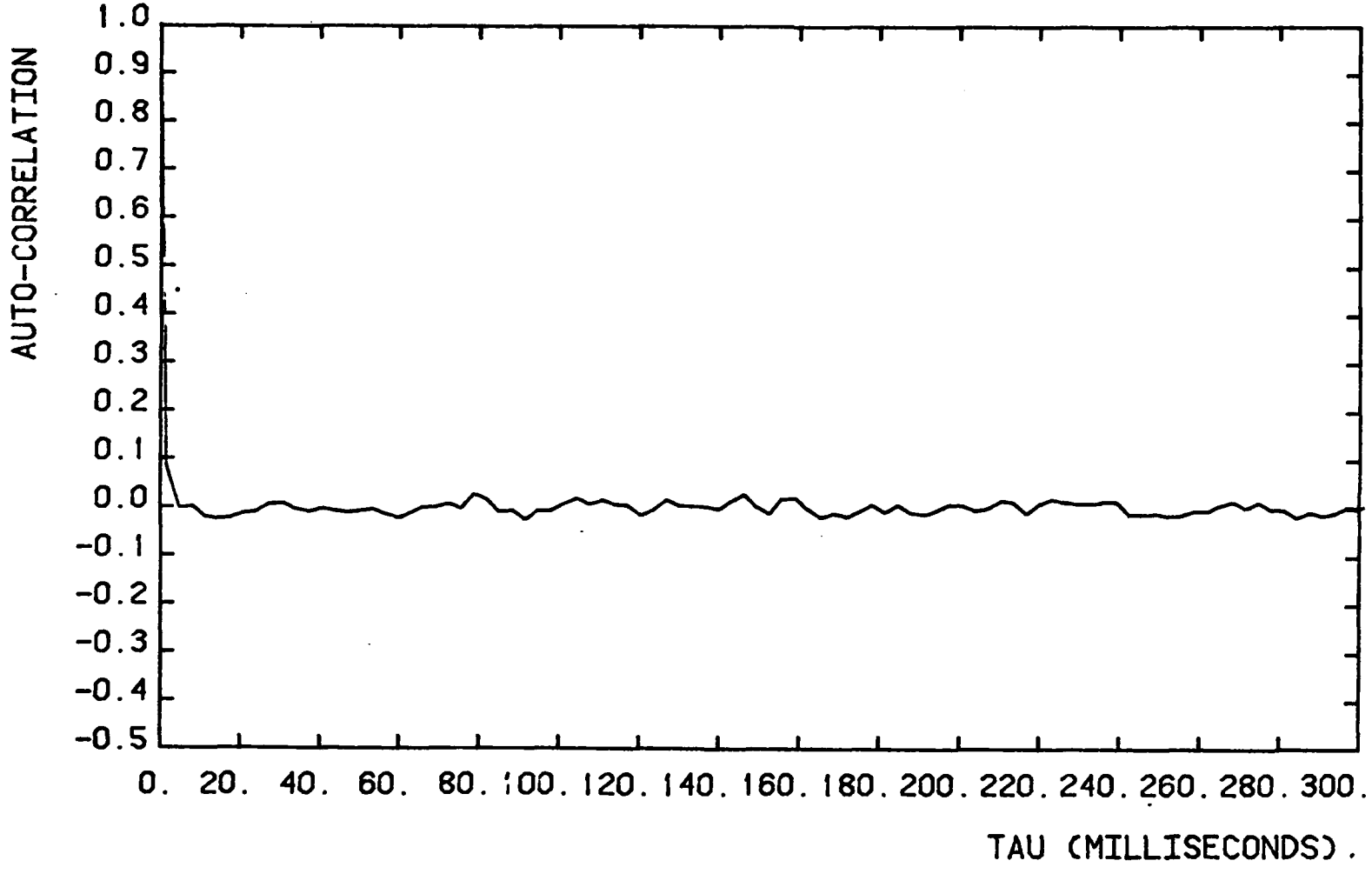

FIG. 31 - UNSTALLED

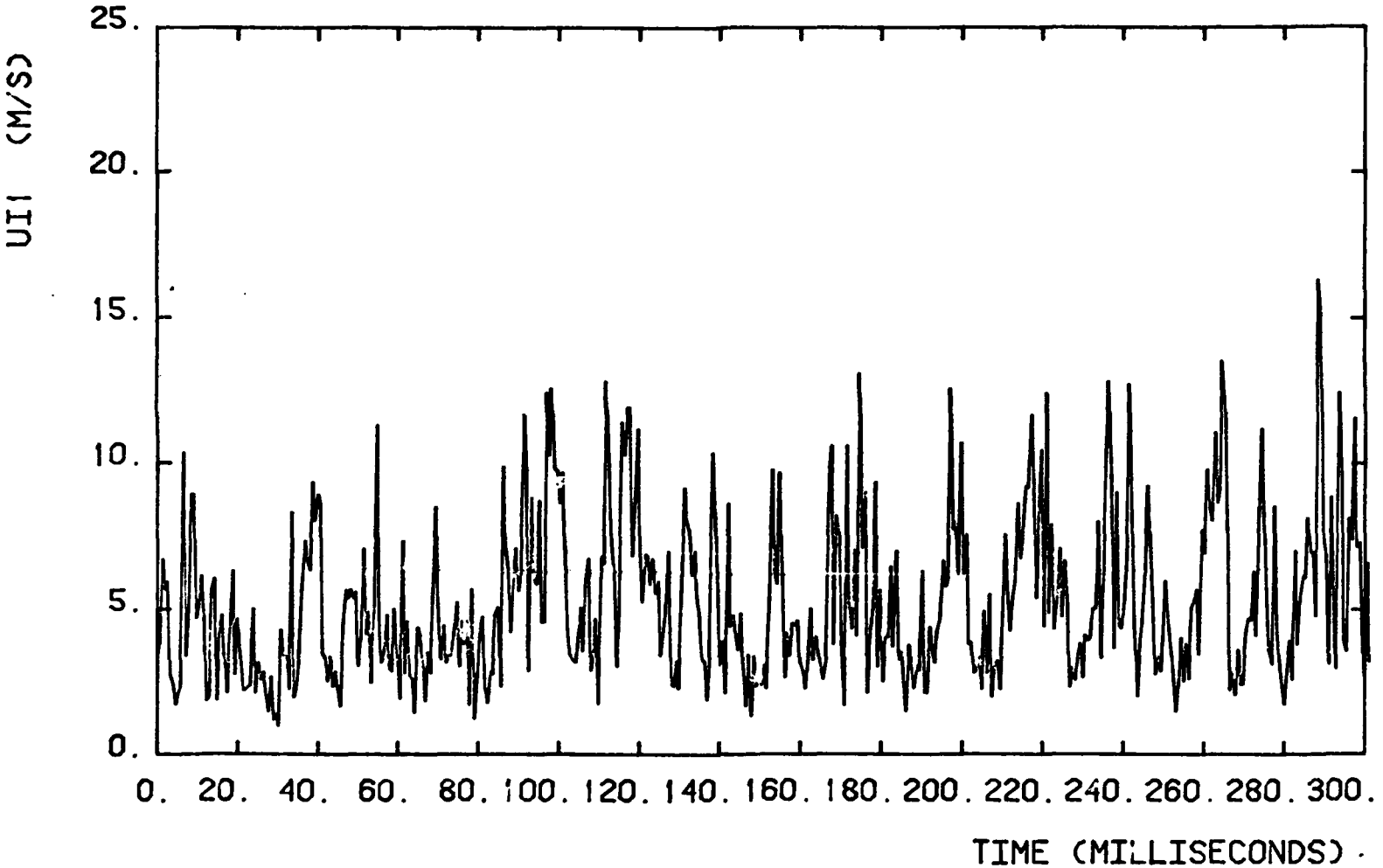

FIG. 32a - S1 CONDITION - FILTER 1562 HZ

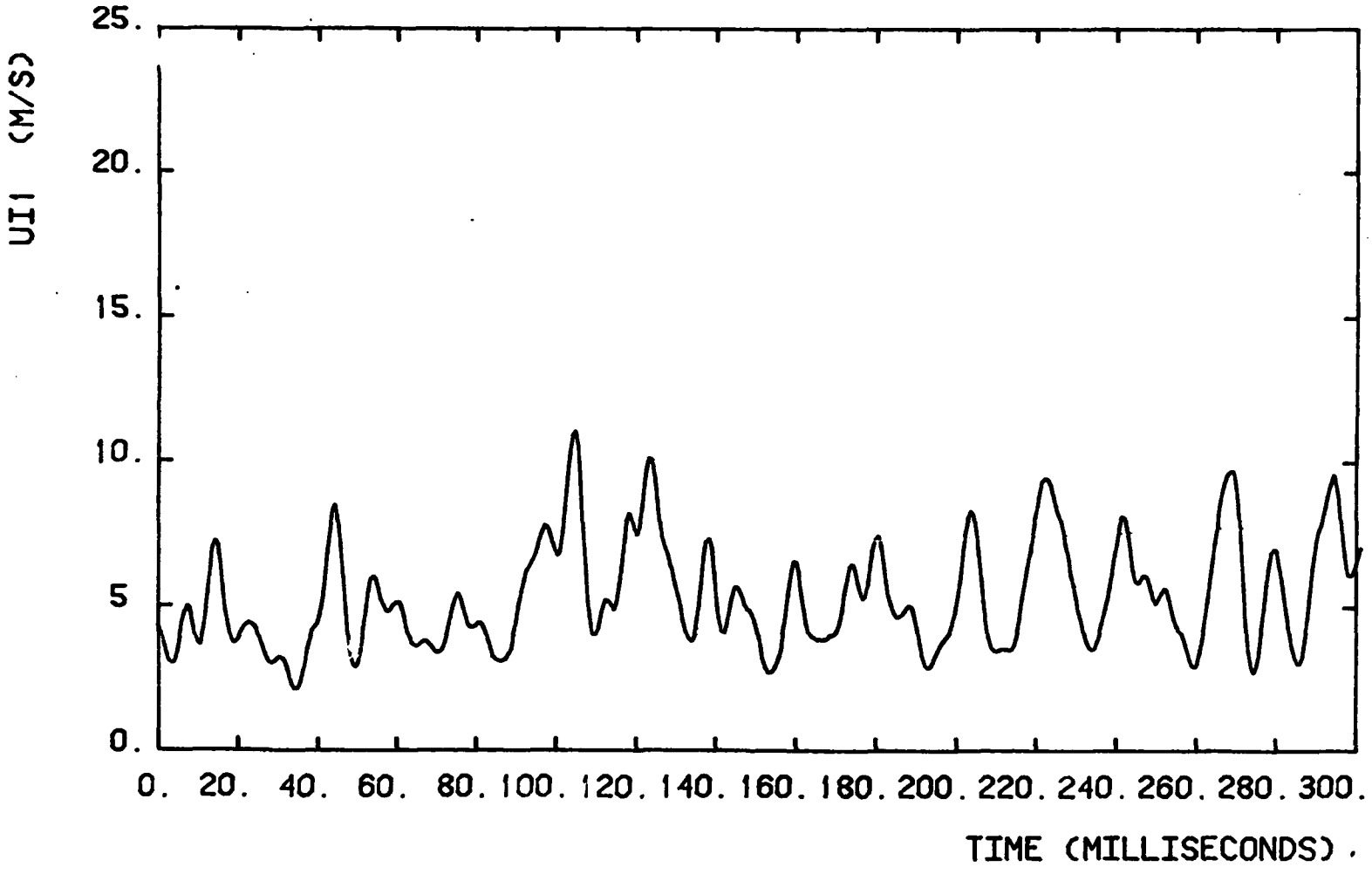

FIG. 32 b - S-1 CONDITION - FILTER 125 H Z

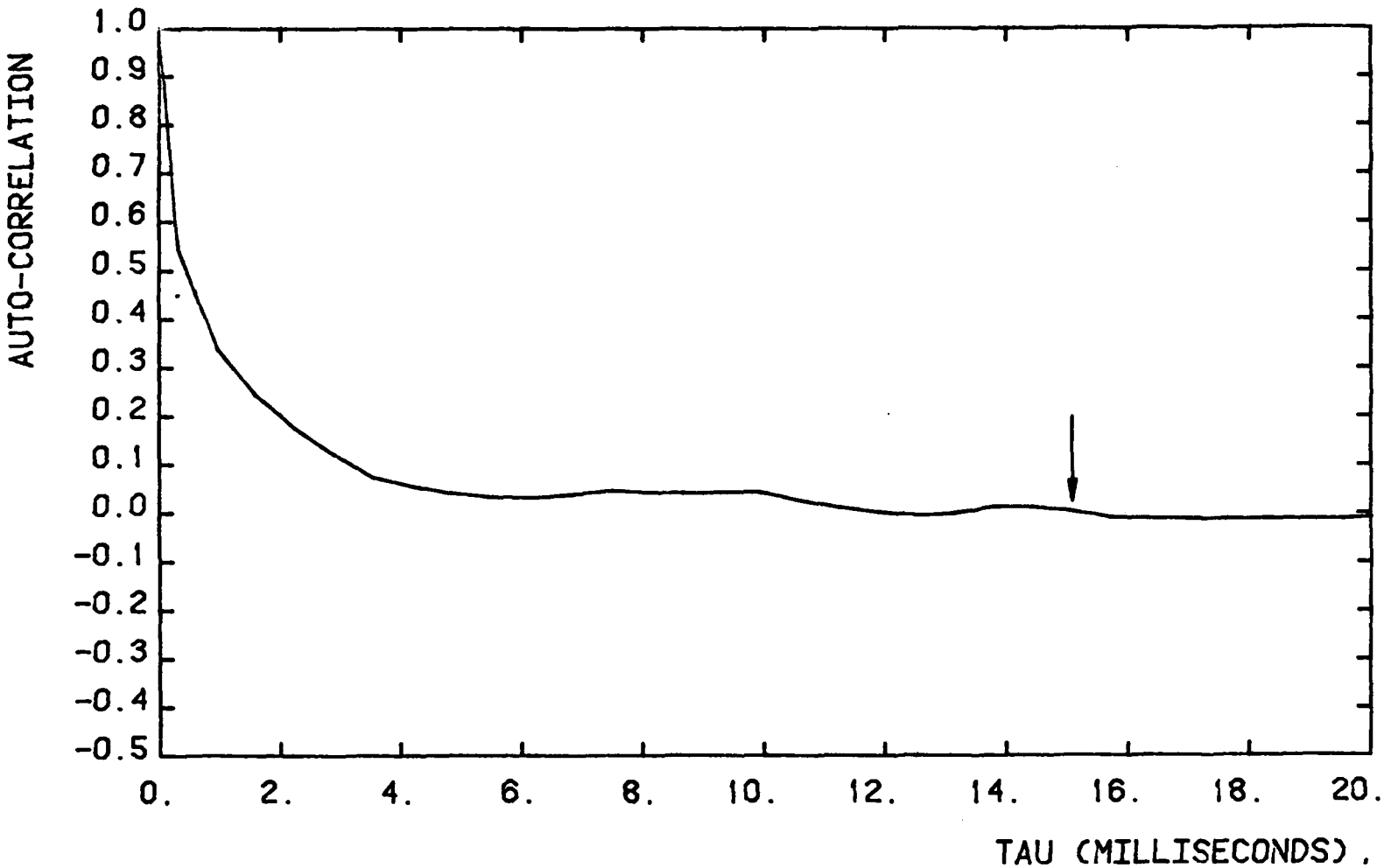

FIG. 33 - S-1 CONDITION

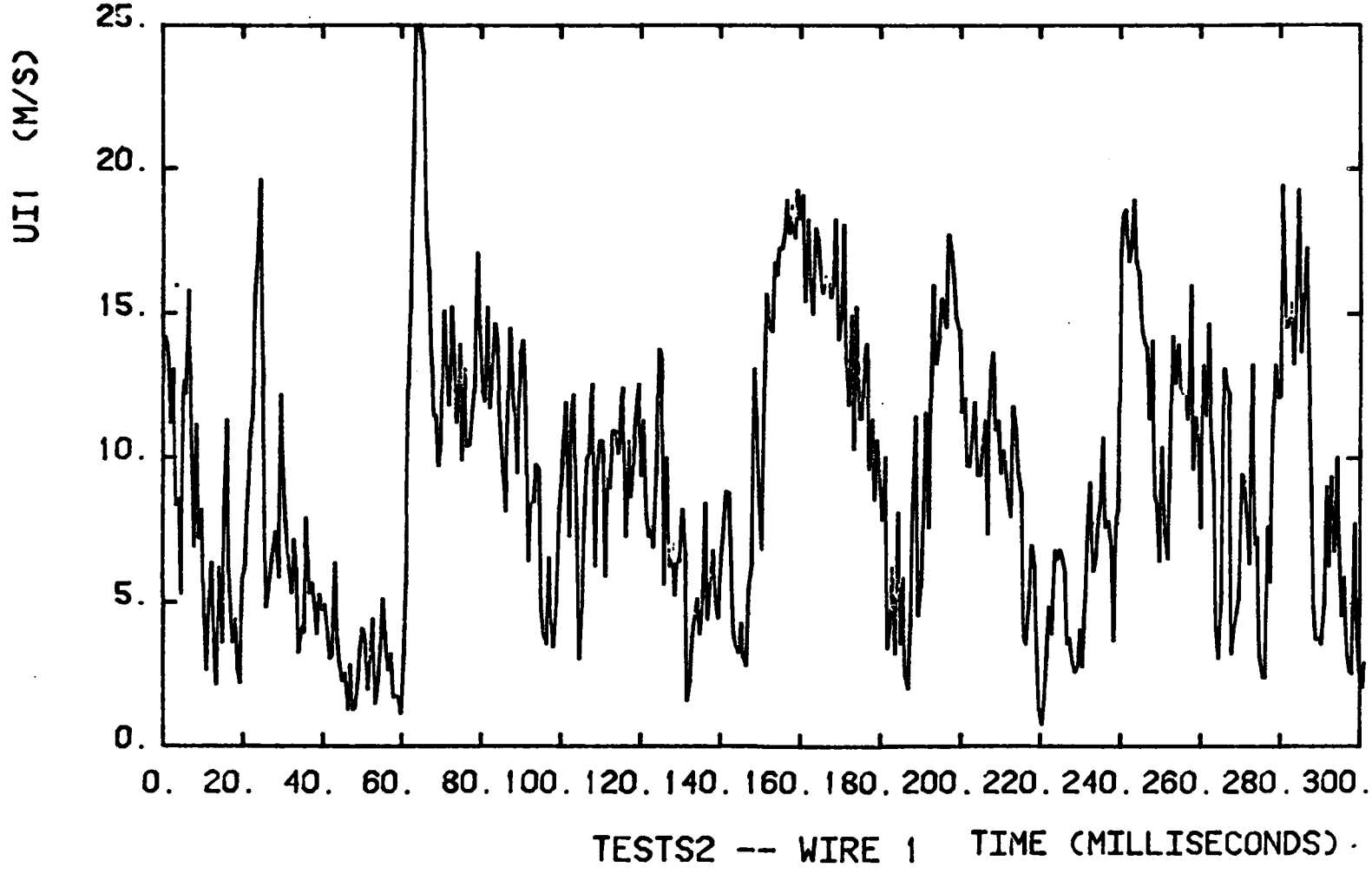

FIG. 34 a - S-2 CONDITION - FILTER 1562 HZ

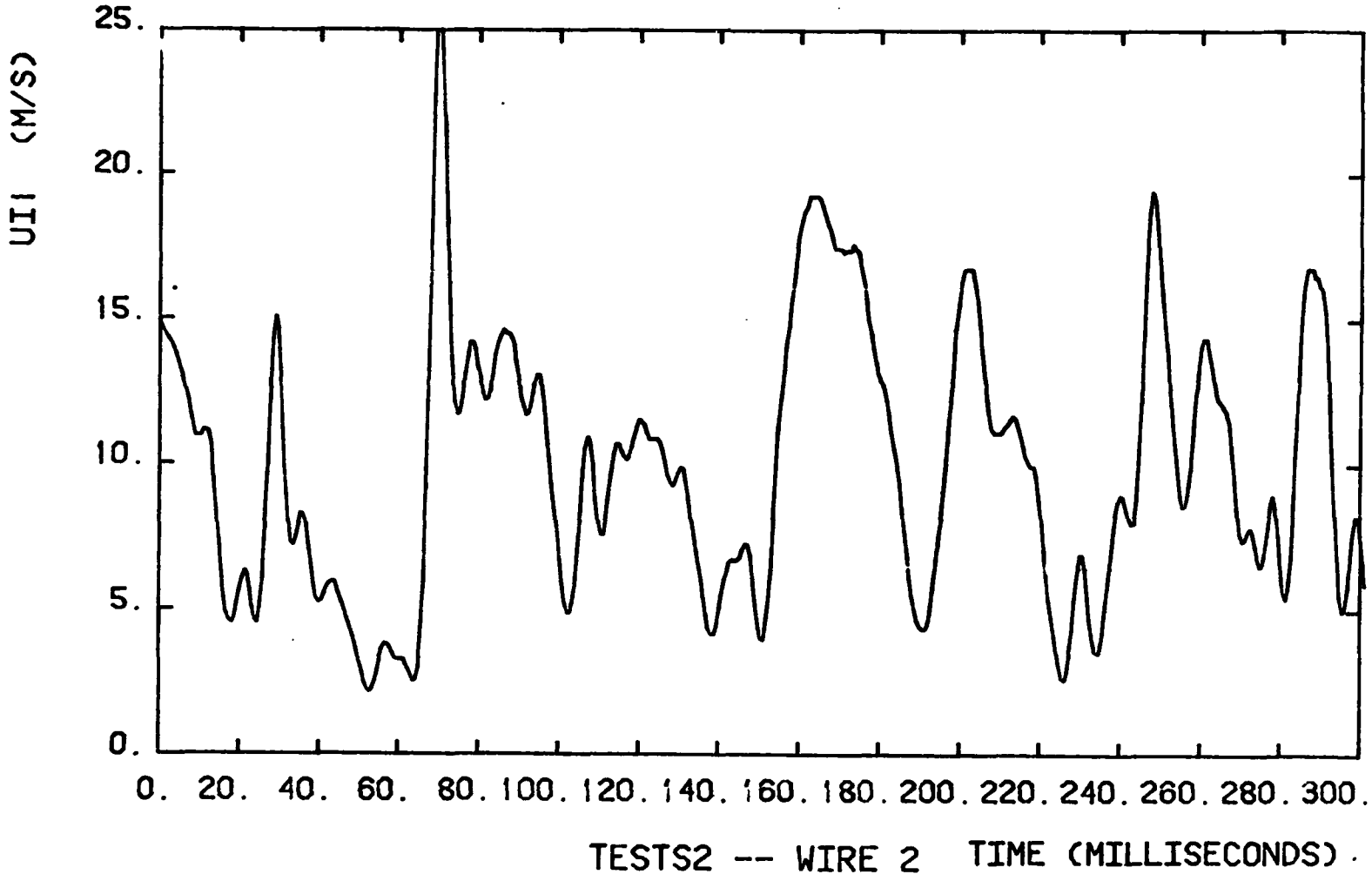

FIG. 34b - S-2 CONDITION - FILTER 125 HZ

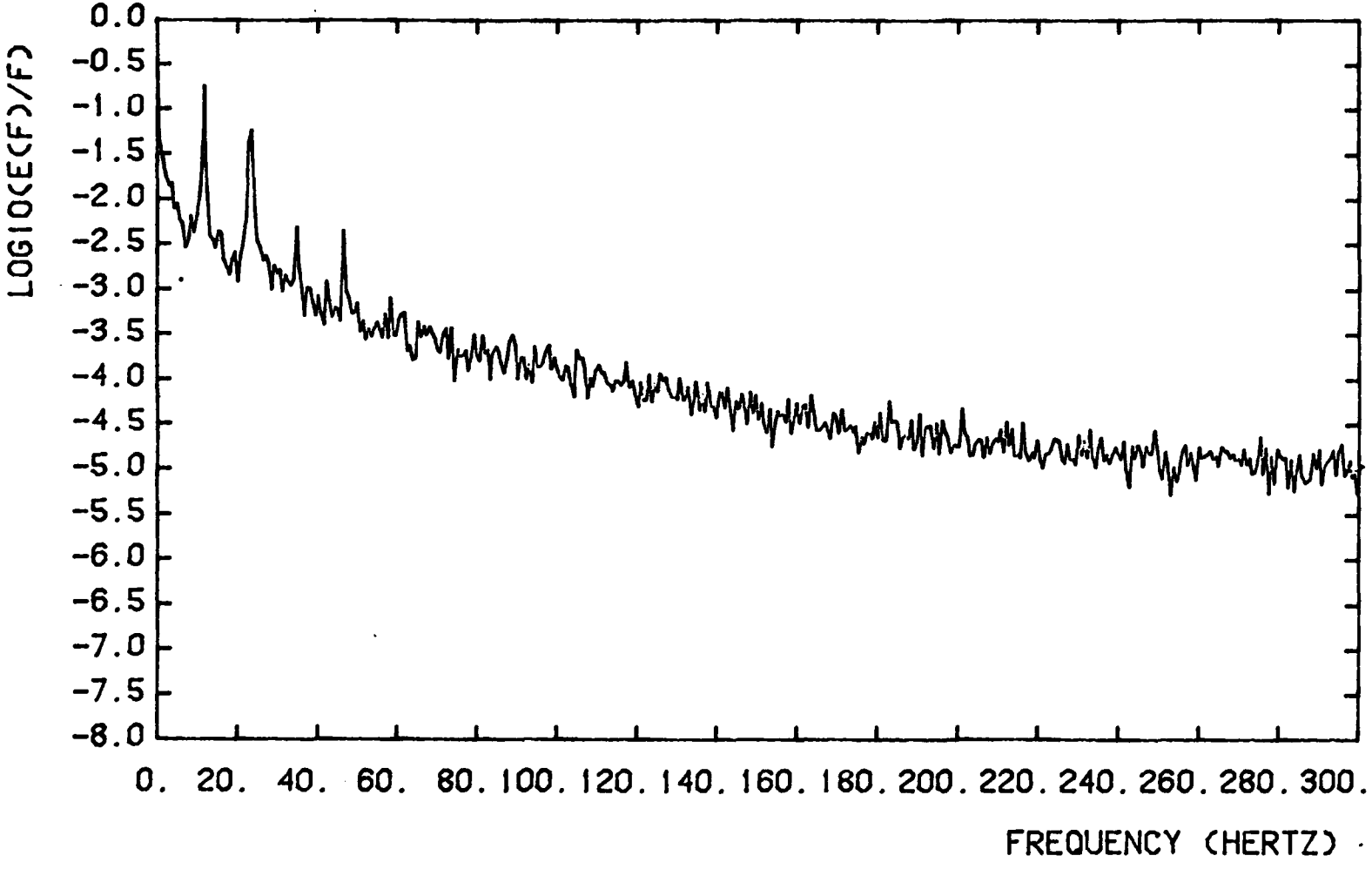

FIG. 35 a - S-2 CONDITION

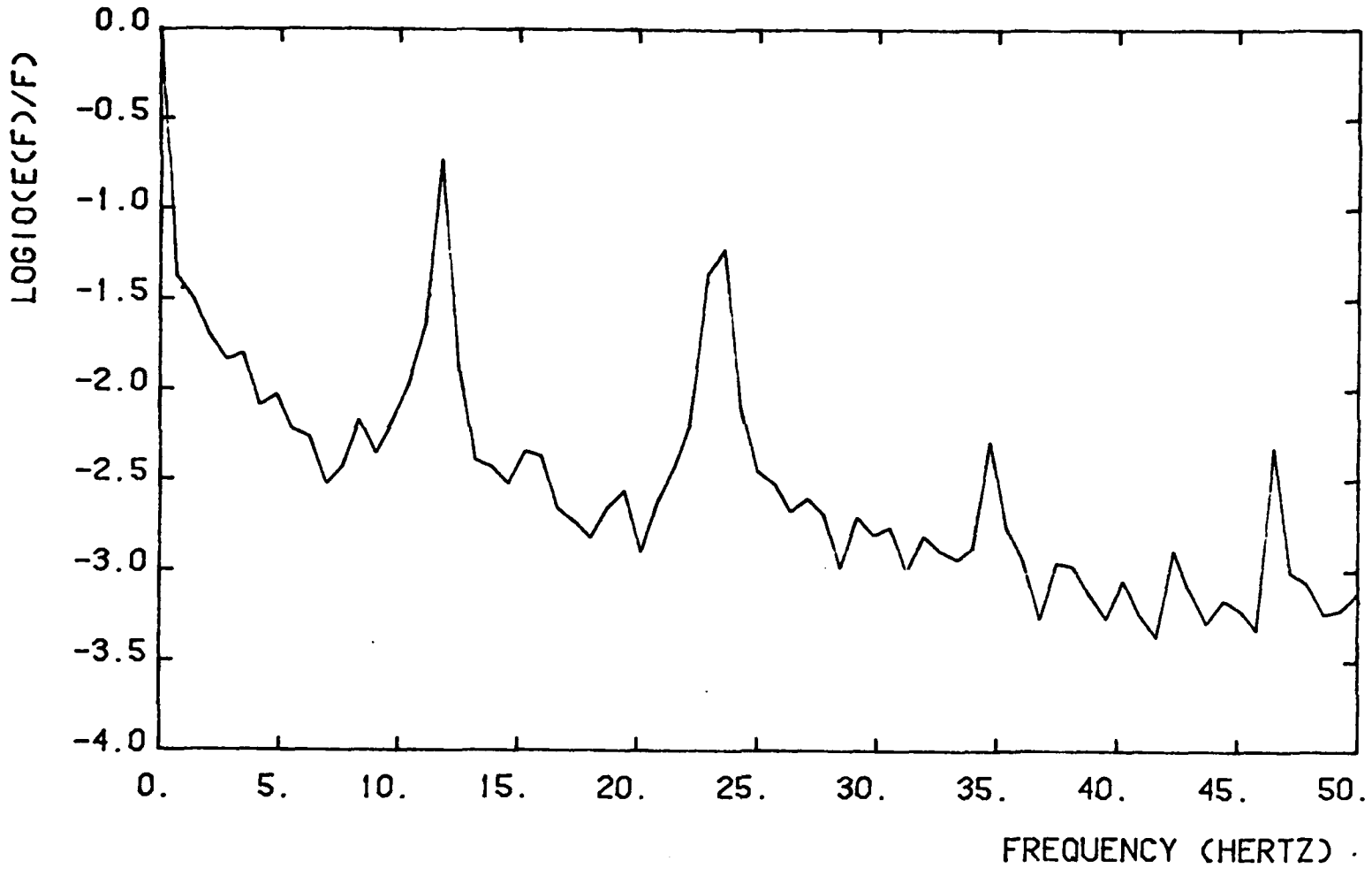

FIG. 35b - S-2 CONDITION

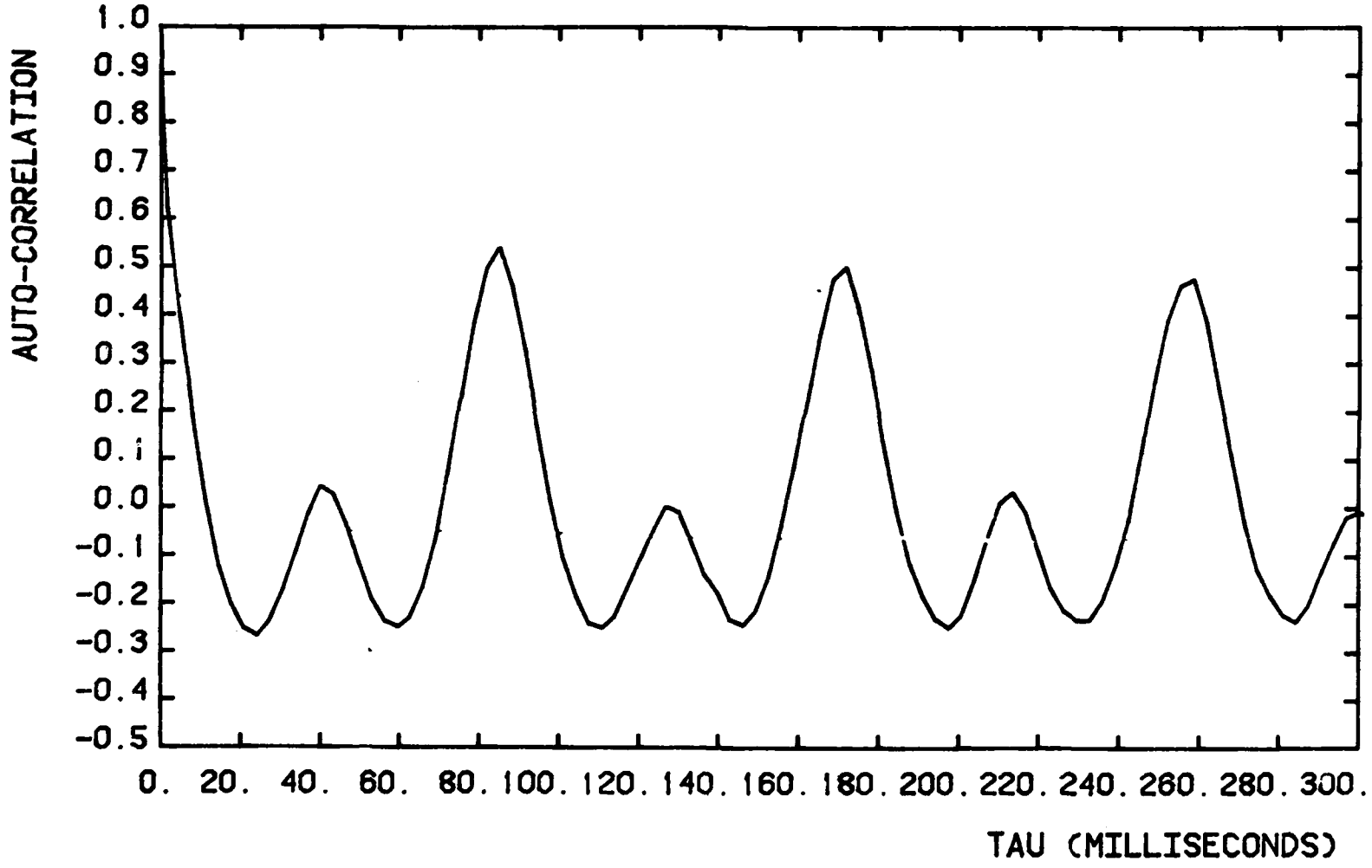

FIG. 36 - S-2 CONDITION

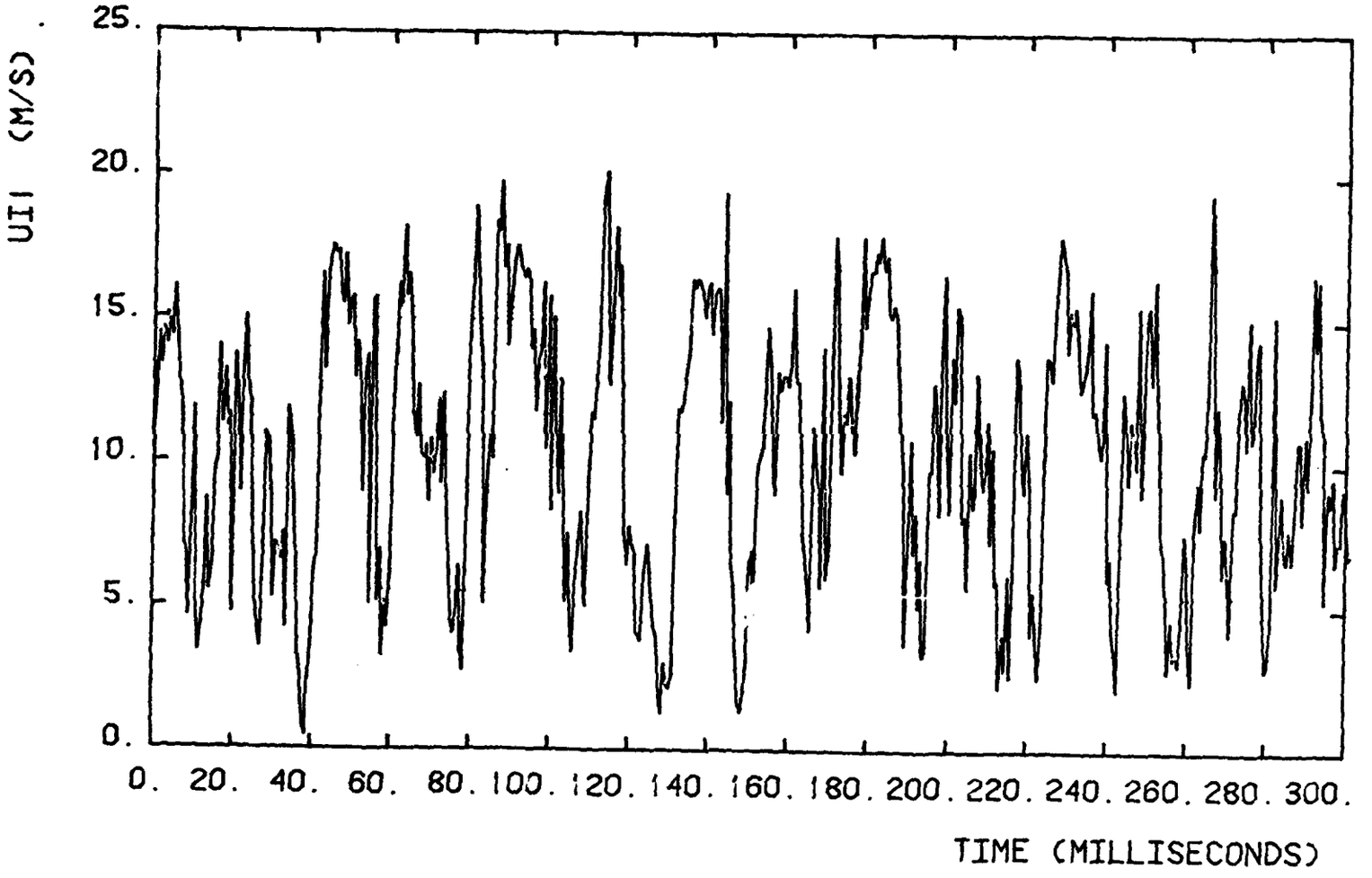

FIG. 37a - S-3 CONDITION - FILTER 1562 HZ

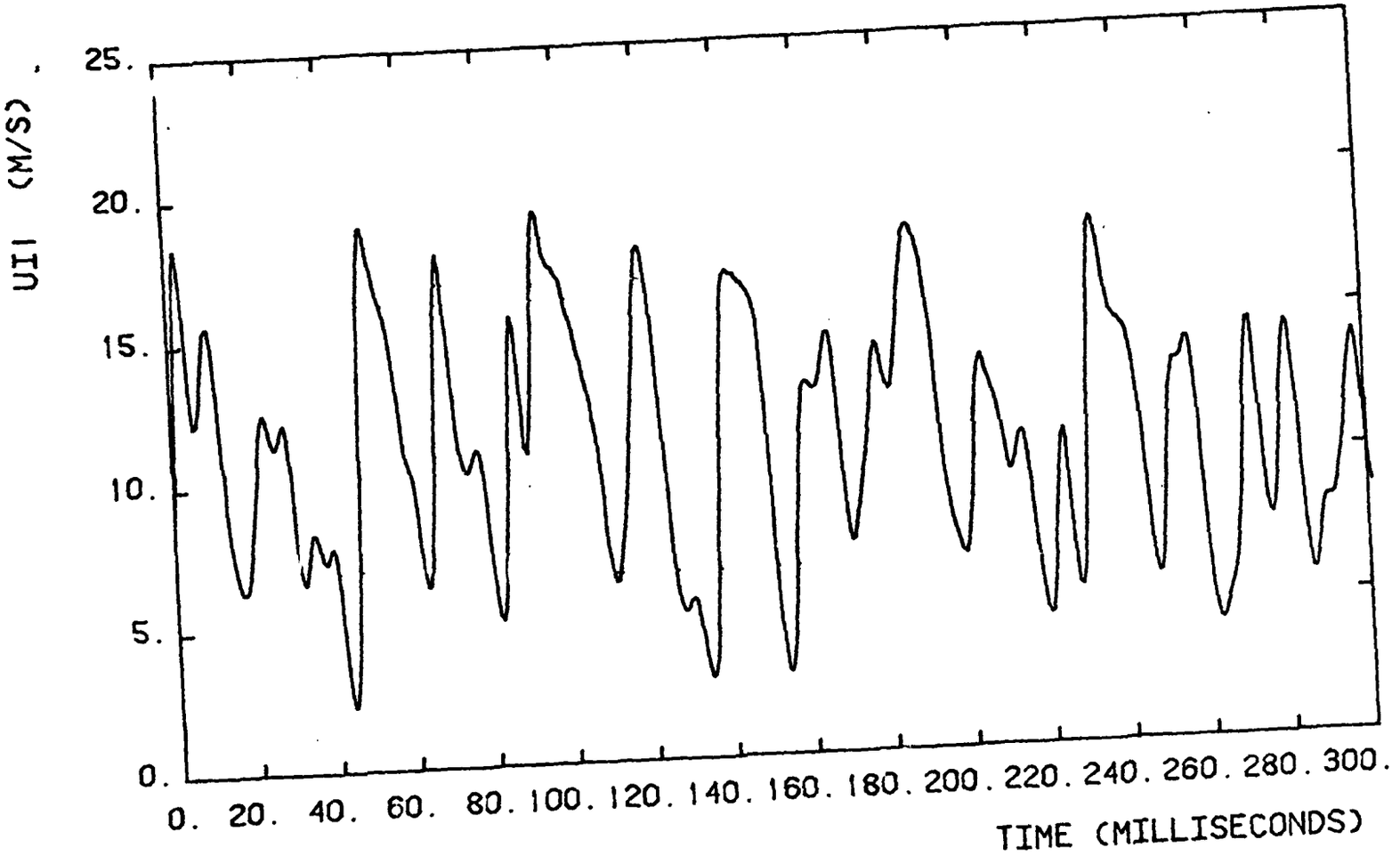

FIG. 37b - S-3 CONDITION - FILTER 125 HZ

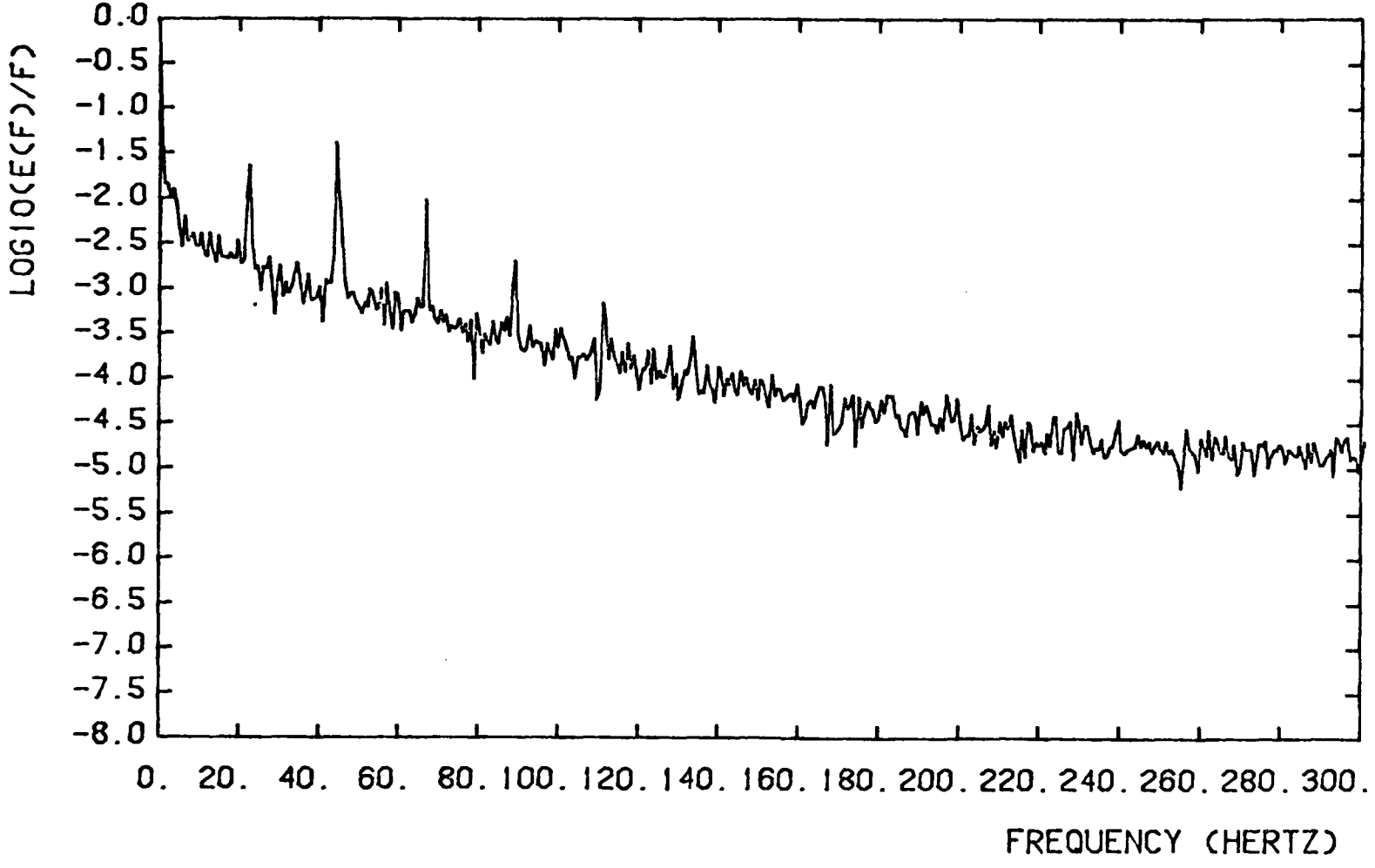

FIG. 38a - S-3 CONDITION

AD-A114 627 VON KARMAN INST FOR FLUID DYNAMICS RHODE-SAINT-GENESE--ETC F/G 20/4
ROTATING STALL IN AN AXIAL FLOW SINGLE STAGE COMPRESSOR. ON-BLA--ETC(U)
APR 82 B GYLES, P LIGRANI, F A BREUGELMANS AFOSR-80-0119B
UNCLASSIFIED EOARD-TR-82-10 NL

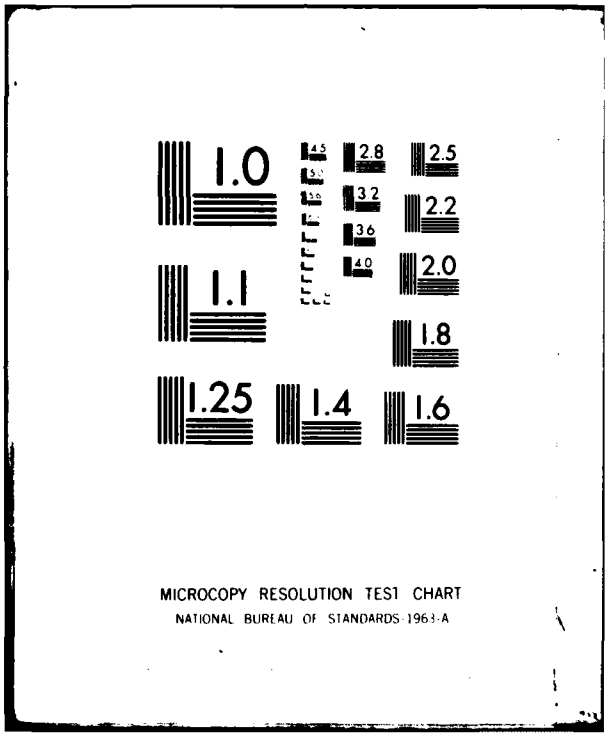
1.0
1.1
1.25
1.4
1.6
1.8
2.0
2.2
2.5
2.8
3.2
3.6
4.0
MICROCOPY RESOLUTION TEST CHART
NATIONAL BUREAU OF STANDARDS-1963-A

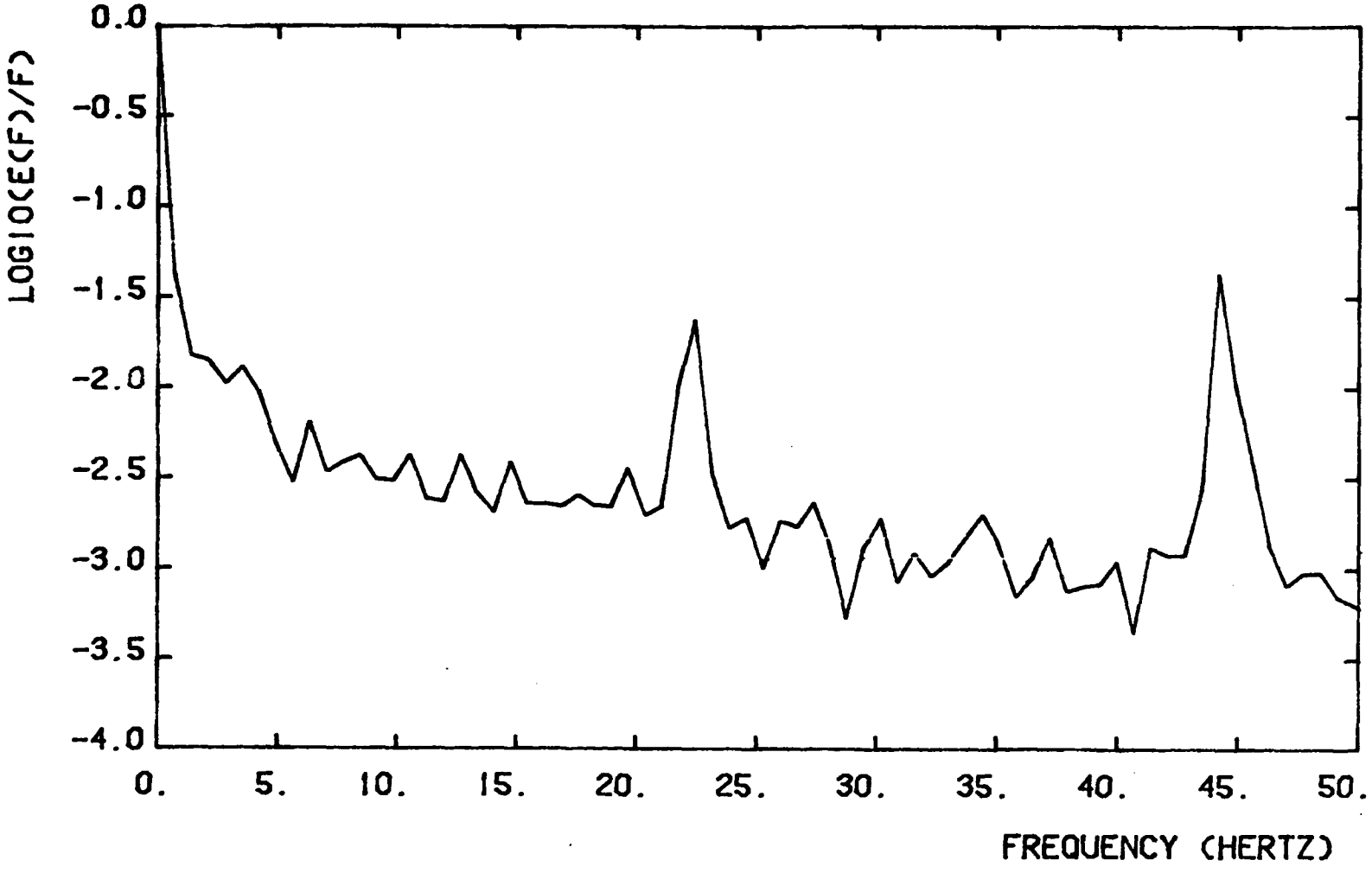

FIG. 38b - S-3 CONDITION

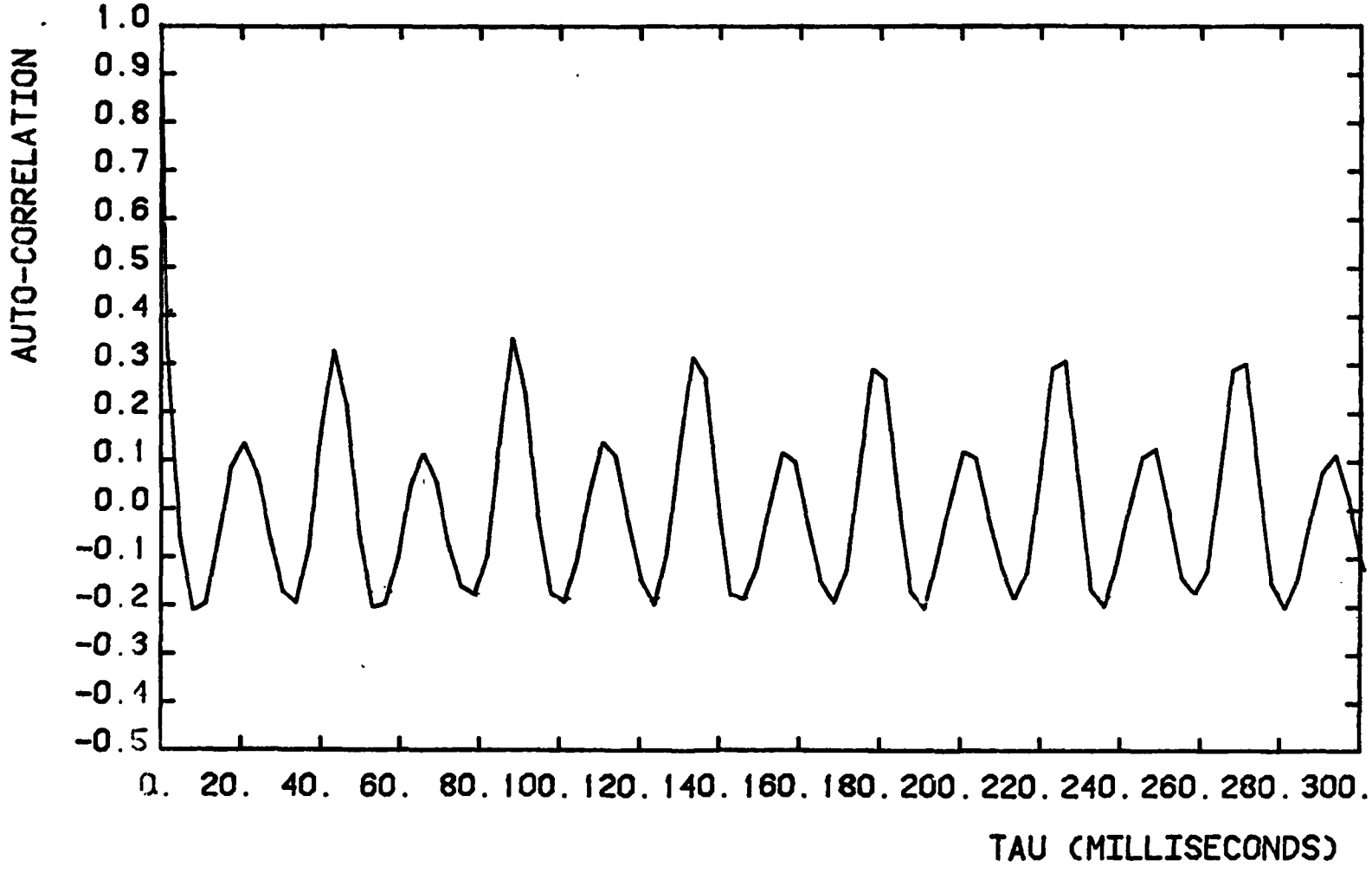

FIG. 39 - S - 3 CONDITION

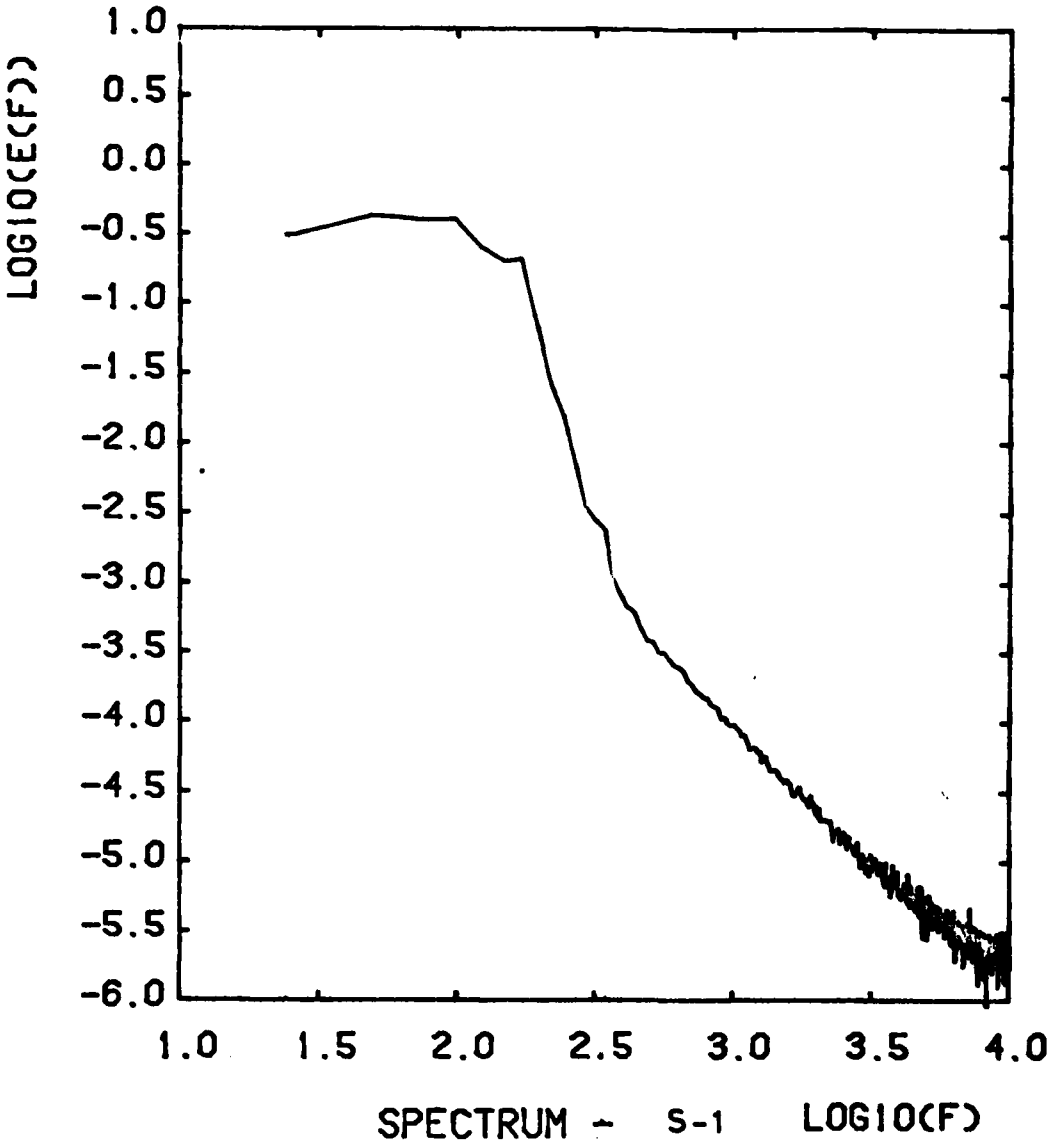
LOG10(E(F))
1.0
0.5
0.0
-0.5
-1.0
-1.5
-2.0
-2.5
-3.0
-3.5
-4.0
-4.5
-5.0
-5.5
-6.0
1.0
1.5
2.0
2.5
3.0
3.5
4.0
SPECTRUM - S-1 LOG10(F)

FIG. 40a

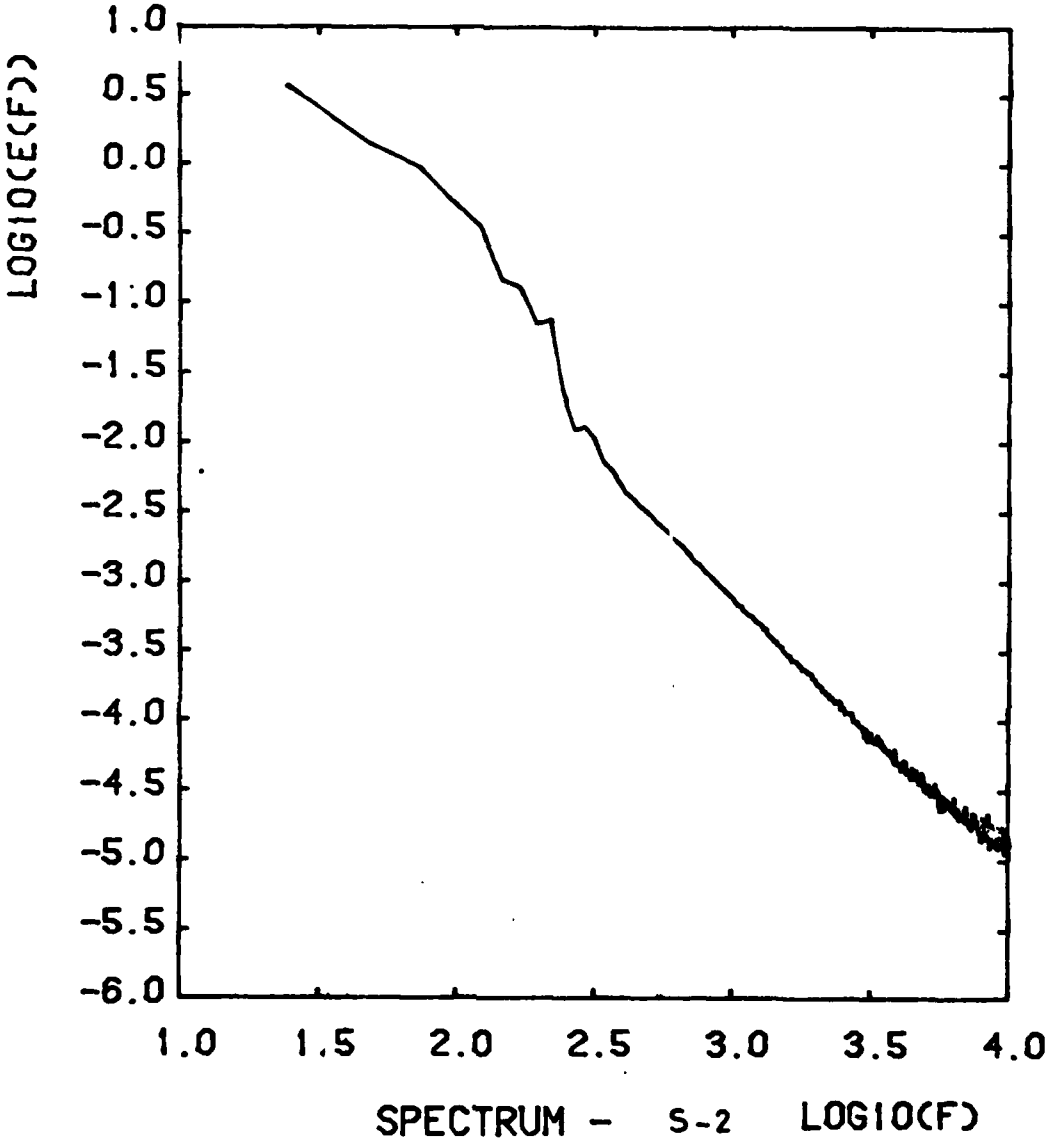
LOG10(E(F))
1.0
0.5
0.0
-0.5
-1.0
-1.5
-2.0
-2.5
-3.0
-3.5
-4.0
-4.5
-5.0
-5.5
-6.0
1.0
1.5
2.0
2.5
3.0
3.5
4.0
SPECTRUM - S-2 LOG10(F)

FIG. 40 b

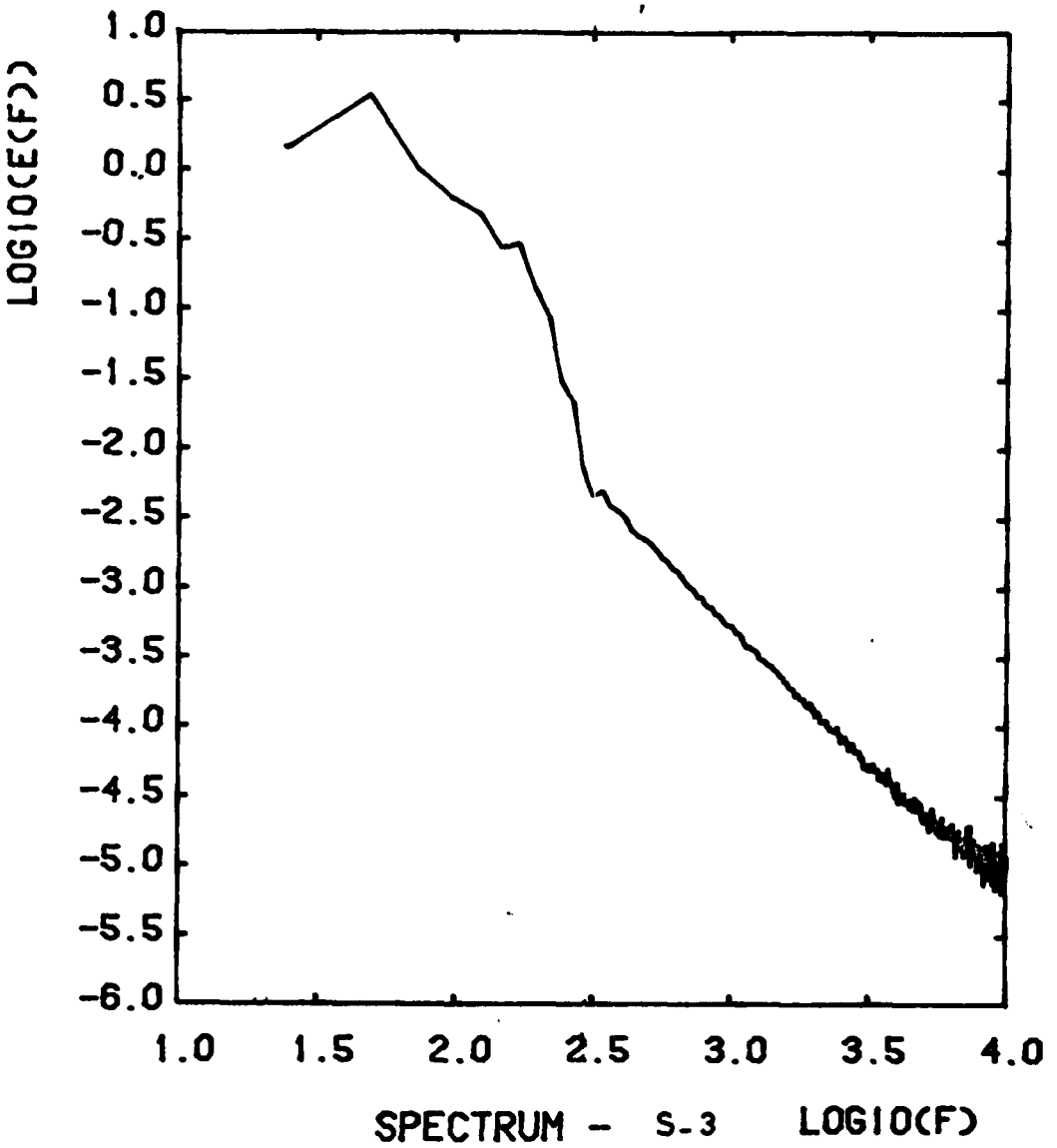
LOG10(E(F))
1.0
0.5
0.0
-0.5
-1.0
-1.5
-2.0
-2.5
-3.0
-3.5
-4.0
-4.5
-5.0
-5.5
-6.0
1.0
1.5
2.0
2.5
3.0
3.5
4.0
SPECTRUM - S-3
LOG10(F)

FIG. 40 c

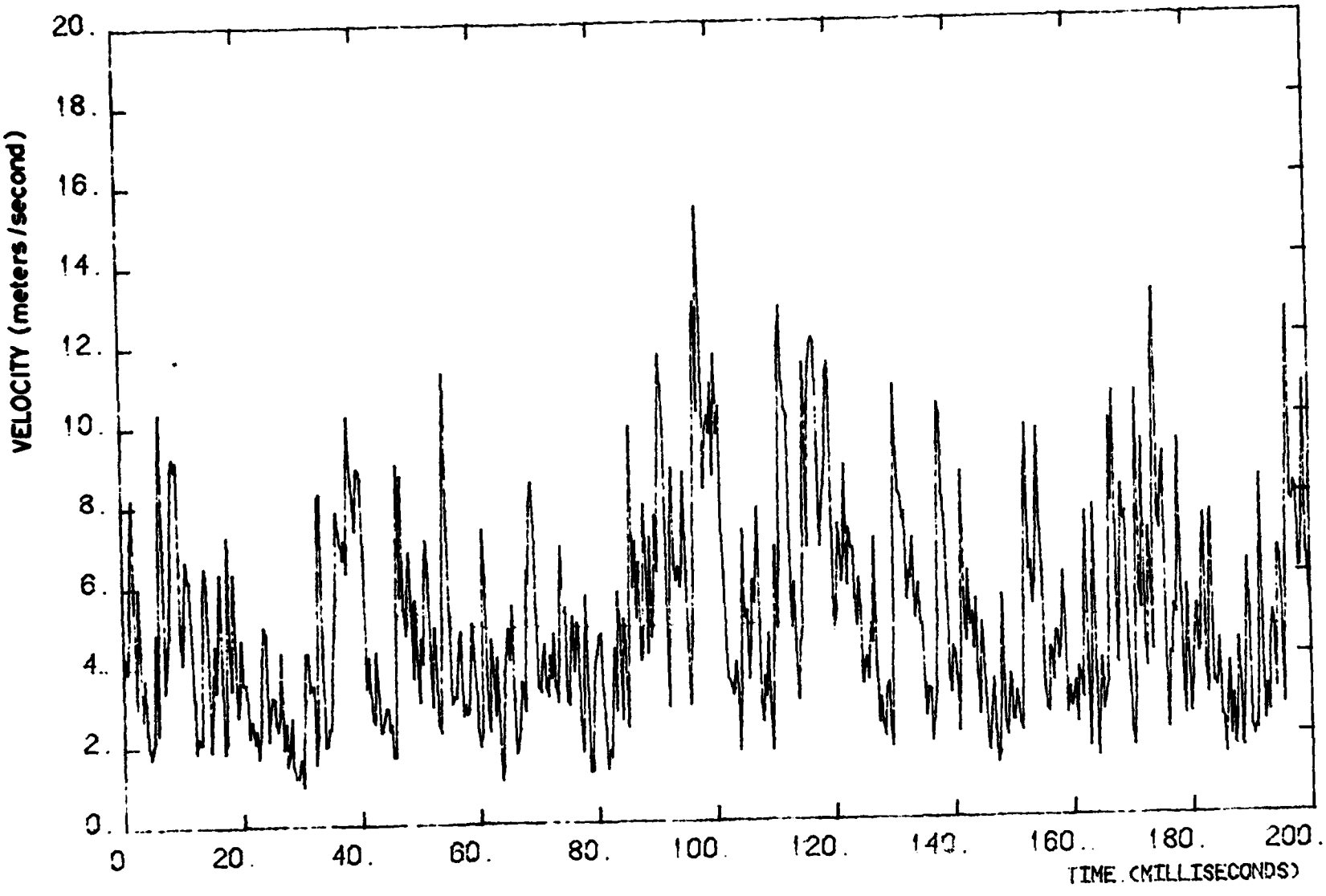

FIG. 41 a - S-1 CONDITION

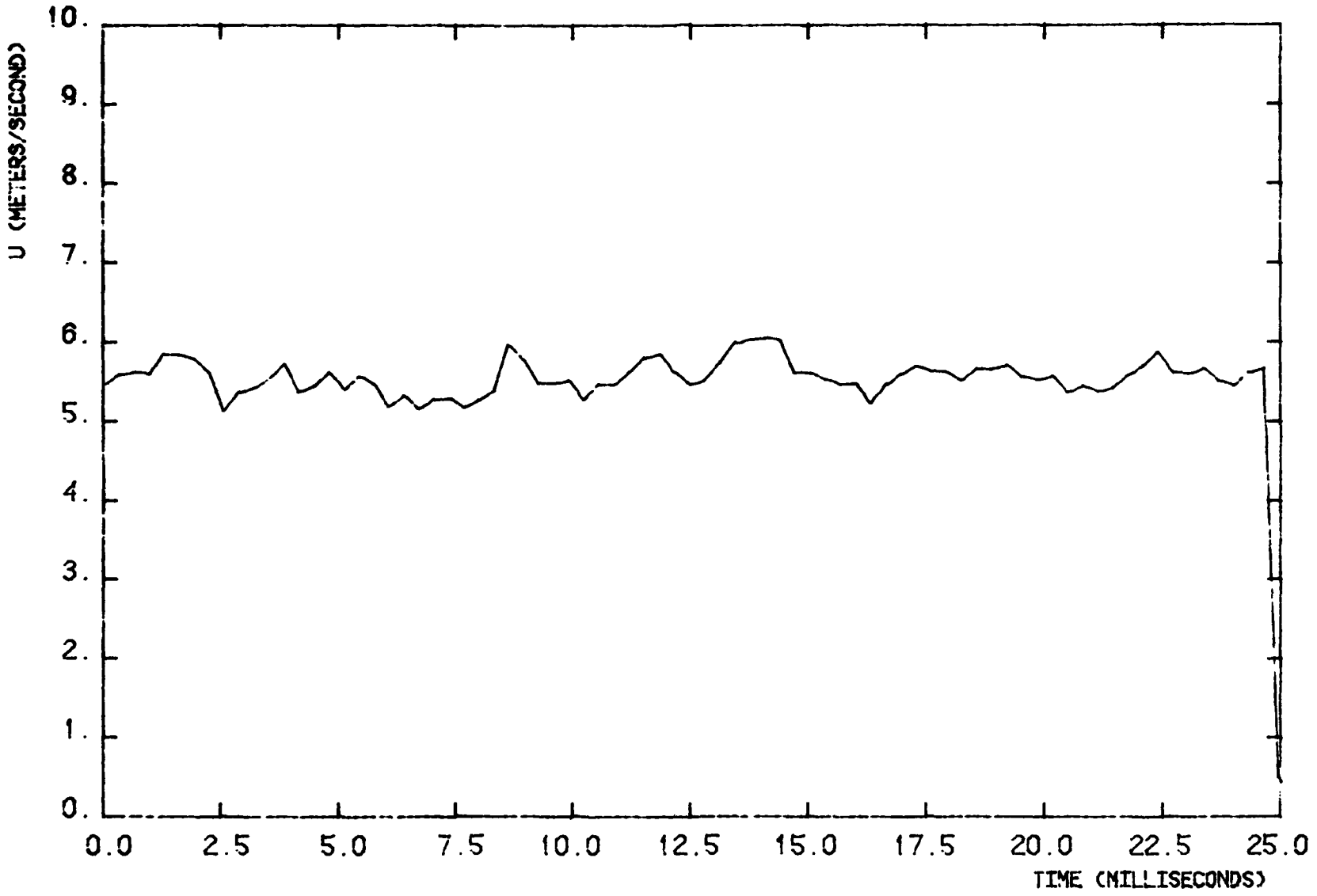

FIG. 41 b - S-1 CONDITION

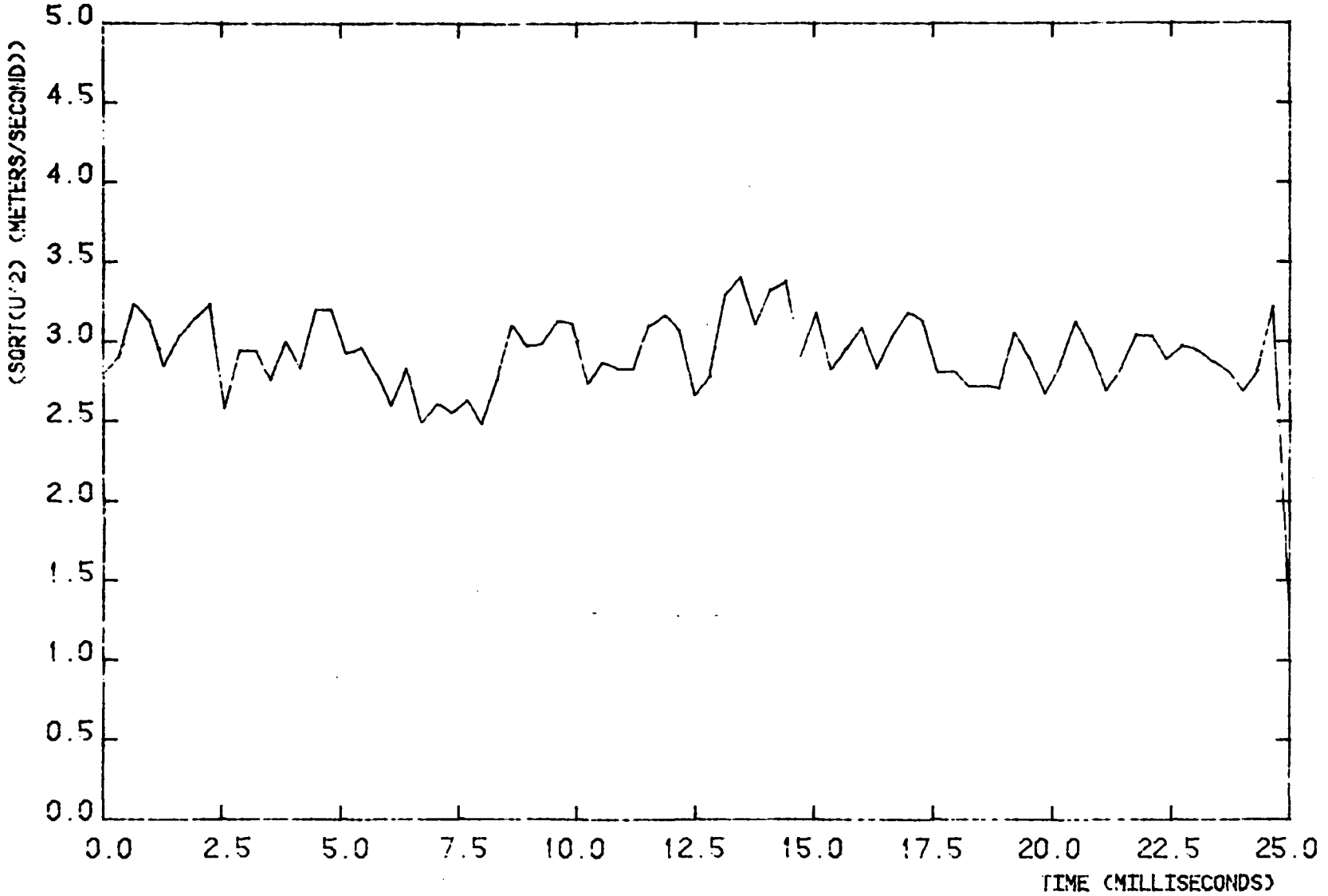

FIG. 41 c - S-1 CONDITION

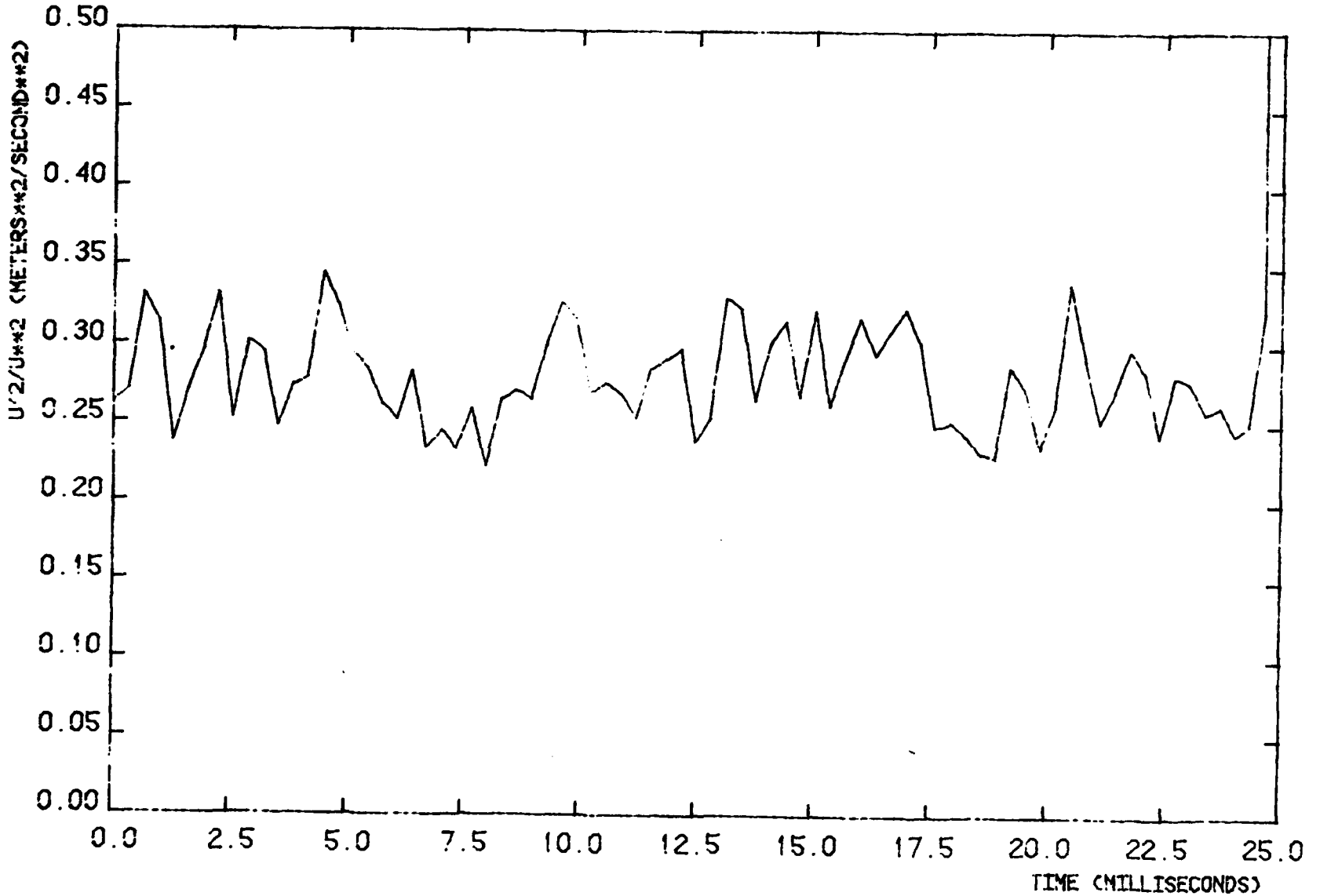

FIG. 41d - S-1 CONDITION

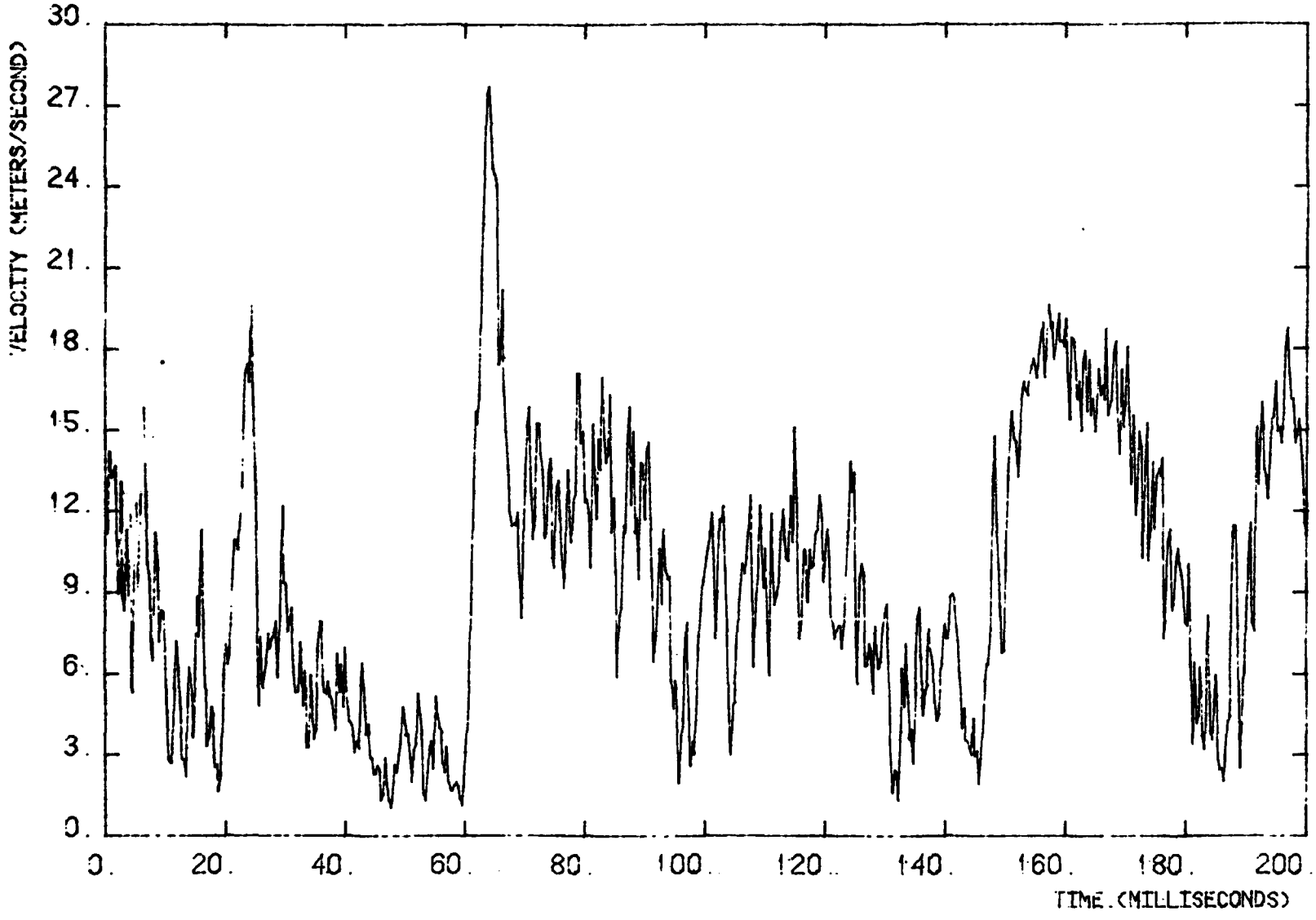

FIG 42 a - S-2 CONDITION.

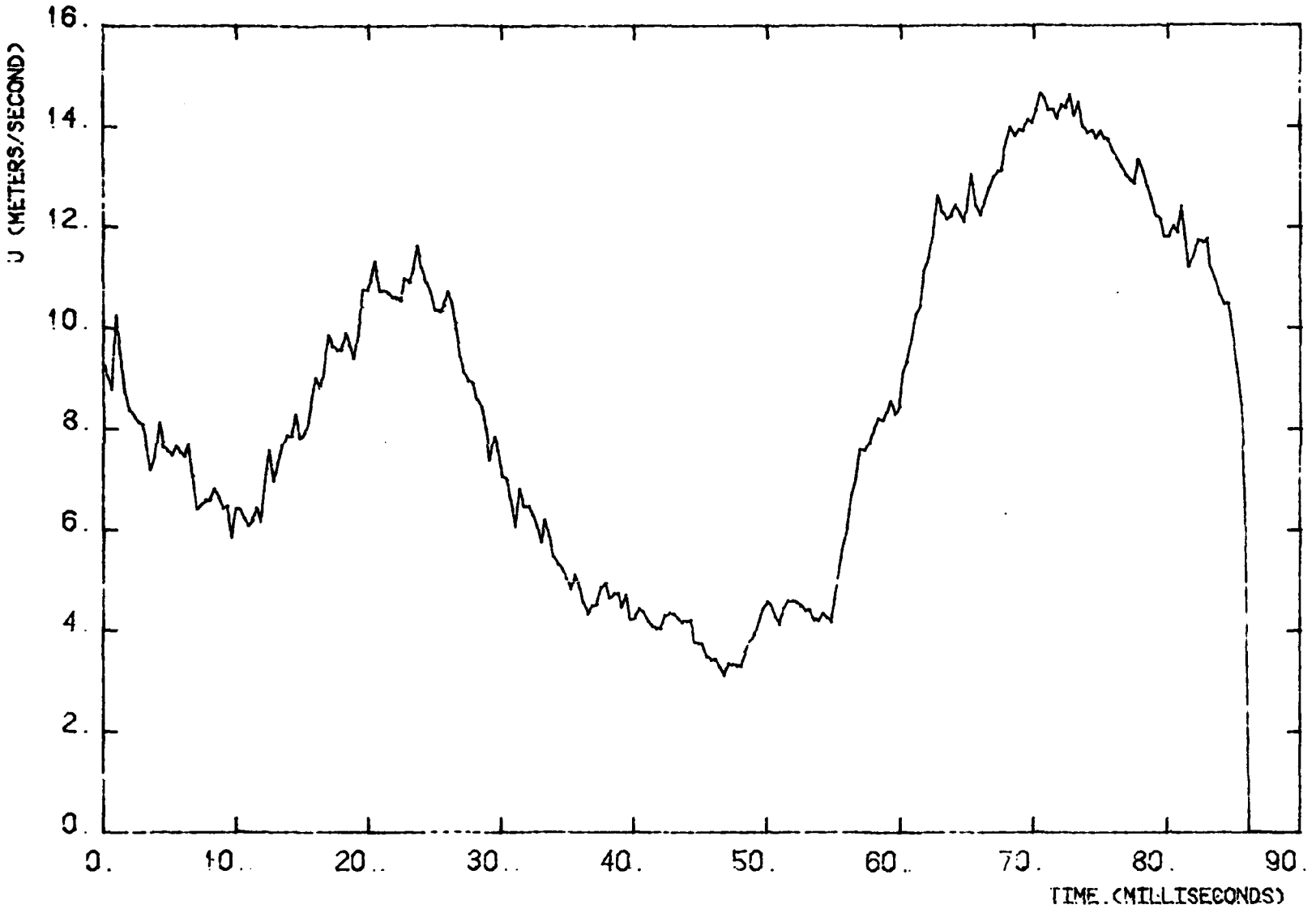

FIG. 42 b - S-2 CONDITION

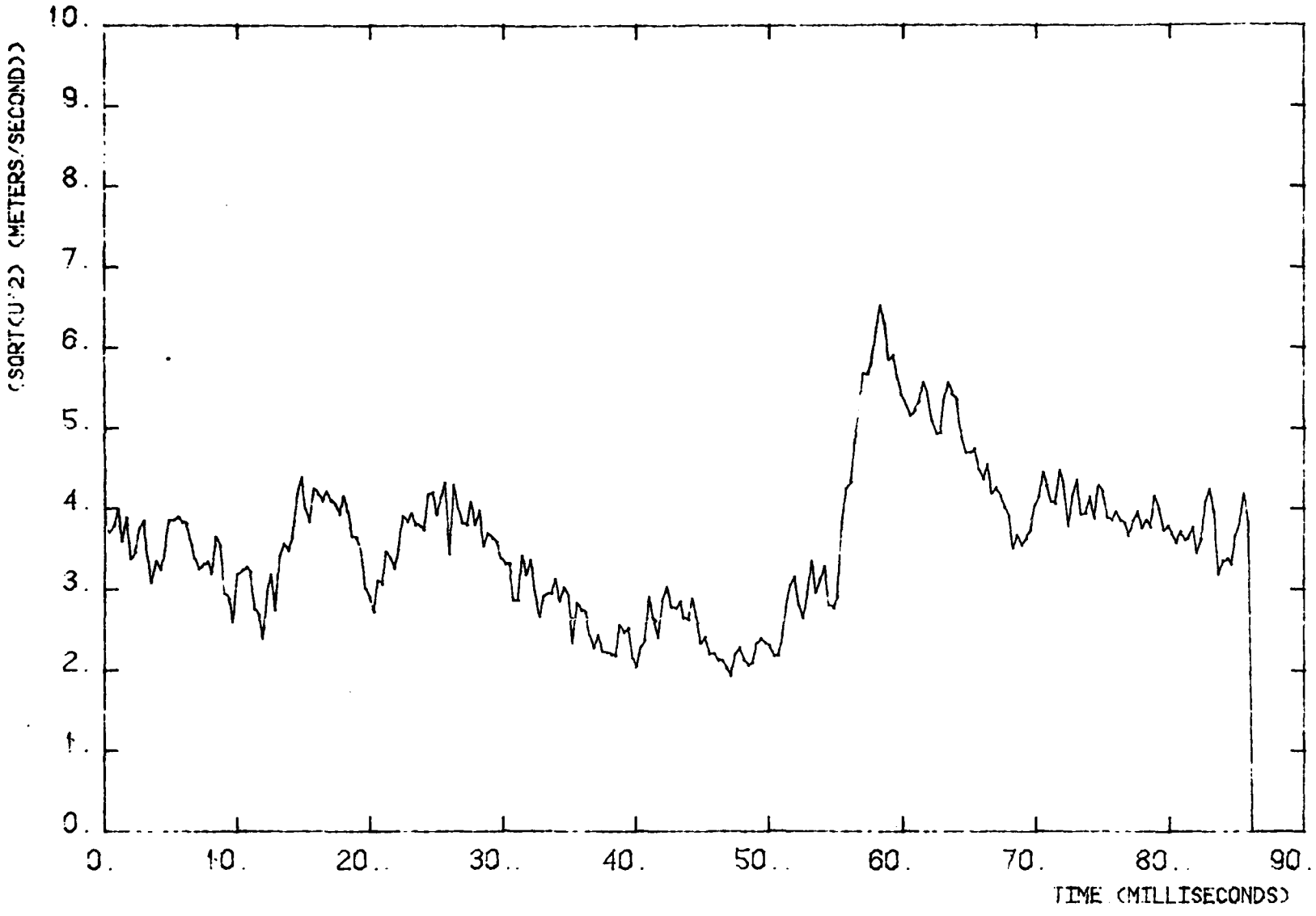

FIG. 42 c- S - 2 CONDITION

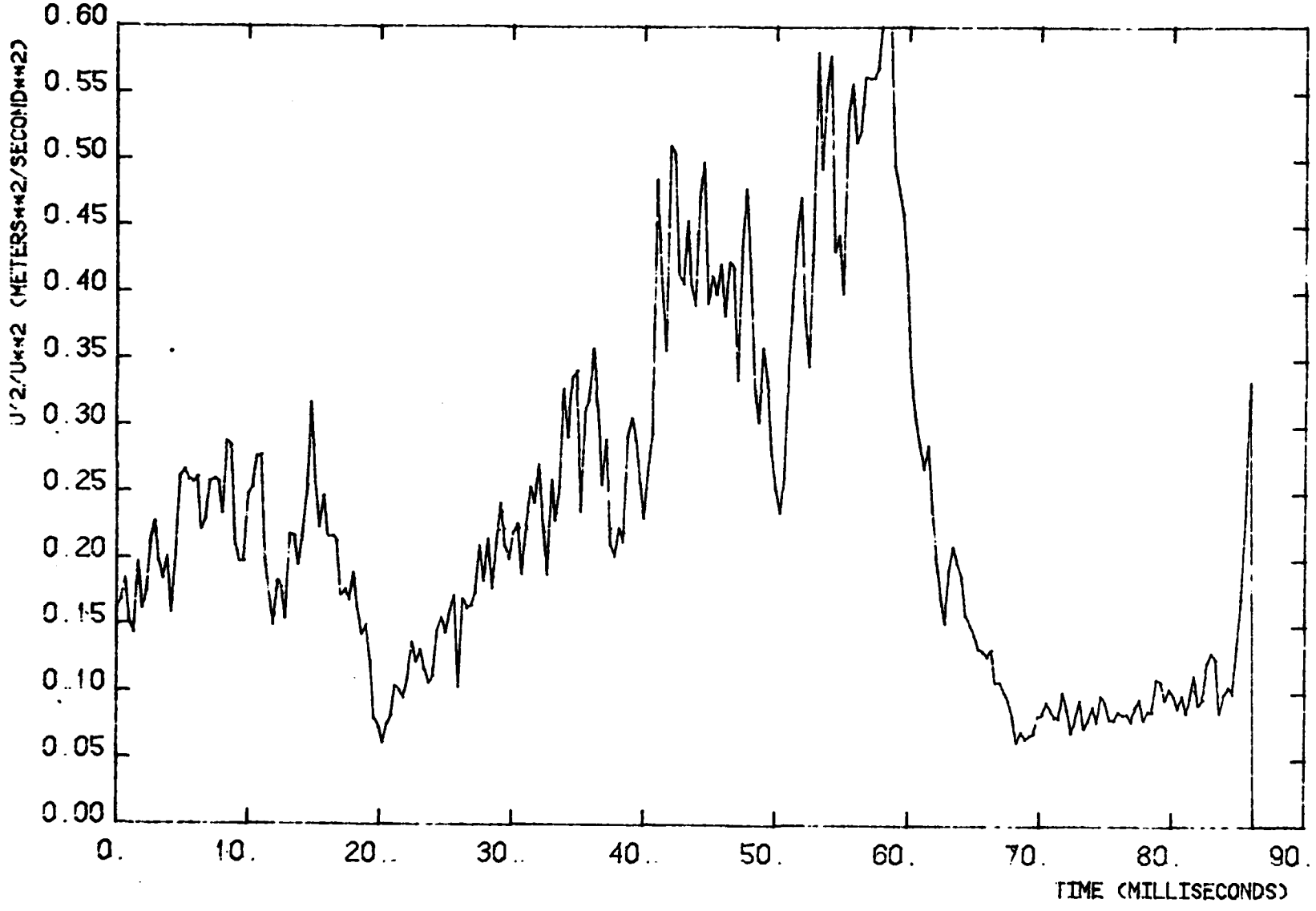

FIG. 42 d - S-2 CONDITION

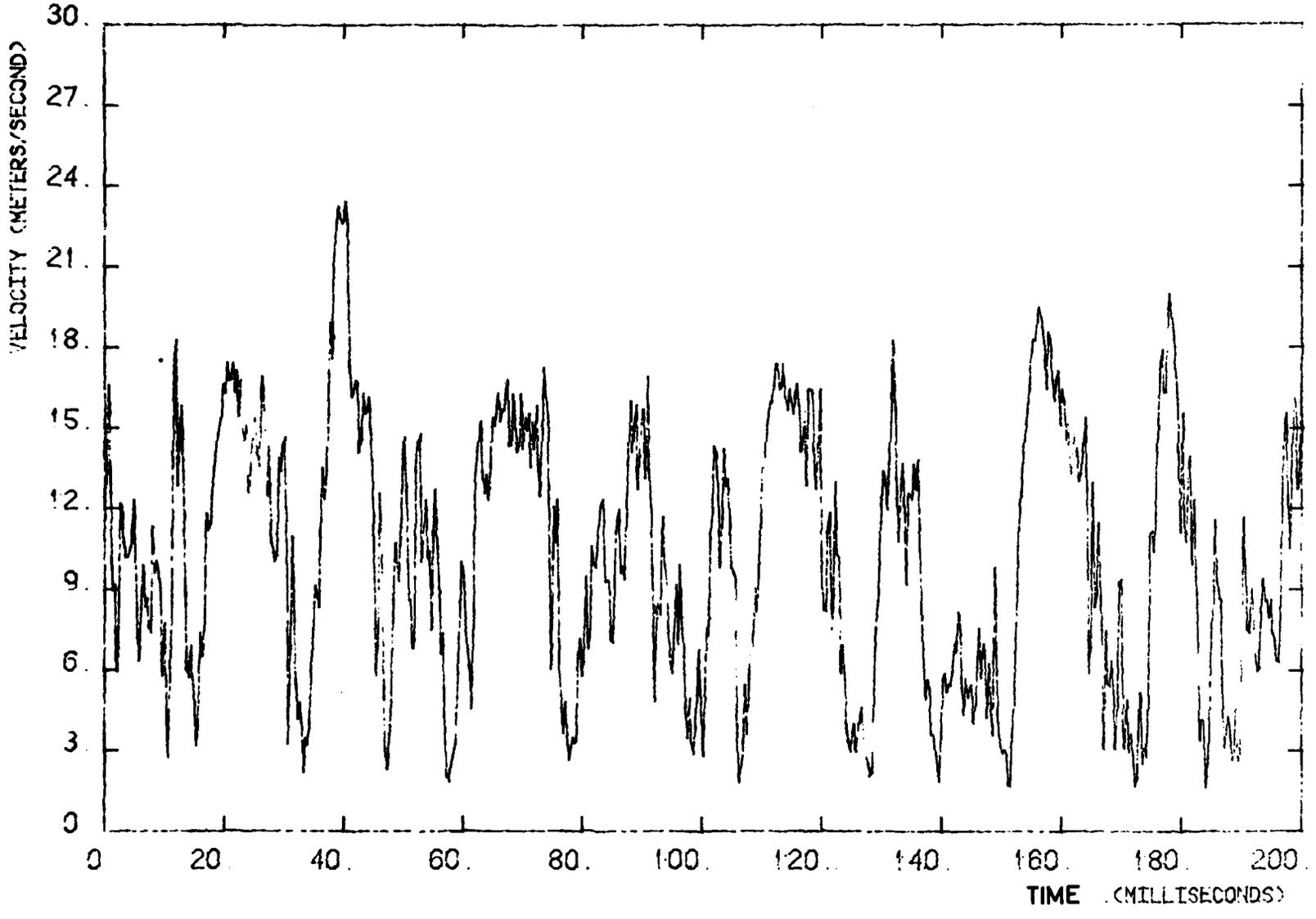

FIG. 43 a - S-3 CONDITION

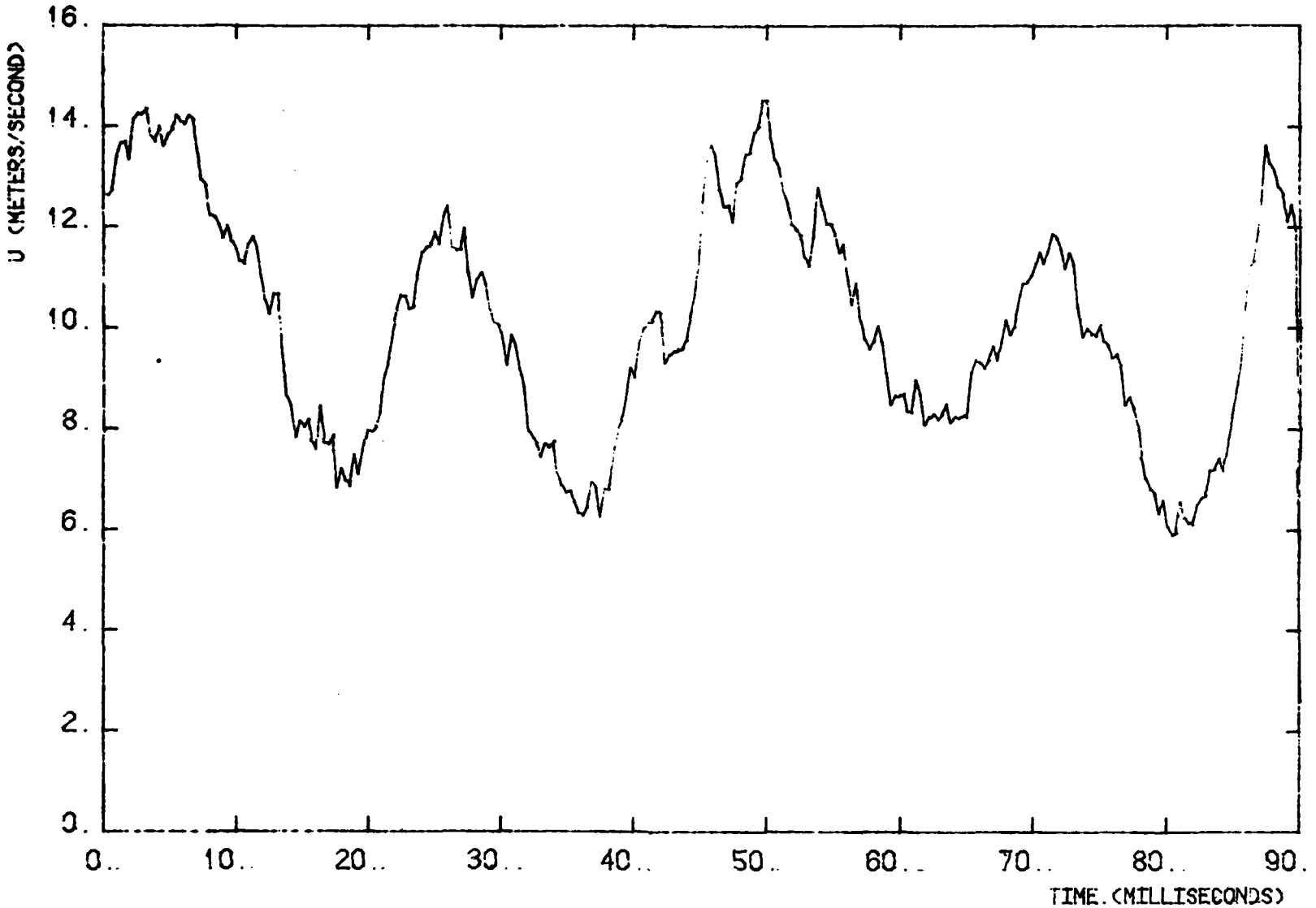

FIG 43 b - S-3 CONDITION

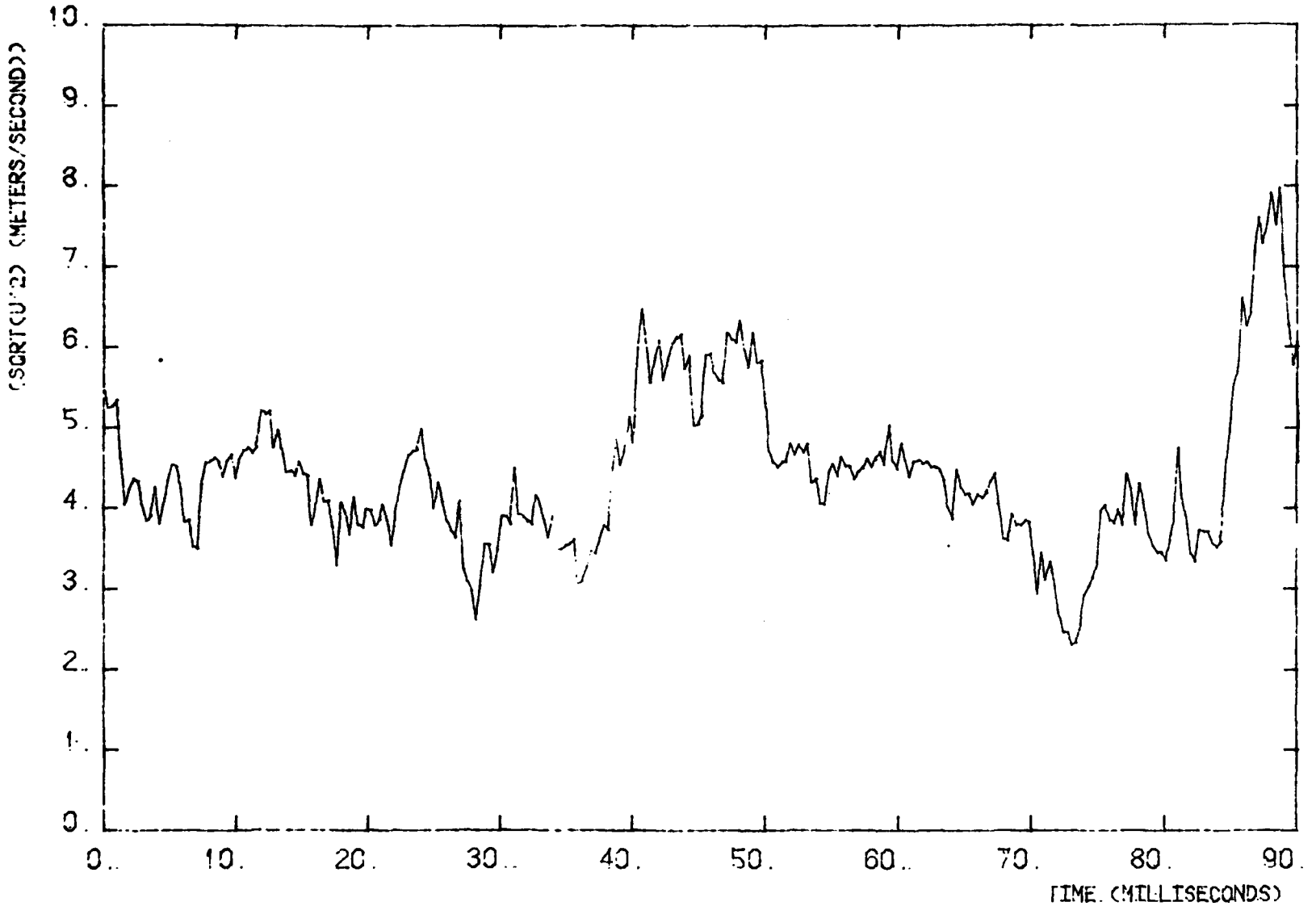

FIG. 43 c - S - 3 CONDITION

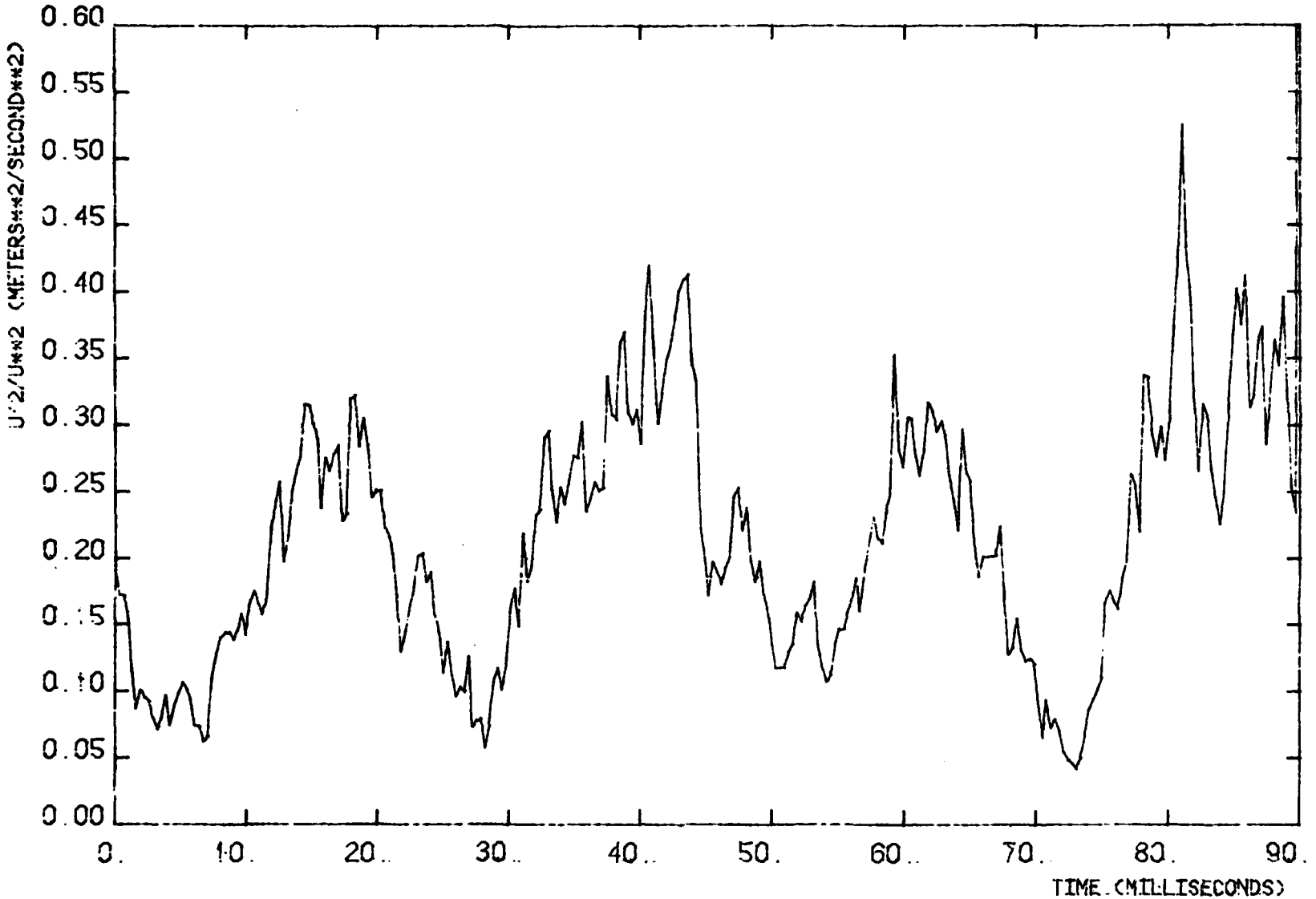

FIG. 43 d - S-3 CONDITION

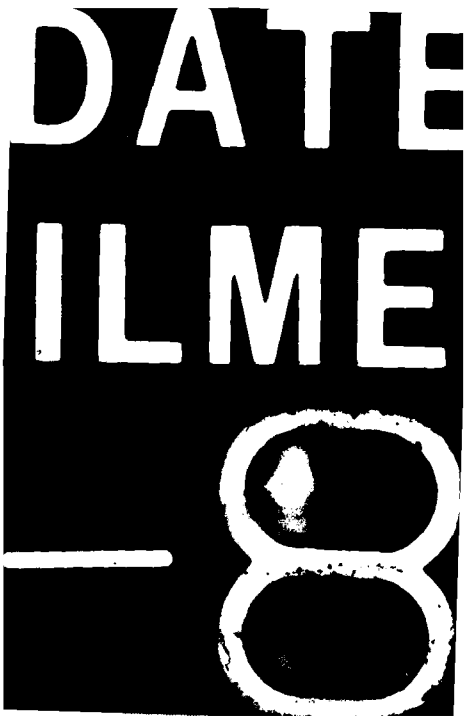
DATE:
ILME
8